JAERI 1266

JAERI 1266

A Study of Reactor-Neutron-Induced Reactions: Double Neutron Capture Process and the Systematics of the (n, 2n) Reaction

June 1980

日 本 原 子 力 研 究 所

Japan Atomic Energy Research Institute

JAERI レポート

この報告書は，日本原子力研究所で行なわれた研究および技術の成果を研究成果編集委員会の審査を経て，不定期に刊行しているものです．

入手（資料交換による），複製などのお問合わせは，日本原子力研究所技術情報部（〒319-11 茨城県那珂郡東海村）あて，お申しこみください．なお，このほかに，財団法人原子力弘済会資料センター（茨城県那珂郡東海村日本原子力研究所内）で，複写による実費頒布を行なっております．

JAERI Report

Published by the Japan Atomic Energy Research Institute

Inquiries about the availability of reports and their reproduction should be addressed to the Division of Technical Information, Japan Atomic Energy Research Institute, Tokai-mura, Naka-gun, Ibaraki-ken, Japan.

編集兼発行　日本原子力研究所
印　　刷　コビキ印刷株式会社

JAERI 1266 正誤表

頁	行	誤	正
6	Table2, 2	Io	I_o'
7	下16	ot	to
8	下12	pyrophoshate	pyrophosphate
9	下 7	soution	solution
	下 3	erros	errors
11	下 9	my	may
15	下 3	nickel of 0.2 mm	nickel foil of 0.2 mm
18	下13	ons	one
23	下 7	imipurities	impurities
29	下 2	ocontribute	contribute
30	6	thertfore	therefore
	下 8	engry	energy
31	7	experimenally	experimentally
33	下 6	Johson	Johnson
41	下 4	metastadle	metastable
42	9	availailble	available
47	下 2	correponds	corresponds
48	7	correponds	corresponds
	(A2, 1)	$\hat{\sigma}$g	$\hat{\sigma}_g$
	(A2, 3)	ti	t_1
49	(A2, 5)	si	s_1
	下13	nncleus	nucleus
51	3	intermittnt	intermittent

A Study of Reactor-Neutron-Induced Reactions: Double Neutron Capture Process and the Systematics of the (n, 2n) Reaction

Toshiaki Sekine and Hiroshi Baba

Division of Radioisotope Produdtion, Radioisotope Center
Japan Atomic Energy Research Institute
Tokai-mura, Naka-gun, Ibaraki-ken, Japan

Received June 4, 1979

Cross sections of the second neutron capture in the double-neutron-capture process were studied in the irradiation of ^{26}Mg, ^{64}Ni, ^{93}Nb, and ^{164}Dy with reactor neutrons. Weak radioactivities produced were determined with sufficient accuracy by taking advantage of high resolution Ge(Li) detectors. The neutron spectrum at the irradiating site was defined with Westcott's epithermal index determined by the use of the cadmium ratio method.

The isomer cross-section ratio was obtained with the ^{94}Nb target. The statistical theory was found to be applicable to such an unstable or odd-odd nuclide as ^{94}Nb. Cross sections of isomers of ^{165}Dy were determined. The capture cross section of the ground state nuclei was found greater than that of the metastable state nuclei in this case. This differs from the other four isomers observed so far.

Cross sections of $^{28}Al(n,p)^{28}Mg$ and $^{58}Ni(n,2n)^{57}Ni$ reactions with fission neutrons were also measured. A simple formula was proposed for the systematics of (n, 2n) reaction cross sections, which enabled prediction of the cross section more accurately than the previously proposed formulae.

Key words: Double Neutron Capture, (n, 2n) Cross Section, Systematics, Thermal Neutron, Fission Neutron, Isomer Ratio, $^{27}Mg(n,\gamma)^{28}Mg$, $^{65}Ni(n,\gamma)^{66}Ni$, $^{94}Nb(n,\gamma)^{95m,g}Nb$, $^{165m,g}Dy(n,\gamma)^{166}Dy$, $^{58}Ni(n,2n)^{57}Ni$, $^{28}Al(n,p)^{28}Mg$

原子炉中性子誘起核反応の研究：二重中性子捕獲過程と(n, 2n)反応の系統性

関根俊明，馬場　宏

日本原子力研究所アイソトープ事業部製造部

1979年6月4日　受理

原子炉の強い中性子束のもとでは，1個の中性子を捕獲して生成した放射性核が崩壊しないうちに更に中性子を捕獲（二重中性子捕獲）する確率を無視しえない。本研究では，この過程による微弱な放射能を高感度のGe(Li)検出器によって測定し，2個目の中性子を捕獲する断面積を求めた。実験には ^{26}Mg，^{64}Ni，^{93}Nb，^{164}Dy をターゲット核に選び，化学分離によって放射能検出の感度を上げることは勿論，カドミウム比法によって Westcott のエピサーマル・インデックスを求めて原子炉のスペクトルの影響を考慮するなどの点において注意を払った。

断面積のデータは反応による生成量の算出，burn-out の補正に用いられるが，核反応機構の点からも興味ある知見が得られる。すなわち，^{93}Nbをターゲット核とする実験では^{95}Nbの核異性体生成比が得られたが，これは今まで知られていない不安定な奇—奇核をターゲット核としている点で興味がある。本実験により，安定核をターゲット核とする場合と同じく不安定核の場合も統計モデルによって良く説明できることが明らかにされた。一方，^{164}Dyをターゲットとする実験により，^{165}Dy の核異性体の熱中性子捕獲面積を求めた。核異性体の断面積が知られている例がほかに4核種あって，いずれも準安定状態の方の断面積が大きいが，^{165}Dy の場合は逆となった。この結果から，核異性体の断面積の比をそれぞれの核異性体から生成する複合核の準位密度との関連において理解することを試みた。

二重中性子捕獲の実験に伴なって得られた ^{28}Al(n, p)^{28}Mg 反応，^{58}Ni(n, 2n)^{57}Ni 反応の断面積についても記述した。また，核分裂中性子による（n, 2n）反応の平均断面積の系統性を表わすために，これまでに発表されている式よりも正確に実験値を再現する式を提案した。

Contents

目　次

1. Introduction

A huge amount of data has been accumulated on the cross section of neutron-capturing nuclear reactions[1]. There are theoretical works by Weisskopf[2] and Lynn[3] for the interpretation of these data. However, cross sections for low-energy neutrons, especially for thermal neutrons of most importance among pile-neutron reactions, are still unpredictable by any theoretical or empirical means. Though it is true that one can set the lower limit for the cross section with relatively high reliability[4], there is no way of knowing accurate cross-section value of the thermal neutron capture reaction unless one measures it.

When a stable nucleus ${}^{A}_{Z}N$ of the atomic number Z and the mass number A is irradiated with neutrons, the following successive reactions take place;

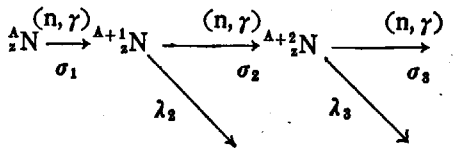

Here, λ_i and σ_i denote the decay constant and the (n,γ) reaction cross section in the ith step of the reaction, respectively. The phenomenon that the product nucleus ${}^{A+1}_{Z}N$ in the first neutron capture absorbs another neutron before it decays is called double neutron capture. Observations on σ_2 are quite scarce contrary to abundance of the σ_1 data. Knowledge of σ_2 is important from the following reasons:

(1) The σ_2 value is necessary in the evaluation of the reaction rate of the neutron capture reaction of ${}^{A+1}_{Z}N$ and the yield of ${}^{A+2}_{Z}N$ nuclide. The former concerns the burn-out correction in the neutron-flux monitoring with activation detectors. For example, the effect of transmutation of ^{198}Au into ^{199}Au is not negligible in the flux measurement by means of activation of gold foil via ^{197}Au(n,γ) ^{198}Au reaction. The latter comes into question as an impurity in the radioisotope (RI) product by the (n,γ) reaction, like ^{199}Au in the ^{198}Au product. Furthermore, one faces σ_2 in two-step reactions other than the double neutron capture, as in the case of the formation of ^{28}Mg from ^{27}Al.

(2) Here, we like to point out a positive significance of the double-neutron-capture reaction, instead of the above-mentioned subsidiary roles. Namely, the double-neutron-capture reaction itself can be a means of the production of a useful RI, in the case where the half-life of ${}^{A+1}_{Z}N$ is considerably short as compared with ${}^{A+2}_{Z}N$. Generally speaking, the product nuclide ${}^{A+2}_{Z}N$ is already known via charged-particle-induced reaction of fission. However, this does not necessarily mean the required amount of the activity is acquired by such reactions. Production by means of double neutron capture can occasionally be promising[14] in cases where both σ_1 and σ_2 are large enough.

So far we have counted the aspects of the application of the double-neutron-capture reaction. Let us consider then its physical meaning. The reaction mechanism of capture of low-energy neutrons is known[3] to consist of the compound and direct processes.

In the compound process, the nearest resonance level to the thermal energy (about 0.025 eV) contributes the most to the capture cross section among several existing levels. The portion of the direct process except for resonace reaction can be estimated[4,5] with certain reliability. On the contrary, there is no way of predicting the energy and the level width of the nearest level which are indispensable to know the absolute magnitude of the cross section. If we, however, look at relative values instead of the absolute magnitude of the cross section, it becomes possible to interpret the data

as stated below.

In the compound processes, formation cross-section ratio between the metastable and the ground state nuclei, the isomer ratio, possesses particular significance among nuclearchemical works. As it is shown by Huizenga and Vandenbosch[6], the isomer ratio highly depends on the properties of not only the target and the final isomers but also of the compound nucleus, and supplies information on the spin cutoff parameter for the level density of the compound nucleus. They first applied the theory to the thermal-neutron-capture reactions and obtained satisfactory agreement with observed data, though they introduced several approximations for simplicity. Now, more realistic way is available[7] for the calculation of the isomer ratio free from the approximations set by Huizenga *et al.*

(3) If we look at the double-neutron-capture reaction in which the final nuclide $^{A+2}_{Z}N$ has an isomeric state, we can measure the isomeric yield ratio and consequently extract the information on the level density.

(4) Conversely, there is a case in which the first product $^{A+1}_{Z}N$ has an isomeric state. In such a case, we are interested in comparing the capture-cross-section values between the excited and the ground-state nuclei. At present, such cross-section data are known only for the four cases: ^{58}Co [48], ^{60}Co [12, 13], ^{104}Rh [1], and ^{148}Pm [49]. They all give one order of magnitude greater value for the excited state than for the ground state. In comparison of capture cross sections between the isomers, the position of the nearest resonance level of each isomer becomes important with respect to the thermal neutron energy. Since this kind of information is not available, one should add more data sufficient for the statistical treatment of the problem.

Studies of the double-neutron-capture process has been reported since an early time as 1949 [8-47] (measured nuclide is given in the bracket following the reference number in the bibliogrphy). Most of the works were concentrated in the fifties, in which activity determination was carried out by measuring β rays with GM counter. Appearance of the NaI(Tl) scintillation detector and multi-channel pulse-height analyzer brought about remarkable improvement of the technique of γ-ray measurement, and consequently the NaI(Tl) detector became the main probe in the successive experiments during the sixties, though the energy resolution was far from satisfaction.

Now, solid-state detectors with high resolution and sufficient detection efficiency are available as a probe for γ rays, whose energy resolution is an order of 2 keV at 1.33 MeV whereas that of the NaI(Tl) detector is ordinarily 70 keV. By means of the solid-state detector, we are now in a position of as well repeating experiments with better precision for nuclides measured once as exploiting the subject among nuclides never investigated. Thus, we picked up four target nuclides, ^{26}Mg, ^{64}Ni, ^{93}Nb, and ^{164}Dy, for studying the double-neutron-capture process from the above-mentioned four points of view; namely, (1) finding σ_2 for the correction of the estimated activity yield, (2) obtaining σ_2 as a useful data for radioisotope production, (3) measuring the isomer yield ratio, and (4) observing the capture cross section of unstable nuclei.

^{27}Mg, described in chapter 3, was chosen mainly from the first point of view. In an attempt of detecting dineutrons by Otozai *et al.*[50], the object nuclide ^{28}Mg can also be produced via a side reaction, ^{27}Al(n, p)^{27}Mg(n, γ)^{28}Mg, and, therefore, the cross section value is required to know for ^{27}Mg(n, γ)^{28}Mg reaction.

In the case of ^{64}Ni in chapter 4, the second product ^{66}Ni possesses a half-life of 55 hr while ^{65}Ni decays with half-life of 2.5 hr, and it can be a useful isotope as a tracer: the case (2). The published data on this nuclide[14,15] are considerably apart from each other.

The cross section for thermal neutron capture was determined with ^{94}Nb mainly from the reason (3) in chapter 5. ^{94}Nb is an odd-odd nuclide, whose spin is 6. It was interesting to see if theories could reproduce the observed isomer ratio of an odd-odd nucleus with such a high spin value, which has never been measured.

In chapter 6, the cross sections of ^{165m}Dy and ^{165g}Dy shall be discussed from the viewpoint of (4). ^{164}Dy is a good activation detector for thermal neutron flux because its neutron-capture cross section follows well the $1/v$ law[2]. The cross section data of ^{165m}Dy and ^{165g}Dy are to be used for the burn-out correction in the flux monitoring with ^{164}Dy.

In the experiment with nickel target, the (n, 2n) reaction cross section of ^{58}Ni was measured for fast neutrons besides detection of ^{66}Ni produced via double neutron capture. There have been published systematic works on (n, 2n) reactions[59, 72], the predicted value of which, however, greatly deviates from observed data for ^{58}Ni. Therefore, we attempted re-determining the cross section experimentally on one hand, and deriving an empirical formula which reproduces (n, 2n) reaction cross sections better on the other hand.

2. Measurement of the Neutron Flux

2.1. Activation detectors for flux monitoring

Cobalt-aluminum alloy was used as the thermal-neutron-flux monitor in the long-term irradiation, while gold foil was activated in the case of short-term irradiation. The former, obtained from Reactor Experiments Co., was a wire of 0.7 mm in dia. and contained 0.475% of cobalt. The thickness of the gold foil was 0.02 mm (39 mg/cm^2). Cadmium tubes used in the measurement of cadmium ratio were 1 mm in inner dia. and 0.5 mm thick (supplied by Reactor Experiments Co.), in which the monitors were sealed. Monitors sealed in the cadmium tube were irradiated in a separate capsule if the capsule was not big enough since existence of a gross amount of cadmium caused attenuation of the neutron flux. Data of the reactor characteristic tests[51] were used in the case where the cadmium ratio was not measurable.

Nickel foil of 0.2 mm thick or wire of 0.25 mm in dia. made by Johnson Matthey Co. was used for monitoring the fast neutron flux.

2.2. Determination of the activity

Activities induced in the flux monitors were determined by measuring γ rays with coaxial-type Ge(Li) detectors or a 3″ϕ×3″ NaI(Tl) scintillator. The full width at half-maximum of the full energy peak of the used ORTEC Ge(Li) detectors ranged from 2.1 to 2.6 keV for the 1.332-MeV ^{60}Co γ ray, while the peak detection efficiency lay between 8 and 20% with respect to that of the 3″ϕ×3″ NaI (Tl) detector. Output pulses, amplified and shaped with an amplifier such as JAERI model 156 or CANBERRA model 1413, were fed to a 1024-channel pulse height analyzer of Nuclear Data 2200 series. Spectrum data in the pulse height analyzer were output in the form of paper tape or stored in a cassette tape, which were input into an electronic computer. Ge(Li) γ-ray spectra were analyzed by BOB73 code[52], and NaI(Tl) γ-ray spectra were treated with NAISAP code[52,53].

Pulse pile-up effect was carefully eliminated by adjusting the source distance from the detector surface so that the total count rate might be kept below 2000 cps[54]. The peak detection efficiency at each source position was determined with the calibrated sources from IAEA, RCC, LMRI, etc. In **Fig. 2.1.** is given an example of the resulting efficiency curves.

The activity A is given by the following equation:

$$A=\frac{N}{t\cdot\varepsilon_p\cdot b\cdot G_\gamma},$$

where N is the peak area, t gives the counting duration, ε_p denotes the counting efficiency for the full energy peak, b is the emission rate of the relevant γ ray per disintegration, and G_γ represents a correction factor for the self-absorption of the source against the γ ray. The values of b and G_γ are listed together with the half-lives in **Table 2.1.** Here, G_γ was evaluated by means of the equation, $G_\gamma = e^{-\mu\bar{x}}$, with the calculated total absorption cross section of elements for γ rays[55], where μ is the linear absorption coefficient and $\bar{x}$ is the mean traveling distance of γ rays in the source. The former was evaluated from the total absorption cross section against γ rays calculated by Storm *et al.* for various elements[55]. $\bar{x}$ was taken to be a half thickness for foil sources, while it was equated to $\pi R/2$ in the case of wire of radius R.

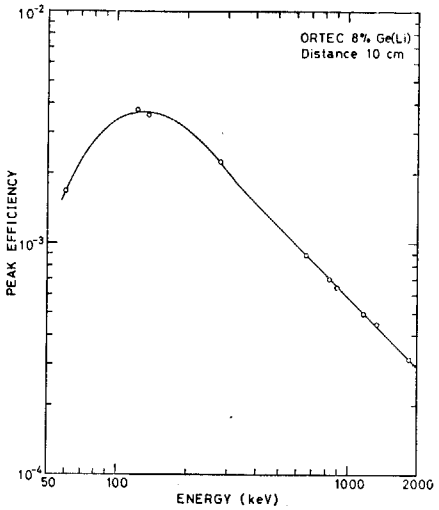

Fig. 2. 1 An example of a peak-efficiency curve of a coaxial Ge(Li) detector.

Table 2. 1 Nuclear data[57] and self-shielding factor, G_r, for the γ ray used for the determination of radioactivities induced in activation detectors with neutrons.

Nuclide	Half-life	γ-ray energy (keV)	γ intensity (per decay)	Gr
^{58}Co	71. 3 d	810	0. 99	0. 994
^{60}Co	5. 263 y	1173	1. 00	0. 992
		1332	1. 00	0. 992
^{198}Au	2. 697 d	412	0. 95	0. 992

2. 3. Calculation of the neutron flux

When the effective cross section $\hat{\sigma}$ for reactor neutrons is expressed by the Westcott convention[56], the "neutron flux" nv_0*) is given by the following equation:

$$nv_0 = \frac{A}{N_0 \hat{\sigma} f_g f_c} , \tag{2. 2}$$

where N_0 is the number of the target nuclei, and

$$\hat{\sigma} = \sigma_0 (g \cdot G_{th} + r \cdot \sqrt{T/T_0} \cdot s_0 G_{epi}) \tag{2. 3}$$

$$f_g = \sum_i (1 - e^{-\lambda t_i}) \cdot e^{-\lambda r_i} \tag{2. 4}$$

$$f_c = e^{-\lambda t_c} . \tag{2. 5}$$

Equation (2. 3) shall be explained in detail in **Appendix 1**. Here, σ_0 is the reaction cross section with 2200 m·sec^{-1} neutrons, and g is a measure of the deviation of the cross section from the $1/v$ law in thermal energy region. Furthermore, $r \cdot \sqrt{T/T_0}$ is a quantity giving the fraction of epithermal neutrons in the neutron spectrum, and s_0 is defined by $s_0 = (2/\sqrt{\pi}) \cdot (I_0'/\sigma_0)$ with I_0', the resonance integral minus its $1/v$-component. The two quantities, G_{th} and G_{epi}, are the self-shielding

*) nv_0 is not equal to the neutron flux in the strict sense, but is called so conventionally.

factors against thermal and epithermal neutrons, respectively. λ in Eq. (2. 4) denotes the decay constant, and the suffix i implies the ith partial irradiation in an intermittent neutron irradiation; t_i gives the length of the partial irradiation and τ_i corresponds to the elapsed time from the end of the partial irradiation to the end of the entire irradiation. Equation (2. 5) gives the decay factor by the time of the start of measurement after irradiation. Parameters appearing in Eq. (2. 3) are listed in **Table 2. 2.**

Table 2. 2 Data used for the determination of nv_0 and $r\sqrt{T/T_0}$ from radioactivities in activation detectors[58].

Target nuclide	σ_0 (b)	I_0 (b)	g	G_{th}	G_{epi}	K
^{59}Co	37. 2	60. 2	1. 00	1. 00	1. 00	2. 07
^{197}Au	98. 8	1491	1. 01	0. 969	0. 394	2. 07

Fission neutron flux ϕ_f was determined with ^{58}Ni(n, p)^{58}Co reaction. The analysis of the results was relatively troublesome because of existence of a metastable state in the product nuclide which decays into the ground state via isomeric transition with half-life of 9. 2 hr[57] and the non-negligible burn-out effect of both states due to large (n, γ) cross sections. The situation became worse in the case of intermittent irradiation. In **Appendix 2** are given details of the calculation for such a case. **Table 2. 3** summarizes cross-section data necessary for the calculation.

Table 2. 3 Reaction cross sections used for the determination of fission neutron flux.

Reaction	Cross section (b)	Reference
^{58}Ni (n, p) ^{58m}Co	0. 0354	59
^{58}Ni (n, p) ^{58g}Co	0. 078	59
^{58m}Co (n, γ) ^{59}Co	136000*	1
^{58g}Co (n, γ) ^{59}Co	1880*	1

* Thermal cross section. The contribution of epithermal neutrons was neglected.

3. Thermal-Neutron-Capture Cross Section of ^{27}Mg

In irradiation of ^{26}Mg with neutrons, one can expect the following successive reactions:

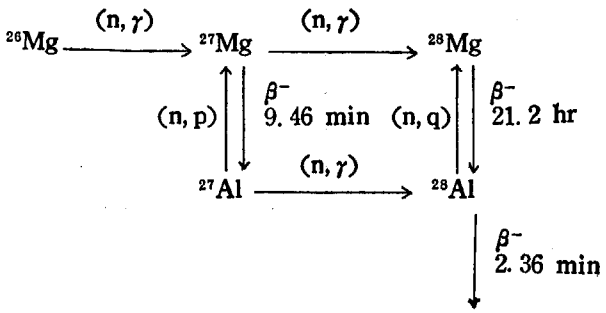

Here, the cross section of the $^{27}Mg(n, \gamma)^{28}Mg$ reaction was studied by Roy and Yaffe[59]. They attempted to detect the ^{28}Mg activity by measuring β rays with GM counter. They reported the cross-section value was less than 0.04 b because they failed in identifying the formation of ^{28}Mg.

One should be careful for contamination of the least amount of lithium impurity in the magnesium target. Tritons produced via $^{6}Li(n, \alpha)^{3}H$ reaction with thermal neutrons would provoke the $^{26}Mg(t, p)^{28}Mg$ reaction[60]. Contamination of lithium as little as 0.1 ppm, though it is undetectable by the spectrophotometrical means, will interfere the result.

The interference by lithium can, however, be corrected experimentally by looking at the neutron-flux dependence of the ^{28}Mg yield. The yield of ^{28}Mg by double-neutron-capture process is proportional to the second power of the neutron flux whereas that via (t, p) reaction is proportional to the first power of the flux. In the present work, we used the purest of commercially available reagents of magnesium oxide and also the above-mentioned technique in order ot exclude the interference of lithium.

Formation of ^{28}Mg is also probable via $^{27}Al(n, \gamma)^{28}Al(n, p)^{28}Mg$ or $^{27}Al(n, p)^{27}Mg(n, \gamma)^{28}Mg$ reaction. In this case, one only knows the upper limit of the $^{27}Mg(n, \gamma)^{28}Mg$ reaction cross section as described in 3.1.2. Here, we like to note that Vandenbosch *et al.* have attempted in vain to detect ^{28}Mg as the product from either dineutron or tetra-neutron reaction in the neutron irradiation of aluminum[61].

The (n, γ) reaction cross section is possibly treated by the current direct reaction theory[70], especially in the case of the mass number below 40. We tried the analysis of the cross section by means of the theory as explained in subsection 3.2.

3.1. Double-neutron-capture process of ^{26}Mg

3.1.1. Neutron irradiation

One to three grams of spectroscopically pure magnesium oxide supplied by Johnson Matthey Co., sealed in a quartz ampoule, was irradiated together with flux monitors in the JRR-2, JRR-3, or JRR-4 reactor for 12 to 290 hr. In **Table 3.1**, are shown the experimental conditions such as those of irradiation. Here, the length of irradiation implies the net irradiation time excluding the reactor shutoff period.

Table 3.1 Details of the experimental condition for irradiation of magnesium oxide.

Run No.	Reactor	Irradiation hole	Irradiation period(hr)*	Weight of target(g)	Chemical yield(%)
1	JRR-2**	HR	65.0	2.26	44
2	JRR-2	HR	65.0	2.83	48
3	JRR-2	VT-1	260	1.01	61
4	JRR-2	VT-1	289	0.79	72
5	JRR-3§	Pn	42.1	0.97	60
6	JRR-4§§	T	13.5	2.38	77
7	JRR-4	T	13.5	1.90	77
8	JRR-4	S	12.0	2.69	69

* This value gives the duration for net irradiation excluding the intermittent period during which the reactor was turned off. Therefore, the effective duration for the growth and decay of ^{28}Mg becomes rather smaller than the listed value.

** A CP-5-type reactor.

§ A heavy-water-moderated natural-uranium-fuelled-type reactor.

§§ A swimming-pool-type reactor.

3.1.2. Chemistry

Irradiated samples were unsealed one to three days after irradiation (or immediately in the case of Run 8). Purification of magnesium was carried out in order to eliminate a large amount of ^{24}Na induced via ^{24}Mg(n, p)^{24}Na reaction and other activities arising from impurities in the target.

The solution obtained by dissolving the powder sample with conc. HCl and distilled water was dried up under an infrared lamp. The residue dissolved with 15 ml of conc. HCl was mounted on an anion exchange column (Diaion SA♯100, 100—200 mesh, 20 mmϕ×180 mm) saturated with conc. HCl. Mg^{2+} ions were eluted in the first fraction with 45 ml of conc. HCl. The eluate was dried up, 10 ml of distilled water was added, and the resulting solution was mounted on a cation exchange column (H-type Diaion SK♯1, 100—200 mesh, 30 mmϕ×250 mm).

Mg^{2+} ions were eluted with 1.5 ℓ of 1N HCl following two preceding fractions, 200 ml of distilled water and 1.3 ℓ of 0.5N HCl; the ^{24}Na activity was removed with the latter fraction. The eluting speed was 300 ml/hr. Magnesium was precipitated in the form of $MgNH_4PO_4$ with 200 ml of the 10% solution of $(NH_4)_2HPO_4$ and conc. NH_4OH. The precipitate was filtered, and dissolved with conc. HCl. The solution was transferred to a volumetric cylinder, diluted to 40 ml with distilled water, and subjected to the γ spectrometry. The chemical yield of magnesium was determined by the gravimetric analysis with magnesium pyrophoshate.

3.1.3. Activity measurement

The γ-ray spectrum of the ^{28}Mg solution was taken with Ge(Li) detectors described in chapter 2. The source and the detector were shielded in a lead shield of 5—10 cm thick. The length of each counting time ranged from 40 to 80 ksec. An example of the obtained γ-ray spectrum is shown in **Fig. 3.1**. Observed were the γ rays of 401, 942, and 1342 keV arising from the decay of ^{28}Mg and the 1779-keV γ ray[62] due to the decay of the daughter nuclide ^{28}Al (half-life 2.36 min). **Figure 3.2** gives the decay curve of the 1779-keV γ ray. The obtained half-life value of 21 hr agreed well with the reported one of 21.2 hr[57]. Thus, formation of ^{28}Mg was concluded to have been confirmed.

The yield of ^{28}Mg was determined with the peak area of the 1779-keV γ ray, the emission rate of which is 1.00 per disintegration[62]. Hydrochloric acid solution containing a known amount of ^{60}Co was used in order to obtain the counting efficiency of the full energy peak for the above-mentioned

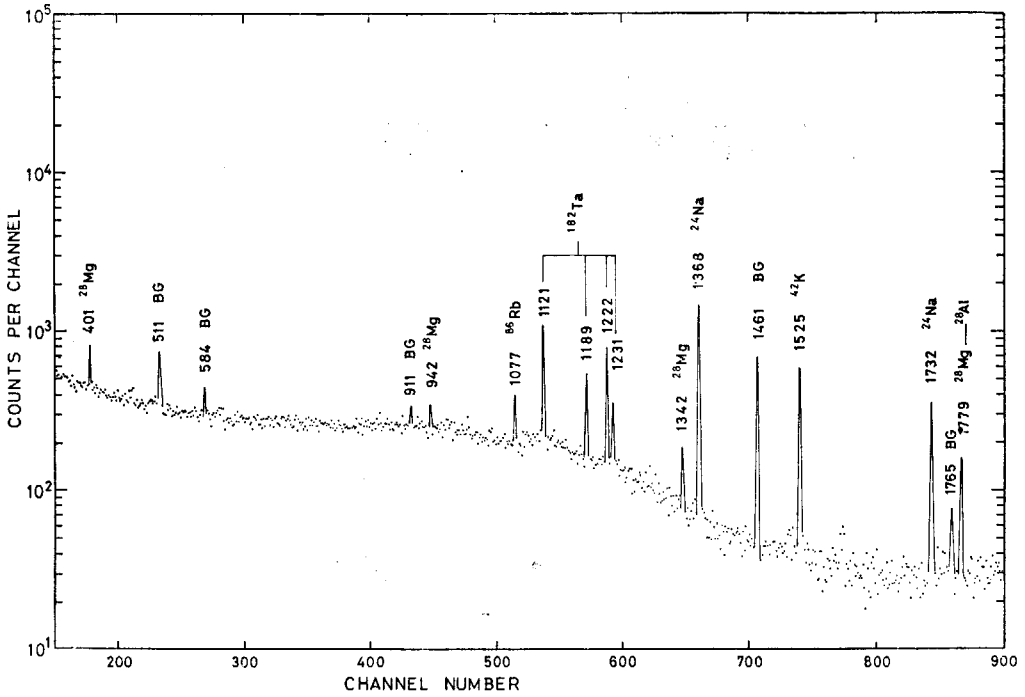

Fig. 3. 1 A Ge(Li) γ-ray spectrum of the magnesium source irradiated for 65 hr (Run 2), measured after the 43 hr cooling. The counting period is 40 ksec. The symbol BG implies that the relevant peak is due to the natural backgound. The 401-, 942-, 1342-, and 1779-keV γ rays are assigned to ^{28}Mg.

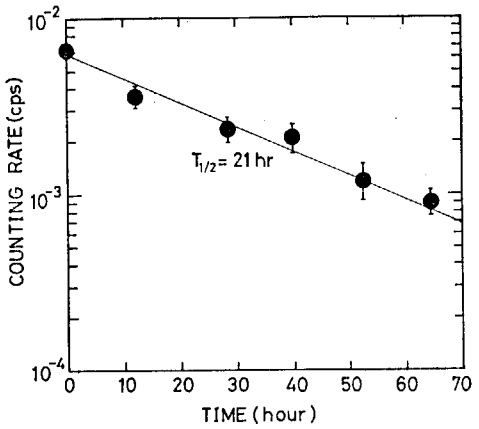

Fig. 3. 2 The decay curve of the 1779-keV γ ray, measured afrer the 43 hr cooling (Run 2).

source geometry. First, the counting efficiencies for 1173- and 1332-keV γ rays were found using the above soution of the same volume in an identical vessel as the sample. Here, the correction for the sum coincidences of the two γ rays was estimated to be less than 4% [63]. Then, the efficiency at 1779 keV was obtained by extrapolating the values at 1173 and 1332 keV to 1779 keV with regard to the energy dependence of the efficiency curve for point sources (cf. **Fig. 2. 1**).

Here, we like to mention that the erros attached to the numerical data throughout the present work represent the uncertainty of confidence level of 67%, i. e., the standard deviation. The confidence level of 99% is, therefore, acquired with three times the quoted error.

3.2. $^{27}Al(n, p)(n, \gamma)^{28}Mg$ reaction

3.2.1. Neutron irradiation

3.20 grams of aluminum grains were used for the target. The purity of the target grains which were supplied by Yokozawa Chemicals Co. was more than 99.99%. The target was wrapped with an aluminum foil, and irradiated together with flux monitors in the pneumatic tube of JRR-2 reactor for 41.6 hr.

3.2.2. Chemistry

The capsule was opened immediately after irradiation. An intense ^{24}Na activity induced via $^{27}Al(n, \alpha)^{24}Na$ reaction and other activities arising from impurities in the target material were removed by the following chemical procedure to prepare the ^{28}Mg source for activity measurement[50].

20 mg of Mg^{2+} ions (20 ml of 6.2% $Mg(NO_3)_2$) and 5 ml of 10% $FeCl_3$ were added to the beaker containing the sample grains. The grains were then dissolved with conc. HCl in contact with a platinum plate under heating for accelerating the dissolving rate. Magnesium hydroxide and ferric hydroxide were precipitated by adding an excess amont of conc. NaOH to the obtained solution, while aluminum ions were retained in the solution. The supernatant was discarded after centrifugation for 5 min. The precipitate was dissolved in a small amount of conc. HCl and re-precipitated with 10N NaOH. The previous procedure of centrifugation, decantation of the supernatant, and dissolution with conc. HCl was repeated, and the resulting solution was dried up under an infrared lamp.

The residue was dissolved in a small volume of conc. HCl, and was mounted on an anion exchange column (Diaion SA#100, 100—200 mesh, 15 mmϕ×150 mm) saturated with conc. HCl, ^{24}Na was eluted with 200 ml of 0.5N HCl following elution of 30 ml water, and then magnesium ions were eluted with 250 ml of 1N HCl.

The purified magnesium was precipitated in the form of magnesium oxinate[64], collected on a filter paper of 2.6 cm in dia. by sorption filtration, dried for 3 min at 110°C, and taped on Mylar film.

After the activity measurement was over, the source was stripped from the Mylar membrane, dried at 150—160°C for 30 min, and weighed after 30 min cooling in a desiccator. The chemical yield was determined by comparing the obtained weight with that of magnesium oxinate precipitated from the original solution of magnesium carrier. The yield was found 56%. This value was confirmed by an alternative method of determination. Magnesium oxinate was dissolved with a little amount of 2N HCl and diluted to 100 ml with distilled water. 10 ml of distilled water was added to 10 ml of the solution taken in a beaker, and the pH value was adjusted to 4.0 by adding 1N NaOH dropwise. The quantity of magnesium was determined by EDTA titration after oxine had been removed from the solution by chloroform extraction.

3.2.3. Activity measurement

Measurement of ^{28}Mg activity was carried out with an ORTEC coaxial-type Ge(Li) detector (full width at half-maximum being 2.1 keV and relative efficiency being 15% at 1332 keV). The sample was placed at the closest approach to the detector surface, and shielded in a lead shield of 10 cm thick. The counting efficiency of the detector for a disk source was obtained with ^{65}Ni (hallf-life 2.56 hr[57]) of known intensity precipitated as nickel dimethylglyoxime in the same shape.

Two nickel foils of 0.2 mm thick, one being 10 mg and the other being 2 mg, were irradiated together for 2 min with neutron flux nv_0 of 5×10^{13} n·cm^{-2} sec^{-1}. The former was used as a point source as it was. The latter was dissolved with *aqua regia* after nickel sponge was added. Nickel

dimethylglyoxime was precipitated by the procedure described in section 4.1, and was mounted in a disk of the same diameter as that of the oxinate source.

The activity of ^{65}Ni was determined by the use of the peak area of the 1482-keV γ ray measured with the above point source at 9 cm apart from the detector surface, while that contained in the nickel dimethylglyoxime precipitate was deduced with consideration of the weight ratio between the nickel targets, the chemical yield, and the ^{65}Ni activity in the point source. The nickel dimethylgly oxime source was then measured with the same geometry as that of the magnesium oxinate source to obtain the counting efficiency for the 1482-keV γ ray. Here, one needs not worry about the counting loss due to sum coincidences because there is no cascade γ rays accompanied with the 1482-keV γ ray. Furthermore, required nuclear data are the half-life values only since γ branching ratio is cancelled in the procedure. The counting efficiency for the relevant 1779-keV γ ray was in turn determined as described before.

3.3. Results and Discussion

3.3.1. Double-neutron-capture cross section of ^{26}Mg

For the yield of ^{28}Mg by double-neutron-capture process of ^{26}Mg, one obtains the following equation system:

$$\left.\begin{aligned}\frac{dN_2}{dt} &= N_1 n v_0 \hat{\sigma}_{12} - \lambda_2 N_2 \\ \frac{dN_3}{dt} &= N_2 n v_0 \hat{\sigma}_{23} - \lambda_3 N_3\end{aligned}\right\}, \tag{3.1}$$

where N_1, N_2, and N_3 are respectively the numbers of atoms of ^{26}Mg, ^{27}Mg, and ^{28}Mg, and $\hat{\sigma}_{12}$ and $\hat{\sigma}_{23}$ represent effective neutron-capture cross sections of ^{26}Mg and ^{27}Mg, respectively. Furthermore, λ_2 and λ_3 are the decay constants of ^{27}Mg and ^{28}Mg. Here, we neglected the burn-out effect for ^{26}Mg, ^{27}Mg, or ^{28}Mg during irradiation.

The solution of Eqs. (3.1) is expressed as

$$\lambda_3 N_3 = \frac{N_1 \cdot \hat{\sigma}_{12} \cdot \hat{\sigma}_{23} (n v_0)^2}{\lambda_2 (\lambda_2 - \lambda_3)} [\lambda_2 (1 - e^{-\lambda_3 t}) - \lambda_3 (1 - e^{-\lambda_2 t})]. \tag{3.2}$$

Equation (3.2) is reduced to

$$\lambda_3 N_3 = \frac{N_1 \hat{\sigma}_{12} \hat{\sigma}_{23} (n v_0)^2}{\lambda_2} (1 - e^{-\lambda_3 t}) \tag{3.3}$$

in the case of $\lambda_2 \gg \lambda_3$ and $\lambda_2 t \gg 1$, which is actually satisfied in the present system.

The results of the experiment described in 3.1.1 are summarized in **Table 3.2**. One my notice from Eq. (3.3) that the quantity $\lambda_3 N_3 / [N_1 (1 - e^{-\lambda_3 t})]$, appeared in **Table 3.2**, is nearly proportional to the second power of $n v_0$. We do observe in **Fig. 3.3** that the above quantity lies on a linear line of gradient 2 when it is plotted versus $n v_0$ on the log-log scale, except for the region of small $n v_0$ values. Deviation for small $n v_0$ values is considered due to a small quantity of lithium impurity.

Since the contribution of lithium impurity is proportional to the amount of target, N_1, the flux, $n v_0$, and the saturation factor, $(1 - e^{-\lambda_3 t})$, Eq. (3.3) is modified by taking it into account as

$$\frac{\lambda_3 N_3}{N_1 n v_0 (1 - e^{-\lambda_3 t})} = k + \frac{\hat{\sigma}_{12} \hat{\sigma}_{23}}{\lambda_2} n v_0 , \tag{3.4}$$

where k is the proportionality constant. Now, we must consider the neutron-spectrum dependence of

Table 3.2 nv_0, $r\sqrt{T/T_0}$, and yields of ^{28}Mg in the irradiation of magnesium oxide.

Run	nv_0 (10^{13}n·cm^{-2}sec^{-1})	$r\sqrt{T/T_0}$	$\lambda_3 N_3/[N_1(1-e^{-\lambda_3 t})]$ (10^{-21} sec)
1	3.8±0.1	0.023	7.1±1.2
2	5.0±0.2	0.023	8.4±1.4
3	15.2±0.3	0.075	91±23
4	11.9±0.2	0.075	47±9
5	2.17±0.04	0.017	2.1±0.5
6	1.47±0.07	0.030	4.1±1.0
7	1.76±0.09	0.030	5.2±1.2
8	1.82±0.09	0.030	2.5±0.5

the quantity in the right-hand side of Eq. (3.4). The constant k does not depend on the epithermal index, $r\sqrt{T/T_0}$, for the cross section of ^{6}Li(n, α)^{3}H reaction follows the $1/v$ law very well[65] and, therefore, it is determined only by the lithium content. The contribution of the epithermal index term to $\hat{\sigma}_{12}$ is concluded to be less than 2% considering $s_0=0.24$ [66]. Hence, $\hat{\sigma}_{12}$ can be regarded as constant within the present accuracy. Finally, $\hat{\sigma}_{23}$ is deduced to be less than 0.11 b from **Fig. 3.3.** There is unlikely a resonance level lying in the vicinity of thermal energy in the process giving such a small cross section. This leads to the conclusion that $\hat{\sigma}_{23}$ least depends on the epithermal index. Now, we can say the right-hand side of Eq. (3.4) does not depend on the epithermal index, and consequently obtain a linear relationship between the left-hand side of Eq. (3.4) and nv_0 as shown in **Fig. 3.4.**

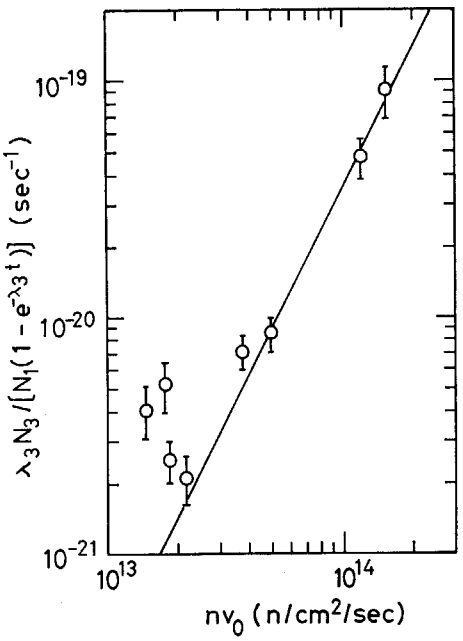

Fig. 3.3 The relation between the neutron flux nv_0 and the yield of ^{28}Mg. The symbols are explained in the text.

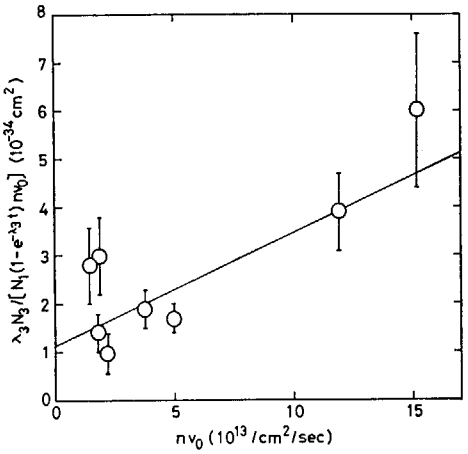

Fig. 3.4 Partition of the yield of ^{28}Mg into two components; the double neutron capture of ^{26}Mg and the ^{26}Mg (t, p)^{28}Mg reaction induced by lithium impurity. The quantity plotted on the ordinate in **Fig. 3.3** is divided by nv_0 and is plotted in this figure.

The main source of the error attached to each datum in **Fig. 3.4** was from the statistical uncertainty due to the weakness of the detected ^{28}Mg activity, amounting 13—23% (cf. **Table 3.2**). The

other sources considered were the error in the calibration of counting efficiency by ±3%, the uncertainty of nv_0 (cf. **Table 3.2**), and the error due to the non-uniformity of nv_0 which was estimated to be ±2—4% depending on the target size. The error given in **Fig. 3.4** was calculated with those errors by the law of the propagation of errors[106]. Despite the fairly large errors, one may recognize that the relationship expressed by Eq. (3.4) exists. The intersect at zero and the slope of the line in **Fig. 3.4** respectively give

$$k \approx 1 \times 10^{-34}\text{cm}^2 \tag{3.5}$$

and

$$\frac{\hat{\sigma}_{12}\hat{\sigma}_{23}}{\lambda_2} = (0.22 \pm 0.06) \times 10^{-47}\text{cm}^4\text{sec.} \tag{3.6}$$

Equation (3.5) indicates, with regard to the ^{28}Mg yield for magnesium-lithium alloy by Mellisch and Crookford[60], that 0.1 ppm of lithium was contained in the presently used magnesium oxide.

For $\hat{\sigma}_{12}$, several values are reported; that is, 0.048±0.010 b by Seren *et al.*[67], 0.025±0.002 b by Lyon *et al.*[68], and 0.034±0.010 b by Spiling *et al.*[69] Ryves gives $\sigma_{12}^0 = 0.0382 \pm 0.008$ b[66] as the cross section for 2200 m·sec^{-1} neutrons, which is considered approximately equal to $\hat{\sigma}_{12}$ as discussed before. One obtains

$$\hat{\sigma}_{23} = 0.07 \pm 0.02 \text{ b} \tag{3.7}$$

by using Ryves' value as $\hat{\sigma}_{12}$ which is probably the most reliable and 9.46 min[57] for the half-life of ^{27}Mg.

Equation (3.7) gives a higher value than the upper limit 0.04 b by Roy and Yaffe[8]. We are at present unable to compare them directly because the $\hat{\sigma}_{12}$ value used to evaluate $\hat{\sigma}_{23}$ and data essential for the neutron flux measurement are not described in the reference. However, the present result would not necessarily be inconsistent with the reference, if they used, for example, the $\hat{\sigma}_{12}$-value by Seren *et al.* which may have been available for the time.

3.3.2. Yield of ^{28}Mg in neutron irradiation of aluminum

The yield of ^{28}Mg via ^{27}Al(n, p)^{27}Mg(n, γ)^{28}Mg and ^{27}Al(n, γ)^{28}Al(n, p)^{28}Mg is given by

$$\lambda_3 N_3 = N_1 \left(\frac{\sigma_{12}\hat{\sigma}_{23}}{\lambda_2} + \frac{\hat{\sigma}_{12'}\sigma_{2'3}}{\lambda_{2'}}\right)\phi_f n v_0 (1 - e^{-\lambda_3 t}) , \tag{3.8}$$

where suffixes 2 and 3 denote ^{27}Mg and ^{28}Mg as before, while 1 and 2′ represent ^{27}Al and ^{28}Al, respectively. N gives the number of nuclei, λ is the decay constant, and ϕ_f represents the fission neutron flux. $\hat{\sigma}_{12'}$ and $\hat{\sigma}_{23}$ denote effective cross sections of the (n, γ) reaction of ^{27}Al and ^{27}Mg, respectively, while σ_{12} and $\sigma_{2'3}$ give (n, p) reaction cross sections of ^{27}Al and ^{28}Al with fission neutrons.

As a result, we obtained that $\phi_f = (1.48 \pm 0.10) \times 10^{12}$n·cm^{-2}·sec^{-1}, $nv_0 = (4.7 \pm 0.2) \times 10^{13}$n·cm^{-2}·sec^{-1} ($r\sqrt{T/T_0} = 0.017$), and $\lambda_3 N_3 = 0.94 \pm 0.09$ dps. The errors attached to ϕ_f and nv_0 were evaluated considering the non-uniformity of neutron flux which was found among the measurements with monitors placed at three positions around the sample, statistical fluctuation in the activity measurement by ±0.5%, and uncertainty of the counting efficiency by ±1.5%. The error in $\lambda_3 N_3$ was deduced by taking into account the statistical error in the activity measurement and uncertainty of the counting efficiency amounting to ±2%.

Substituting the above-obtained results, together with $N_1 = 7.14 \times 10^{22}$ (the error being ±1.5%) and $1 - e^{-\lambda_3 t} = 0.743$, into Eq. (3.8), one obtains

$$\frac{\sigma_{12}\hat{\sigma}_{23}}{\lambda_2} + \frac{\hat{\sigma}_{12'}\sigma_{2'3}}{\lambda_{2'}} = (2.6 \pm 0.3) \times 10^{-49}\text{cm}^4\text{sec.} \tag{3.9}$$

Neglecting the second term in the left-hand side of Eq. (3.9) and substituting $\sigma_{12}=3.5\pm0.2$ mb[59] into it, one finds $\hat{\sigma}_{23}\leqq0.09$ b. This does not contradict $\hat{\sigma}_{23}=0.07\pm0.02$ b deduced for the double-neutron-capture reaction. Conversely, one can conclude $\sigma_{2'3}\leqq2$ mb from Eq. (3.9) by using $\hat{\sigma}_{23}=0.07$ b together with $\hat{\sigma}_{12'}=0.231\pm0.003$ b[1] and $\lambda_2=5.00\times10^{-3}\text{sec}^{-1}$ [57].

The presently obtained result was applied to the experiment carried out by Schiffer and Vandenbosch[27]. It was then concluded that the yield of ^{28}Mg had been only one-tenth of the detection limit under their experimental condition.

3.3.3. Calculation of thermal-neutron-capture cross section of ^{27}Mg by means of a direct reaction model

According to Mughabghab[70], hard sphere capture or potential capture is the main process in the thermal-neutron-capture reaction of the nucleus with the mass less than 40. The cross section $\sigma_{\text{hard sph.}}$ for s-wave neutrons to be captured in the bound-state p-orbit via hard sphere capture is given[70] by

$$\sigma_{\text{hard sph.}}=\frac{0.062}{R\sqrt{\varepsilon'}}\left(\frac{Z}{A}\right)^2\theta_N{}^2\cdot y^2\left(\frac{y+3}{y+1}\right)^2 \text{ b}, \tag{3.10}$$

where

$\theta_N{}^2$ = non-dimensional reduced width of the final state,

y = $k_{Nl}R$,

k_{Nl} = wave number corresponding to the binding energy ε_{Nl} of the state Nl,

R = effective radius of the hard sphere (fm),

ε' = energy of the incoming neutron (eV),

Z = atomic number of the target nucleus,

A = mass number of the target nucleus.

Since the bound-state energy gradually changes with the mass number, the binding energies for $2p_{1/2}$ and $2p_{3/2}$ of ^{28}Mg were estimated to be 2.2 and 3.5 MeV, respectively, from the data given by Bird[71]. Substituting them and $R=1.45A^{1/3}$ fm[5] into Eq. (3.10), one obtains for $\varepsilon'=0.0253$ eV

$$\sigma_{\text{hard sph.}}=\begin{cases}0.12\theta_N{}^2 \text{ b} & \text{for } 2p_{1/2}\\ 0.16\theta_N{}^2 \text{ b} & \text{for } 2p_{3/2}.\end{cases} \tag{3.11}$$

Considering that $\theta_N{}^2\approx1$, one may conclude that the observed cross section 0.07 ± 0.02 b is explainable by the hard sphere capture process.

4. Thermal-Neutron-Capture Cross Section of ^{65}Ni and the ^{58}Ni(n, 2n)^{57}Ni Reaction Cross Section

Irradiation of nickel with reactor neutrons provokes the following reactions:

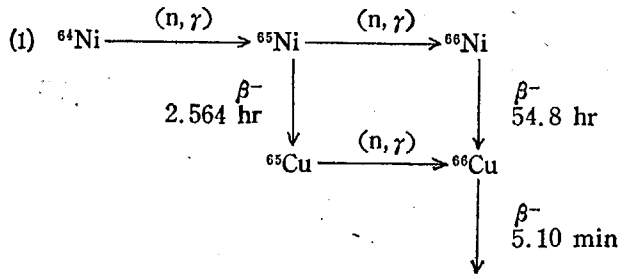

(2) ^{58}Ni(n, p)^{58}Co (71.3 d)

(3) ^{58}Ni(n, 2n)^{57}Ni (36.0 hr)

^{65}Ni produced with the highest yield decays out within a short period after the irradiation, and one observe ^{66}Ni induced by double neutron capture and ^{57}Ni via the third process if ^{58}Co has been separated.

There are two data available on the thermal-neutron-capture cross section of ^{65}Ni: 60—70 b by Pinajian[14] and 24.3±2.4 b by Serment[15]. They are significantly different from each other. It follows that, if they are to be both correct, the ^{65}Ni cross section is highly sensitive to the neutron spectrum and the utilized neutron spectra in the two experiments were largely different from each other.

In the present experiment, the change of the effective cross section of ^{65}Ni was studied with different neutron spectra, and at the same time the yield of ^{57}Ni was obtained to determine the ^{58}Ni (n, 2n)^{57}Ni reaction cross section.

Systematics of the mean cross section of the (n, 2n) reaction is studied by Roy and Hawton[72], and Calamand[59]. The systematics predicts a value six times larger than the empirical ^{58}Ni cross section. In the present work, we propose a new systematics reproducing empirical (n, 2n) reaction cross sections better.

4.1. Experimental

4.1.1. Neutron irradiation

Spectroscopically pure nickel wire of 0.25 mm in dia., supplied by Johnson Matthey Co., or nickel of 0.2 mm thick was used as the target by 4—7 mg in each case. It served at the same time as the flux monitor for fission neutrons. In **Table 4.1** are summarized the experimental conditions such as the length of irradiation time, etc.

Table 4.1 Details of the experimental condition for irradiation of nickel.

Run No.	Reactor	Irradiation hole	Irradiation period(hr)*	Weight of nickel(mg)	Chemical yield(%)
1	JRR-2	VT-1	260	6.14	91
2	JRR-2	VT-1	289	6.06	90
3	JRR-3	VR-2	254	7.45	97
4	JRR-4	S	19.5	4.21	75
5	JRR-4	S	12.0	5.29	91

* This value gives the duration for net irradiation excluding the intermittent period during which the reactor was turned off. Therefore, the effective duration for the growth and decay of ^{57}Ni and ^{66}Ni becomes rather smaller than the listed value.

4.1.2. Chemistry

Gamma-ray spectrum of ^{58}Co produced in the nickel sample was measured a few days after the irradiation. Then, the nickel sample was dissolved with 4 ml of *aqua regia*. The obtained solution was dried up twice by adding 2 ml of conc. HCl to expel nitric acid. The residue was dissolved with conc. HCl, and mounted on an anion exchange column (Diaion SA#100, 100—200 mesh, 10 mmϕ×230 mm), saturated with conc. HCl. Nickel ions were eluted with 25 ml of conc. HCl to be separated from ^{58}Co. The resulting nickel fraction was dried up, dissolved in water, and diluted to 200 ml with water. Nickel dimethylglyoxime was precipitated by adding 5 ml of 1% solution of dimethylglyoxime and 1:1 ammonia water to the above solution heated on a water bath. The precipitate was aged with heat for 20 min, and then collected on a filter paper by sorption filtration. The precipitate was washed sufficiently with 1:200 hot ammonia water and ethanol, heated for 3 min at 110°C, and weighed to determine the chemical yield. The obtained chemical yield are listed in **Table 4.1**. The γ-ray source was prepared by fixing the obtained precipitate on Mylar film with Scotch tape.

4.1.3. Activity measurement

Gamma-ray spectrum measurement of nickel dimethylglyoxime sample was carried out as in the case of magnesium oxinate sample described in 3.2.3. The source was placed as close as possible to the Ge(Li) detector surface, except for Run 3 in which a 3″ϕ×3″ NaI(Tl) detector was used instead of Ge(Li) detector. An example of the obtained Ge(Li) γ-ray spectra is shown in **Fig. 4.1**.

In the yield determination of ^{66}Ni, the value of 0.09 [57] was adopted as the emission rate of the 1039-keV γ ray per disintegration. The 1921-keV γ ray (emission rate 0.14 [57]) was used for the determination of the ^{57}Ni yield. Here, the 1379-keV γ ray was not used despite its large emission probability of 0.86 [57], because the counting loss more than 20% was expected due to the coincidences with annihilation radiation in the β^+ decay.

Half-lives of ^{66}Ni and ^{57}Ni were taken to be 54.8 hr and 36.0 hr[57], respectively.

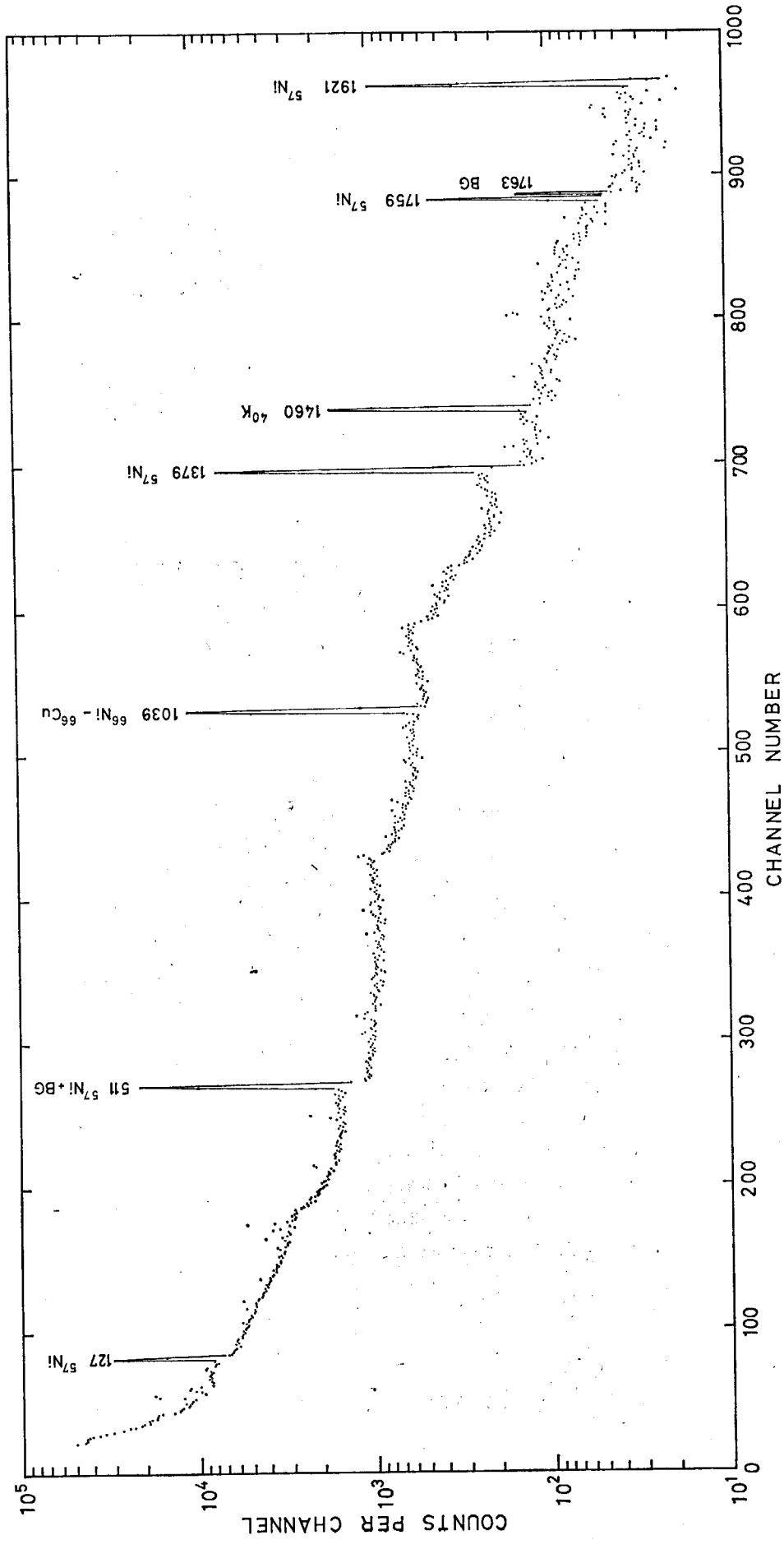

Fig. 4.1 A Ge(Li) γ-ray spectrum of the nickel dimethylglyoxime measured after the 173 hr cooling (Run 2). The counting period was 100 ksec.

4.2. Results and discussion

4.2.1. $^{65}Ni(n,\gamma)^{66}Ni$ reaction cross section

The yield of ^{66}Ni is given by Eq. (3.2). First, the effective cross section of the $^{64}Ni(n,\gamma)^{65}Ni$ reaction, $\hat{\sigma}_{12}$, is estimated as follows. From ref. 1, one knows that $\sigma_0 = 1.49\pm0.03$ b and the resonance integral $I_0 = 1.1\pm0.2$ b. According to the $1/v$ law for the neutron cross section, the $1/v$-component of the resonance integral is $0.45\sigma_0$ when the cutoff energy is taken to be 0.5 eV[1]. Hence, $I_0' = I_0 - 0.45\sigma_0 = 0.4\pm0.2$ b. It follows that $s_0 = 0.3\pm0.2$ and $\hat{\sigma}_{12} = 1.49(1+0.3r\sqrt{T/T_0})$ b. The second term in the parenthesis of $\hat{\sigma}_{12}$ is at most 2% and therefore negligible.

The cross section $\hat{\sigma}_{23}$ for the $^{65}Ni(n,\gamma)^{66}Ni$ reaction obtained by substituting the $\hat{\sigma}_{12}$ value into Eq. (3.2) is shown in **Table 4.2** and plotted versus the epithermal index, $r\sqrt{T/T_0}$, in **Fig. 4.2**. The attached errors were estimated by taking into account the errors involved in the detection efficency ($\pm1.5\%$), chemical yield ($\pm1.5\%$), and $(nv_0)^2$ ($\pm2.5\%$) (cf. **Table 4.2**) besides the statistical error.

Table 4.2 Effective cross section values of the $^{65}Ni(n,\gamma)^{66}Ni$ reaction.

Run No.	nv_0 (10^{18} n·cm^{-2} sec^{-1})	$r\sqrt{T/T_0}$	$\hat{\sigma}_{23}$ (b)
1	14.7±0.2	0.075	22.0±0.9
2	11.9±0.2	0.075	22.1±0.9
3	1.14±0.02	0.022	21.6±2.3
4	1.59±0.02	0.030	23±5
5	1.82±0.03	0.030	21±4

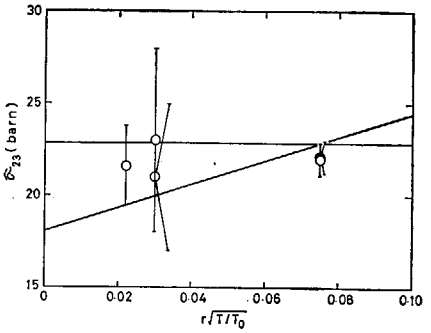

Fig. 4.2 The effective cross section for $^{65}Ni(n,\gamma)^{66}Ni$ reaction plotted vs. the epithermal index $r\sqrt{T/T_0}$. The solid lines indicate the upper and the lower limit for the intersect and the slope in the dependence of the cross section $\hat{\sigma}_{23}$ on $r\sqrt{T/T_0}$.

For $r\sqrt{T/T_0}=0.075$, $\hat{\sigma}_{23}$ could be determined with high precision as 22.0 ± 0.8 b. On the contrary, it is associated with large uncertainty in the case of low values of the epithermal index. This means that ons is unable to know the dependence of $\hat{\sigma}_{23}$ on the epithermal index accurately. Here, we set the upper limit for σ_{23}^0, the cross section for 2200 m·sec^{-1} neutrons, as shown by a horizontal line in **Fig. 4.2**; for there are quite scarce cases where the dependence of the effective cross section on the epithermal index shows a negative slope. On the other hand, the straight line representing the lower limit of σ_{23}^0 gives the upper limit for the resonance integral. Thus, one concludes

$$\sigma_{23}^0 = 20.4\pm2.4 \text{ b}$$
$$I_{23} < 60 \text{ b}.$$

The present $\hat{\sigma}_{23}$-value of 22.0 ± 0.8 b agrees well with 24.3 ± 2.4 b by Serment *et al.*[15] but deviates far from 60—70 b by Pinajian[14]. The same nuclear data are used in the three experiments in the determination of the ^{66}Ni yield; namely, the energy and emission rate of the used γ ray and the cross section $\hat{\sigma}_{12}$. Pinajian has used the thermal neutron flux of 2.45×10^{15}n·cm^{-2} sec^{-1}, which is ten times larger than our flux. However, no information on the used neutron spectra are given in the above two works. In any respect, it seems unlikely that the large discrepancy is due to difference in the neu-

tron spectrum used.

4. 2. 2. ^{58}Ni(n, 2n)^{57}Ni reaction cross section

In **Table 4. 3** are shown the results on the ^{58}Ni(n, 2n)^{57}Ni reaction cross section. Observed values agree well with each other except for Run 3. The threshold 12. 4 MeV of the reaction is much higher than the effective threshold of 4. 3 MeV[59] for the ^{58}Ni(n, p)^{58}Co reaction monitoring the fission neutron flux. There is a possibility that distortion of the neutron spectrum affects the deduced cross-section value. In JRR-3 reactor used in Run 3, thermalization of neutrons is attained in higher proportion, so that the low-energy portion in the fission neutron spectrum is expected to be reduced compared to the cases of other reactors. Similar phenomenon is reported by Hoste *al et.*[73-75] Conversely, the spectrum distortion above 4 MeV is considered small in the remaining runs as a result of the comparison of the (ϕ_f/nv_0)-value with that in refs. 73—75. Therefore, the ^{58}Ni(n, 2n)^{57}Ni reaction cross section was deduced by averaging the data of runs excluding Run 3.

Table 4. 3 Determination of the cross section of the ^{58}Ni(n, 2n)^{57}Ni reaction with fission neutrons.

Run No.	ϕ_f/nv_0	Cross section* (μb)
1	0. 16	3. 7
2	0. 12	3. 9
3	0. 016	7. 8
4	0. 17	4. 1
5	0. 29	3. 4
	mean value	3. 8±0. 5§

* These values contain statistical uncertainties of *ca.* ±10%.

§ The result of Run 3 was excluded in the calculation of the mean value.

The resulting value, 3. 8±0. 5 μb, agrees well with 3. 7 μb given by Schuman *et al.*[76] (re-evaluated by Calamand[59]), and lies within the range of the error of 5. 3±1. 4 μb by Braun *et al.*[77] (re-evaluated by the authors). Kobayashi *et al.*[78], however, report 5. 92±0. 28 μb, which has been deduced from the original literature by the use of 113 mb for the ^{58}Ni(n, p)^{58}Co reaction cross section. They have also measured the cross section of the ^{90}Zr(n, 2n)^{89}Zr reaction, which is eventually three times larger than either the previously observed value or the predicted value from the systematics (cf. the following section). These two (n, 2n) reactions possess threshold energies close to each other. The discrepancy must be investigated hereafter.

4. 3. Systematics of the (n, 2n) reaction cross sections with fission neutrons

Roy and Hawton[72] and Calamand[59] have compiled the (n, 2n) reaction cross sections $\bar{\sigma}_{n,2n}$ averaged over the fission neutron spectrum, and related them with the reaction threshold, $E_{th} = -Q(A+1)/A$. Here, Q is the Q-value of the reaction and A is the mass number of the target nucleus. They have found an empirical equation by plotting the quantity, $\bar{\sigma}_{n,2n} \cdot 25/A^{2/3}$, versus E_{th}, as shown in **Fig. 4. 3.** The empirical equation predicts the $^{58}Ni(n, 2n)^{57}Ni$ reaction cross section so high as 26^{+18}_{-10} μb.

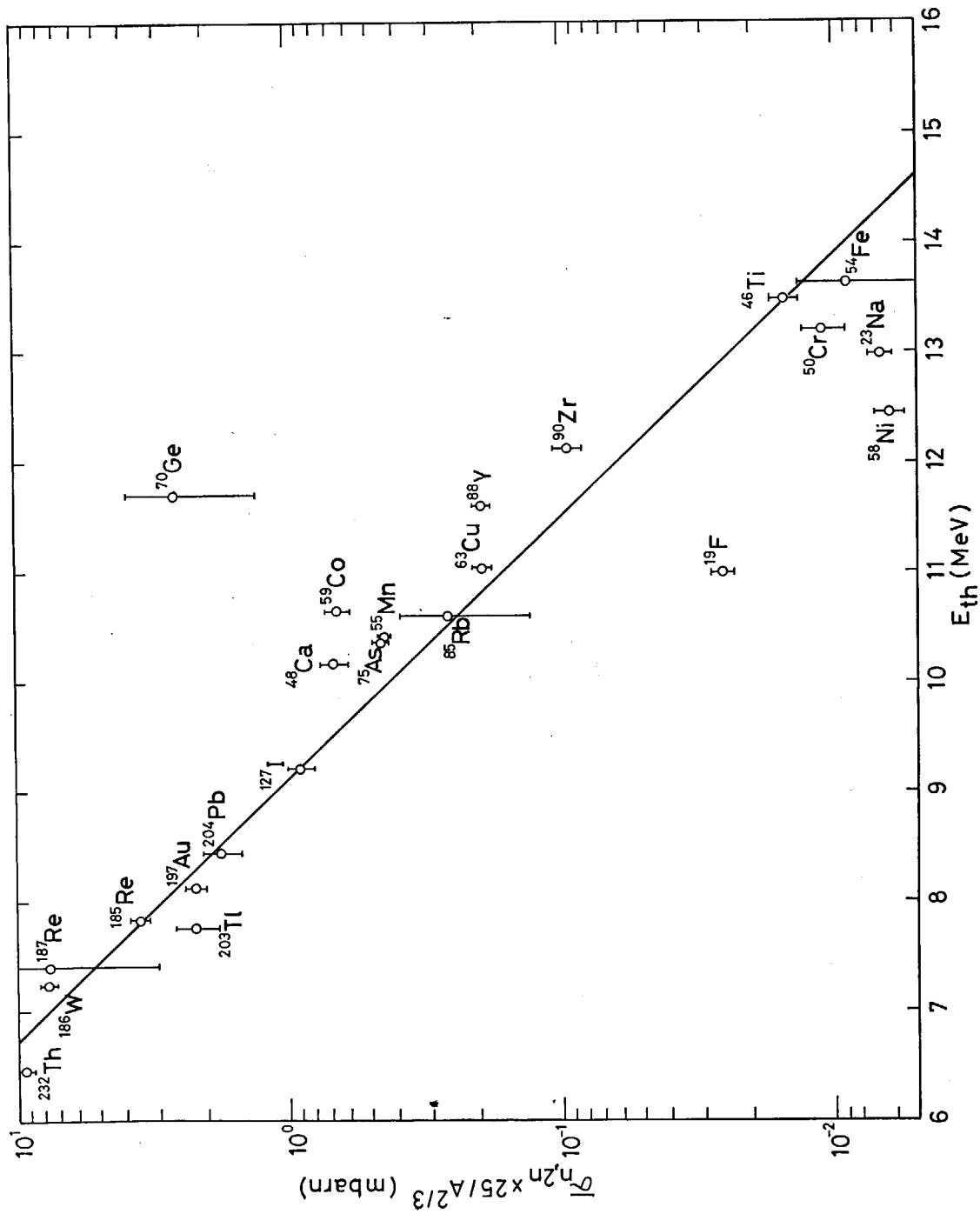

Fig. 4. 3 The systematics of the averaged (n, 2n) cross sections for fission neutrons proposed by Calamand[59].

Pearlstein expresses the (n, 2n) reaction cross section for monochromatic neutrons by the product of three quantities[79] as

$$\sigma_{n,2n} = \sigma_{ne} \cdot \frac{\sigma_{n,M}}{\sigma_{ne}} \cdot \frac{\sigma_{n,2n}}{\sigma_{n,M}}, \tag{4.1}$$

where σ_{ne} is the non-elastic cross section and $\sigma_{n,M}$ gives the sum of the cross sections of the neutron-emitting reactions, such as (n, n'), (n, 2n), (n, 3n), etc. Flerov *et al.*[80] find an empirical equation:

$$\sigma_{ne} = \pi[0.12A^{1/3} + 0.21]^2 \text{ b}. \tag{4.2}$$

Furthermore, Barr *et al.*[81] give the relation:

$$\frac{\sigma_{n,M}}{\sigma_{ne}} = 1 - 1.764 \cdot \exp[-18.14(N-Z)/A] \tag{4.3}$$

for the target nucleus with the atomic number Z, the neutron number N, and the mass number A.

In the case of irradiation experiments with fission neutrons, $\sigma_{n,2n}$ must be averaged with the weight of the neutron flux distribution $\chi(E)$,

$$\bar{\sigma}_{n,2n} = \int_0^\infty \sigma_{n,2n}\chi(E)dE = \sigma_{n,M}\int_0^\infty \frac{\sigma_{n,2n}}{\sigma_{n,M}}\chi(E)\, dE. \tag{4.4}$$

Here, $\sigma_{n,M}$ can be calculated with Eqs. (4.2) and (4.3) while $\sigma_{n,2n}/\sigma_{n,M}$ depends on the nuclear model. As regards $\chi(E)$, several expressions are proposed.

Instead of carrying out the integration of Eq. (4.4), we attempted to evaluate it with empirical data of $\bar{\sigma}_{n,2n}$. If one plots $\log(\bar{\sigma}_{n,2n}/\sigma_{n,M})$ versus E_{th}, one obtains a straight line, as shown in **Fig. 4.4**. Thus, we derived an empirical equation:

$$\bar{\sigma}_{n,2n} = 2.8\times10^3[0.12A^{1/3}+0.21]^2\{1-1.764\cdot\exp[-18.14(N-Z)/A]\}$$
$$\times\exp(-0.794E_{th}) \quad \text{(mb)}. \tag{4.5}$$

As one sees by comparing **Fig. 4.3** with **Fig. 4.4**, Eq. (4.5) reproduces observed cross-section data better than the previous systematics. Particularly, the predicted value for ^{58}Ni agrees very well with the observed one. However, observed cross sections of ^{19}F, ^{23}Na, ^{59}Co, and ^{70}Ge significantly deviate from the systematics as in the case of the previous ones. The first two nuclides ^{19}F and ^{23}Na are classified as the nuclei of $N - Z = 1$ (while $N - Z \geq 2$ for all the others), and Eq. (4.3) is not considered valid for such nuclei[79]. For ^{59}Co and ^{73}Ge, there are reasons to believe the obsered data are possibly inaccurate because of the old experimetal techniques. Particularly in the ^{59}Co experiment, formation of ^{60}Co would considerably interfere the quantitative determination of ^{58}Co. We, therefore, like to trace the experiments with these two target nuclides in near future.

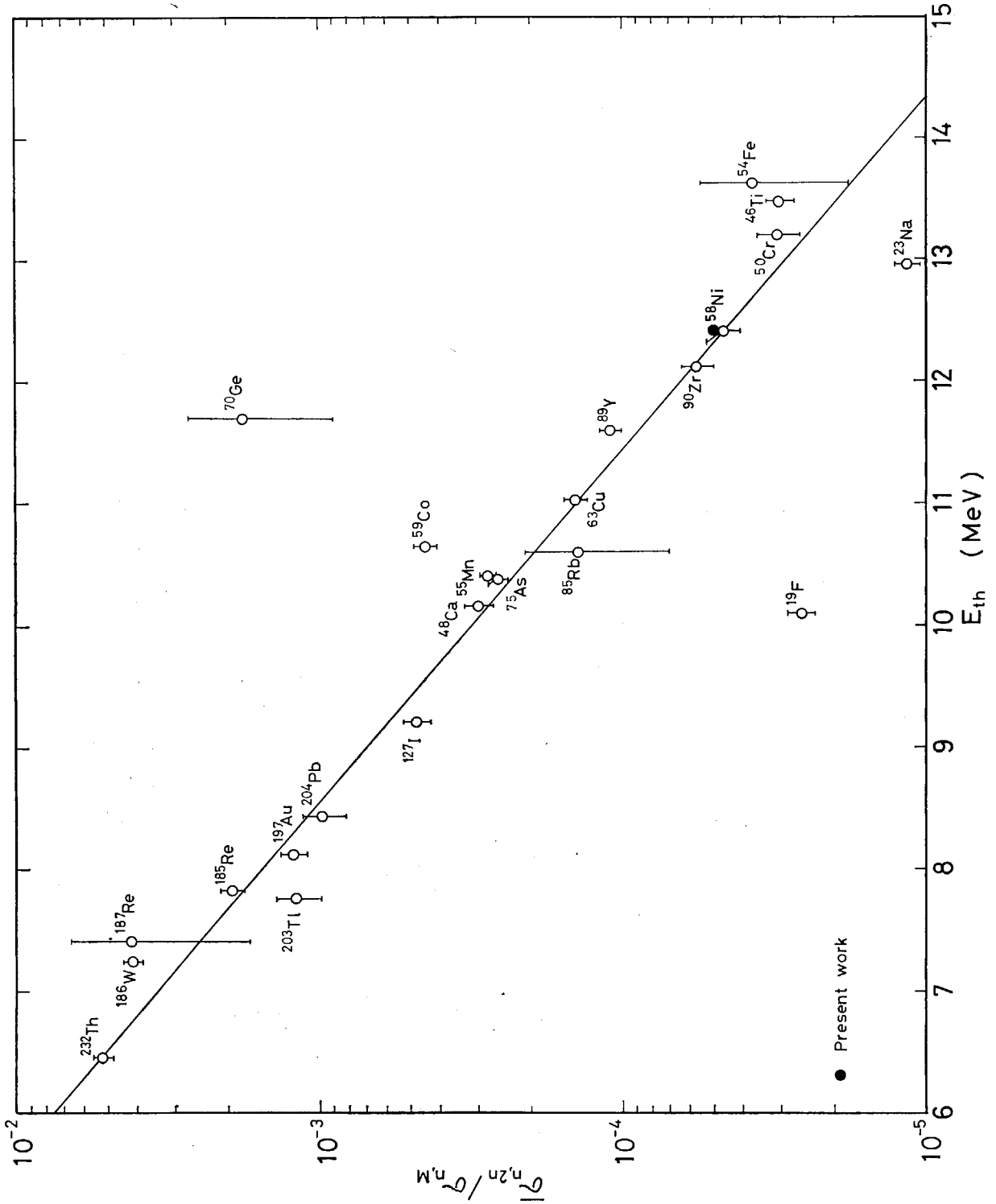

Fig. 4.4 Ratios between the measured (n, 2n) cross section and the calcualted cross section for neutron emission plotted vs. the threshold energy, E_{th}. The experimental data were adopted from reference[59].

5. $^{94}Nb(n,\gamma)^{95m,g}Nb$ Reaction Cross Sections

Neutron irradiation of niobium (^{93}Nb 100%) induces the sequential reactions displayed in **Fig. 5.1**. There are a few reports[20-22] on the thermal-neutron-capture cross section of ^{94}Nb, and the resonance parameters are also available[23]. However, the thermal-neutron cross section for ^{95m}Nb formation is not known. One can obtain the isomeric yield ratio between ^{95m}Nb and ^{95g}Nb if one measures the formation cross section for the former, to which one can apply the statistical model calculation.

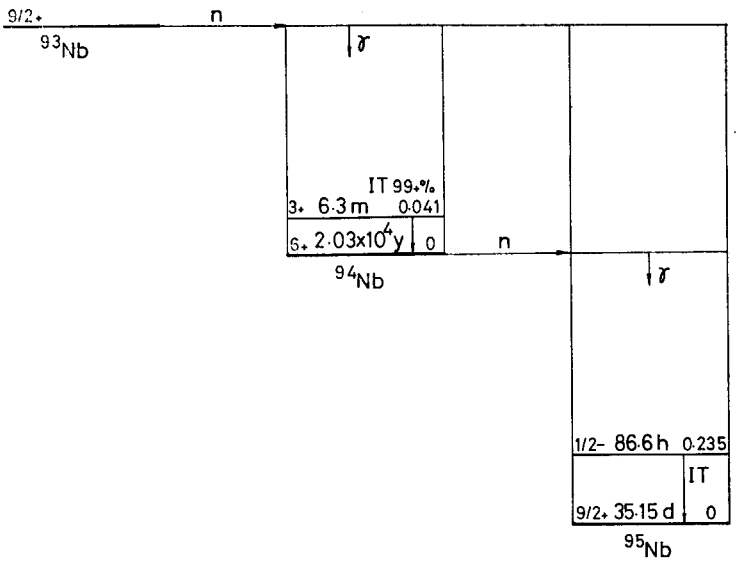

Fig. 5.1 A schematic drawing for the reactions initiated by the neutron capture of ^{93}Nb. Data on energy, spin, parity, and half-life of the metastable and the ground state of ^{94}Nb and ^{95}Nb are indicated.

Neutron capture of ^{93}Nb results in the formation of both ground and metastable states of ^{94}Nb. However, the contribution of the metastable state is negligibly small because the formation cross section of the ground state is 1.0 b while that of the metastable state is 0.1 b and the life time of the latter is much small as compared with former. For example, 100-hr irradiation would yield 7,000 ground-state nuclei per single metastable-state nucleus. As one sees later, change in the irradiation length did not affect the result ; this indicates the contribution of the metastable state was negligible.

5.1. Experimental

Prelimnary irradiation of a commercial reagent of metallic niobium revealed predominant activities due to imipurities such as ^{182}Ta and ^{187}W. Particularly, the long-lived ^{182}Ta was the most interfering radioactive impurity for the present purpose. Therefore, tantalum was chemically separated from niobium target either before or after the irradiation. Namely, the purification was carried out after irradiation in Run 1, while niobium oxide as a purified product from metallic niobium was used as a target in Run 2. Here, the chemical procedure is described in the latter case.

5.1.1. Target preparation

170 mg of spectroscopically pure metallic niobium, made by Johnson Matthey Co., was dissolved in

a polyethylene beaker with 10 ml of 46% HF and 0.5 ml of conc. HNO_3. The resulting solution was transferred to a separatory funnel after 4 ml of conc. HCl, 1 ml of conc. HNO_3, and 40 ml of distilled water were added. By shaking the solution with 40 ml of hexone (methyl isobutyl ketone) for three minutes, tantalum was extracted into the organic phase while niobium was retained in the aquious phase[83]. The extraction procedure was repeated three times. Niobium in the aqueous phase was then precipitated as niobium hydroxide with 16 ml of conc. NH_4OH, and filtered. The filtrate was strongly heated in a porcelain crucible for 1 hr to convert it into Nb_2O_5. The chemical yield was 46%.

5.1.2. Neutron irradiation and activity measurement

30.0 mg of pure niobium oxide obtained above was wrapped in an aluminum foil and irradiated in the VR-2 irradiating hole of the JRR-3 reactor for 216 hr.

The irradiated target in the aluminum foil was unfolded in a nickel crucible filled with distilled water to remove the aluminum foil a few days after irradiation. Niobium oxide in the crucible was heated with an infrared lamp to reduce the water volume, fused by adding 6 ml of 10M KOH with heat, and dissolved with 4 ml of hot water after it cooled off. Black precipitate formed during the fusion process was filtered off. The volume of the resulting solution was 6 ml. 2 ml of the solution was transferred to a polyethylene polar bottle to be subjected to the γ-ray measurement.

A Ge(Li) detector with 8% of the relative detection efficiency was used in the measurement in which the source was placed 10 cm apart from the detector surface. **Figure 5.2** shows an example of the obtained spectrum. The neutron-capture cross section of ^{94}Nb can be obtained from the yielded activity ratios among ^{94}Nb, ^{95m}Nb, and ^{95g}Nb. **Figure 2.1** indicates the energy dependence of the counting efficiency.

5.2. Results

5.2.1. Induced activities and interfering reactions

As shown in **Fig. 5.2**, 702- and 871-keV peaks belonging to ^{94}Nb and the 765-keV ^{95g}Nb peak were clearly observed in the obtained γ-ray spectrum. Though the 236-keV ^{95m}Nb γ ray was very weak, the obtained half-life of 87 hr (cf. **Fig. 5.3**) agreed with the known value of 86.6 hr[85] satisfactorily enough to confirm the formation of ^{95m}Nb.

Table 5.1 Nuclear data and self-shielding factor, G_γ, for the γ ray used for the determination of radioactivities induced in niobium with neutrons.

Radionuclide	Half-life	γ-ray energy (keV)	Intensity (per decay)	G_γ
^{94}Nb	2.03×10^4 y*	702	1.00§	0.913
		871	1.00§	0.921
^{95m}Nb	86.6 hr**	236	0.25§	0.868
^{95g}Nb	35.15 d**	765	1.00§	0.916

* Reference[84]. ** Reference[85]. § Reference[86].

Table 5.1 summarizes half-lives and branching ratios adopted in the calculation of the induced activities. For 236- and 800-keV γ rays, one can not neglect the difference in the self-absorption of the sample matrix; namely, absorption and scattering by water in this case. This effect was corrected by the use of the calculated total cross sections for water given by Storm *et al.*[55] The obtained correction factor G_γ for the self-absorption of γ rays is listed in **Table 5.1**.

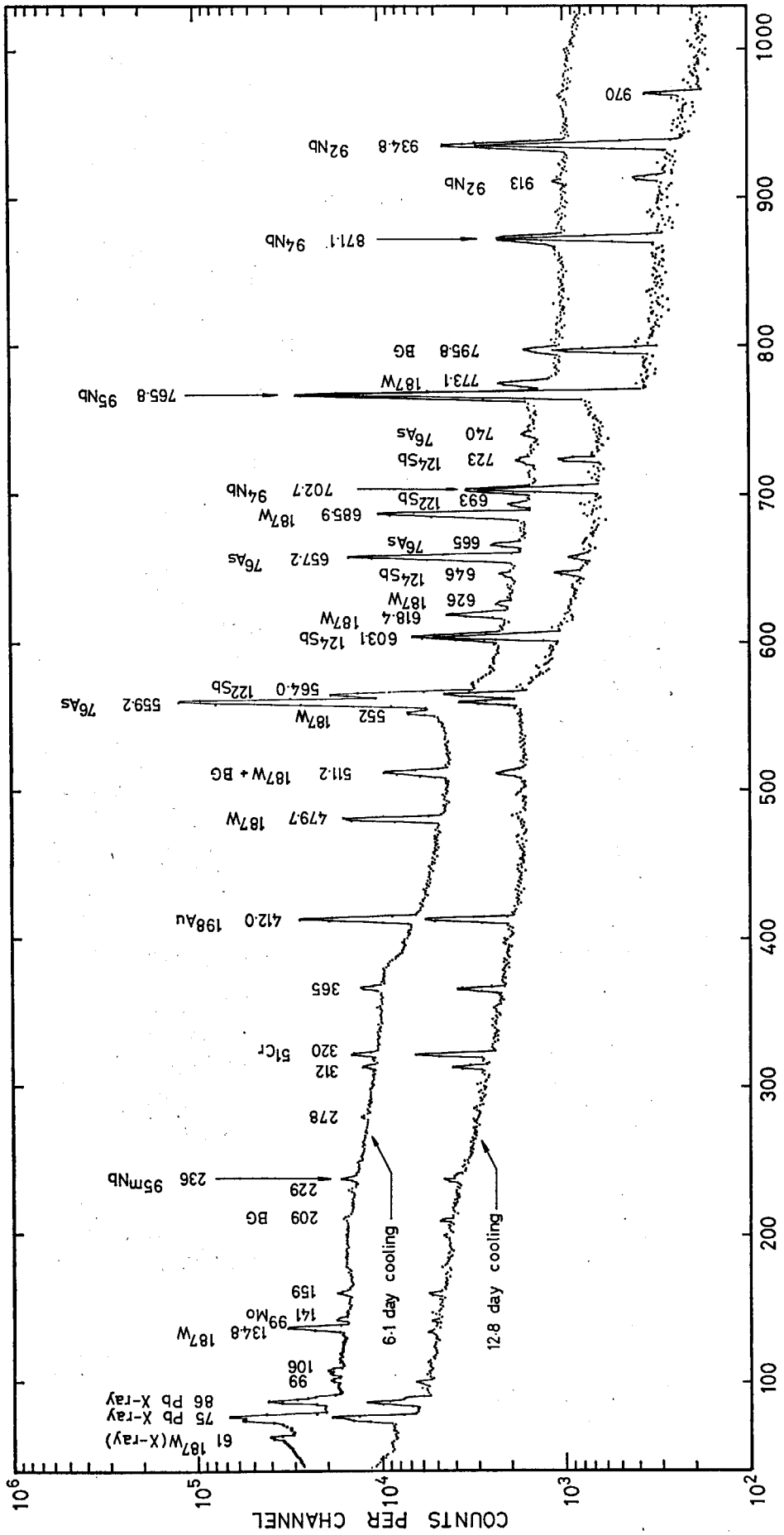

Fig. 5.2 A Ge(Li) γ-ray spectrum of the niobium source, counted for 80 ksec (Run 2).

The corrected values of the radioactivity are given in **Table 5.2**, together with flux nv_0, cumulative irradiation time t, and cooling time t' after irradiation. The epithermal index was found to be 0.022. Errors accompanied with the deduced activities were evaluated with consideration of both the statistical error in the peak area and uncertainty of the counting efficieney ($\pm 1.5\%$ for the 236-keV γ ray or $\pm 1\%$ for the rests). Errors in the γ-branching ratios were, however, not taken into account.

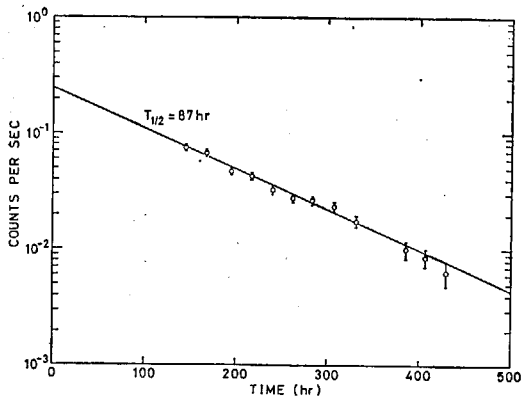

Fig. 5.3 A decay curve of the 236-keV γ ray measured in Run 2. The γ ray was assigned to ^{95m}Nb with the half-life of 86.6 hr[85].

Table 5.2 Observed radioactivities produced in the neutron irradiation of ^{93}Nb.

Run No.	nv_0 (10^{13} n·cm^{-2}sec^{-1})	Irradiation duration(hr)	Cooling time(hr)	Radio-nuclide	Radioactivity (10^2dps)
1	2.11±0.03	282.1	237.2	^{94}Nb	8.71±0.14
				^{95m}Nb	9.1±0.3
				^{95g}Nb	245±3
2	1.59±0.02	193.1	145.7	^{94}Nb	1.28±0.03
				^{95m}Nb	1.76±0.06
				^{95g}Nb	20.6±0.3

Let us consider the possibility of the formation of ^{94}Nb and ^{95m,g}Nb via side reactions. A probable side path for ^{94}Nb is the ^{94}Mo(n, p)^{94}Nb reaction. The yield of ^{94}Nb by the reaction was estimated from tht amount of the detected ^{99}Mo in the sample by the use of the cross sections of ^{98}Mo(n, γ) ^{99}Mo [1] and ^{94}Mo(n, p)^{94}Nb [59] reactions, the neutron flux, and the fast neutron flux. As a result, the amount of ^{94}Nb produced via the side reaction was concluded to be only $1/10^9$ of the observed activity.

There are two by-ways of the ^{95}Nb formation : (1) ^{95}Mo(n, p)^{95}Nb reaction and (2) beta disintegration of ^{95}Zr (half-life 65 d) formed via either ^{94}Zr(n, γ)^{95}Zr or ^{235}U(n, f) reaction. The yield of ^{95}Nb via route (1) was calculated as in the case of ^{94}Nb to be $1/10^6$ of the detected amount, while the possibility of the route (2) was rejected because the 724- and 756-kev γ rays emitted in the decay of ^{95}Zr were not detected at all.

Thus, it was concluded that observed ^{95m}Nb and ^{95g}Nb were produced by the double-neutron-capture process of ^{93}Nb.

5.2.2. Thermal-neutron-capture cross section

The following relations hold for the activities of ^{94}Nb, ^{95m}Nb, and ^{95g}Nb, respectively, produced by irradiation for t and cooling for t':

$$\frac{\lambda_2 N_2}{N_1 \hat{\sigma}_{12} n v_0} = (1-e^{-\lambda_2 t})e^{-\lambda_2 t'} \tag{5.1}$$

$$\frac{\lambda_3 N_3}{N_1 \hat{\sigma}_{12}(nv_0)^2} = \frac{\hat{\sigma}_{23}}{\lambda_2(\lambda_2-\lambda_3)}[\lambda_2(1-e^{-\lambda_3 t})-\lambda_3(1-e^{-\lambda_2 t})]\ e^{-\lambda_3 t'} \tag{5.2}$$

$$\frac{\lambda_4 N_4}{N_1 \hat{\sigma}_{12}(nv_0)^2} = \hat{\sigma}_{23}\{\frac{1}{\lambda_2(\lambda_2-\lambda_3)}[\lambda_2(1-e^{-\lambda_3 t})-\lambda_3(1-e^{-\lambda_2 t})] \times \frac{\lambda_4}{\lambda_4-\lambda_3}(e^{-\lambda_3 t'}-e^{-\lambda_4 t'})$$

$$+ [-\frac{\lambda_3\lambda_4}{(\lambda_2-\lambda_3)(\lambda_2-\lambda_4)}(e^{-\lambda_2 t}-e^{-\lambda_4 t}) + \frac{\lambda_2\lambda_4}{(\lambda_2-\lambda_3)(\lambda_2-\lambda_4)}(e^{-\lambda_3 t}-e^{-\lambda_4 t}) + (1-e^{-\lambda_4 t})] \times e^{-\lambda_4 t'}\}$$

$$+\frac{\hat{\sigma}_{24}}{\lambda_2(\lambda_2-\lambda_4)}[\lambda_2(1-e^{-\lambda_4 t})-\lambda_4(1-e^{-\lambda_2 t})]e^{-\lambda_4 t'}, \tag{5.3}$$

where the suffixes, 1, 2, 3, and 4, designate ^{93}Nb, ^{94}Nb, ^{95m}Nb, and ^{95g}Nb, respectively. λ and N represent the decay constant and the number of nuclei, while $\hat{\sigma}_{ij}$ is the formation cross section of the jth nuclide by the (n, γ) reaction of the ith nuclide.

Since $\lambda_2 \ll \lambda_3$, $\lambda_2 \ll \lambda_4$, $\lambda_2 t \ll 1$, and $\lambda_2 t' \ll 1$, the above equations are reduced to simpler forms:

$$\frac{\lambda_2 N_2}{N_1 \hat{\sigma}_{12} n v_0} = \lambda_2 t, \tag{5.1'}$$

$$\frac{\lambda_3 N_3}{N_1 \hat{\sigma}_{12}(nv_0)^2} = \hat{\sigma}_{23}[t-(1-e^{-\lambda_3 t})/\lambda_3]e^{-\lambda_3 t'}, \tag{5.2'}$$

$$\frac{\lambda_4 N_4}{N_1 \hat{\sigma}_{12}(nv_0)^2} = \hat{\sigma}_{23}\{[t-(1-e^{-\lambda_3 t})/\lambda_3]\cdot\frac{\lambda_4}{\lambda_4-\lambda_3}(e^{-\lambda_3 t'}-e^{-\lambda_3 t'}) + [t-\frac{\lambda_4}{\lambda_3(\lambda_3-\lambda_4)}(e^{-\lambda_3 t}-e^{-\lambda_4 t})$$

$$-(\lambda_3^{-1}+\lambda_4^{-1})(1-e^{-\lambda_4 t})]e^{-\lambda_4 t'}\} + \hat{\sigma}_{24}[t-(1-e^{-\lambda_4 t})/\lambda_4]e^{-\lambda_4 t'}. \tag{5.3'}$$

In the case of the irradiation with a constant flux, $\hat{\sigma}_{23}$ and $\hat{\sigma}_{24}$ can be determined immediately from Eqs. (5.1'), (5.2'), and (5.3'). However, the analysis becomes tedious in the case where the reactor power is shut down during irradiation. There was the power shut-down twice in Run 1 and three times in Run 2. The analysis was carried out by using a program "DOUBLE" written by Baba *et al.*[87]

The yield ratio between ^{94}Nb and ^{95m}Nb gave

$$\hat{\sigma}_{23} = 0.61 \pm 0.03 \text{ b},$$

which in turn resulted in

$$\hat{\sigma}_{24} = 14.6 \pm 0.2 \text{ b}$$

with the yield ratio between ^{94}Nb and ^{95g}Nb.

For the ^{94}Nb(n, γ)^{95}Nb reaction, $\sigma_0 = 13.6 \pm 1.5$ b and $I_0 = 125 \pm 8$ b[22]. This means that $s_0 = 9.9$. By the use of the value of epithermal index, one obtains that

$$g + r\sqrt{T/T_0}\cdot s_0 = 1.22.$$

$\hat{\sigma}_{23}$ or $\hat{\sigma}_{24}$ divided by the above value corresponds to the 2200 m·sec^{-1} cross section σ_0, which is listed in Table 5.3 together with the reported values. Good agreement was attained between the present results and the reported ones, except for ref. 21.

Table 5.3 Thermal neutron capture cross sections of ^{94}Nb.

Reaction	Cross section (b)		Reference
	Present work	Literature	
^{94}Nb(n, γ) ^{95m}Nb	$\hat{\sigma}$ =0.61±0.03*		
^{94}Nb(n, γ) ^{95g}Nb	$\hat{\sigma}$ =14.6±0.3*		
^{95}Nb(n, γ) $^{95m+g}$Nb	$\hat{\sigma}$ =15.2±0.3*	$\hat{\sigma}$ = 15±4§	[20]
	σ_0=12.5±0.3	σ_0= 13.6±1.5	[22]
		σ_0= 16.8±1.5	[21]

* $r\sqrt{T/T_0}$ = 0.022.

§ The value of $r\sqrt{T/T_0}$ is not given.

The isomeric yield ratio is given by

$$\frac{\sigma_m}{\sigma_g} = \frac{\hat{\sigma}_{23}}{\hat{\sigma}_{24}} = 0.042\pm0.002,$$

the analysis of which shall be attempted by the compound nucleus model in the next section.

5.3. Discussion on the isomeric yield ratio in the (n, γ) reaction of ^{94}Nb

Here, we attempt a theoretical explanation of the observed yield ratio with reasonable assumptions. The prescription by Huizenga and Vandenbosch[6] is traced first and, then, more strict method by Pönitz[7] will be tried.

5.3.1. Calculation by the Huizenga-Vandenbosch prescription

In order to simplify the problem, the following assumptions are introduced in this prescription: (1) Gamma rays are emitted by dipole transition. (2) Cascade multiplicity is determined either by experiment or from the mean γ-ray energy. (3) The final stage of the γ cascade determines whether the nucleus finally settles in the ground or the metastable state. (4) The nucleus chooses to feed the metastable or ground state depending on which transition has the smaller spin change in the last γ de-excitation.

According to the first assumption, compound nuclei with spin J_c decay to any levels having one of the three spin values, J_c-1, J_c, and J_c+1 in the first stage of the cascade. The transition probability is proprtional to the spin-dependent term of the nuclear level density [88,89]:

$$\rho(J) \propto (2J+1)\ \exp[-(J+1/2)^2/2\sigma^2], \tag{5.4}$$

where σ is the spin cutoff parameter determining the spin distribution. Nucleus having any one of the above three spins feeds three spin groups as well in the second cascade stage. This procedure is repeated till the emission of (N_γ-1) γ rays, where N_γ is the average number of the cascade multiplicity. The last γ emission then determines the population of the metastable and ground states (assumption (3)). With the assumption (4), the states with spin $J < 5/2$ populate the spin 1/2 state, ^{95m}Nb, while those with $J > 5/2$ populate the spin 9/2 state, ^{95g}Nb. The states possessing $J = 5/2$ feed equally the two states [90,91].

The spin cutoff parameter σ was calculated by the Gilbert-Cameron prescription[92]. For the neutron binding energy 8.496 MeV of ^{95}Nb [82], we obtain the effective excitation energy U = 7.38 MeV, the level density parameter a = 12.4 Mev^{-1}, and σ =4.2.

The spin of ^{94}Nb is 6 and s-wave neutron capture is predominant in the capture process*. Therefore, the spin J_c of the compound nucleus is possibly 11/2 or 13/2. Computation of the isomeric

yield ratio was carried out for the two J_c values and N_γ from 3 to 5. The results are listed in **Table 5.4**. Agreement was obtained between the observed value and the calculated one in the case of J_c = 11/2 and N_γ = 5. N_γ can be evaluated by the equation[93];

Table 5.4 Isomer ratio in the thermal neutron capture reaction of ^{94}Nb calculated by the theory of Huizenga and Vandenbosch[6].

Experimental	Theoretical		
		J_c	
	N_γ	11/2	13/2
0.042±0.002	3	0	0
	4	0.022	0
	5	0.043	0.009

$$N_\gamma = \frac{\sqrt{aU}}{\ell+1}, \tag{5.5}$$

where ℓ is the multipolarity. According to Eq. (5.5), N_γ = 4.8 for the present case, which is consistent with the result in **Table 5.4**.

The above discussion leads to the conclusion that the isomeric yield ratio in the thermal-neutron-capture reaction of ^{94}Nb can be explained by the Huizenga-Vandenbosch prescription and the spin of the compound state is very likely to be 11/2.

5.3.2. Analysis by Pönitz's theory[7]

Pönitz has derived a method requiring none of the assumptions introduced by Huizenga *et al.*[6] In this method, the low-lying levels with known energy, spin, and parity are explicitly considered, and quadrupole transition is included as well as dipole transition.

The occupation probability of the compound state with energy E_c, spin J_c, and parity π_c is expressed as

$$W_{n=0}(E, J, \pi) = \delta(E - E_c) \cdot \delta_{JJ'} \delta_{\pi\pi'} \tag{5.6}$$

where $\delta(x)$ is the Dirac delta function and $\delta_{xx'}$ is Kronecker's delta. The suffix n implies the number of γ rays previously emitted in the cascade process.

Here, we make an approximation that the levels between E_{th} and E_c are continuous while those below the critical energy E_{th} are treated as discrete levels. The occupation probability of a level in the continuous region is written after n γ transitions as

$$W_n(E, J, \pi) = \sum_{J'} \sum_{\pi'} \int_E^{E_c} W_{n-1}(E', J', \pi')\, \rho(E', J', \pi') \frac{S(E', J', \pi' \to E, J, \pi)}{B(E', J', \pi')} dE', \tag{5.7}$$

where

$$B(E', J', \pi') = \sum_{J'} \sum_{\pi'} \int_{E_{th}}^{E'} S(E', J', \pi' \to E, J, \pi) \rho(E, J, \pi) dE + \sum_k S(E', J', \pi' \to E_k, J_k, \pi_k), \tag{5.8}$$

$S(E', J', \pi' \to E, J, \pi)$ represents the transition probability between single levels with (E', J', π') and (E, J, π), and $\rho(E, J, \pi)$ gives the nuclear level density. The suffix k denotes the kth discrete level.

Similarly, the occupation probability for the ith discrete level is expressed as

*) The compound state with J = 9/2 or 15/2 is likely to ocontribute to some extent because the possibility of p-wave neutron capture is expected high in the epithermal region. This effect is, however, neglected in the present discussion.

$$W_n(E_i, J_i, \pi_i) = \sum_{J'\pi'}\sum\int_{E_{th}}^{E_c} W_{n-1}(E', J', \pi')\ \rho(E', J', \pi')\ \frac{S(E', J', \pi' \rightarrow E_i, J_i, \pi_i)}{B(E', J', \pi')}\ dE'$$

$$+\sum_k W_{n-1}(E_k, J_k, \pi_k)\ \frac{S(E_k, J_k, \pi_k \rightarrow E_i, J_i, \pi_i)}{B(E_k, J_k, \pi_k)}, \tag{5.9}$$

where

$$B(E_k, J_k, \pi_k) = \sum_i S(E_k, J_k, \pi_k \rightarrow E_i, J_i, \pi_i). \tag{5.10}$$

The nucleus finally settles in either metastable or ground state. The isomeric yield ratio σ_m/σ_g is, thertfore, given by

$$\frac{\sigma_m}{\sigma_g} = \frac{\sum_n W_n(E_m, J_m, \pi_m)}{\sum_n W_n(E_g, J_g, \pi_g)}. \tag{5.11}$$

Let us consider E1, M1, E2, and M2 transitions in the computation of the transition probability S like Pönitz:

$$S(E', J', \pi' \rightarrow E, J, \pi) = C_{E1}\eta_{E1}(E'-E)^3 + C_{M1}\eta_{M1}(E'-E)^3$$
$$+C_{M2}\eta_{M2}(E'-E)^5, + C_{E2}\eta_{E2}(E'-E)^5, \tag{5.12}$$

where C gives the intensity of transition and η is 1 for allowed transitions and 0 for forbidden ones. In the case where both E2 and M1 transitions are probable, we shall consider only the latter in which the spin difference is smaller. Likewise, E1 transition alone is considered in the case where both E1 and M2 transitions are possible.

The level density in the continuous region is given by

$$\rho(E, J, \pi) = \frac{2J+1}{2\sqrt{2\pi}\cdot\sigma^3}\cdot\exp\left[-\frac{(J+1/2)^2}{2\sigma^2}\right]\cdot\frac{\rho(E)}{2} \tag{5.13}$$

if one assumes that it does not depend on parity. The factor of 1/2 in the last factor in Eq. (5.13) arises from the fact that the levels with either parity alone appear. Gilbert and Cameron[92] give a prescription for the spin cutoff parameter:

$$\sigma^2 = 0.0888(aU)^{1/2}A^{2/3} \tag{5.14}$$

when the level density at high excitation is expressed as

$$\left.\begin{aligned}\rho(E) &= \frac{\sqrt{\pi}}{12}\ \frac{\exp(2\sqrt{aU})}{a^{1/4}U^{5/4}} \\ U &= E - U_0\end{aligned}\right\}, \tag{5.15}$$

where a is the level density parameter, U is the effective excitation enrgy and U_0 is the pairing energy. For $U < U_x = 2.5 + 150/A$ (MeV), the constant-temperature level density

$$\rho(E) = \frac{1}{T}\exp\left(\frac{E-E_0}{T}\right) \tag{5.16}$$

is used instead. Here, the constants T and E_0 are determined so that Eqs. (5.15) and (5.16) may smoothly join at U_x [92].

The computation was carried out with FACOM 230-75. The computer program written in FORTRAN IV and its instruction manual are given in **Appendix 3.**

Integration appeared in Eqs. (5.7) and (5.9) were replaced by summation in the actual computa-

tion, and the spins in the continuous region were restricted within the range in which either metastable or ground state could be reached from the excited levels only by dipole or quadrupole transition.

Though the precision of the summation is improved with increasing the number m of divided intervals of the integration range, the time required for computation increases proportionally with increasing m. An optimum value of m was found to be 20 as a result of test runs. The resulting computation time was 100 sec under this conditon.

Figure 5.4 indicates low-lying levels of ^{95}Nb determined experimenally[95]. There are levels associated with two sets of spin and parity; the spin value can not be definitely assigned yet.

Unknown quantities in the computation are spin and parity, J_c^π, of the compound nucleus and constants in Eq. (5.12). The J_c^π value is not given in the existing data of resonance parameters for ^{94}Nb [23]. However, s-wave neutron capture is predominant for thermal neutrons as stated before. There are two possibilities that $J_c^\pi=11/2^+$ and $13/2^+$ since the spin-parity of the target nucleus is 6^+.

As regards the constants C, it is known that the transition probabilities of E1, M1, and M2 are a few orders of magnitude smaller than the Weisskopf estimate whereas the E2 transition probability is greater than that in many cases[94]. Systematics of the deviation from the Weisskopf estimate such as that found for deformed nuclei[95] is not observed among nuclides in the neighbourhood of the mass number 100. Anyhow, one may assume that probabilities of the E2 and M1 transitions are roughly the same order of magnitude while the probability of M2 transition is more than one order smaller than them[7]. Hence, we assume

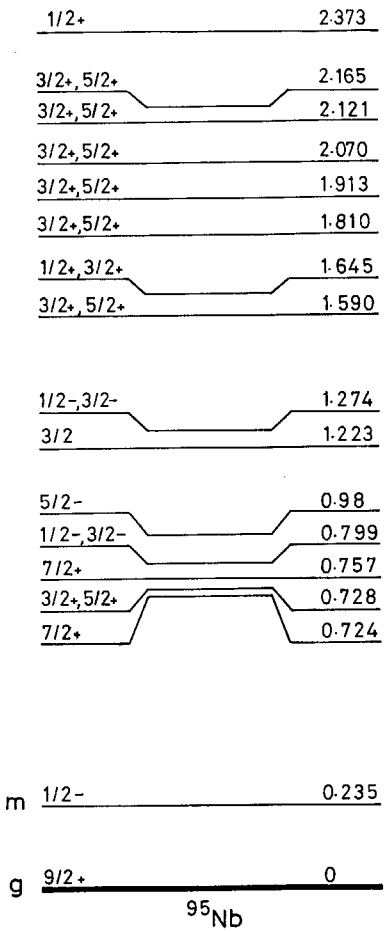

Fig. 5.4 Level scheme used in the calculation of the isomeric cross-section ratio.

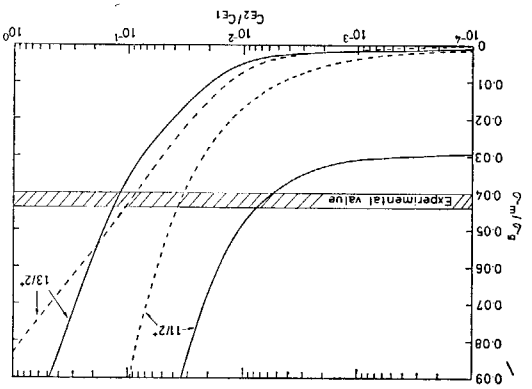

Fig. 5.5 The isomeric cross-section ratio plotted vs. C_{E2}/C_{E1}. The results of the calculation are represented for the two possible values of the spin of the compound nucleus and at the same time for two possible sets for the spin value of the ^{95}Nb discrete levels: the low spin case (solid curves) and the high spin case (dashed curves).

$$C_{E2} = C_{M1} = 10\, C_{M2}. \tag{5.17}$$

The ratio C_{E2}/C_{E1} affects the most the result of computation, which was then treated as an adjustable parameter in the computation. The absolute magnitude of C is indifferent to the result.

The results of computation are shown in **Fig. 5. 5** both for $J_c^\pi = 11/2^+$ and $13/2^+$. The full line represents the case in which all levels assigned with alternative spin-parity values were assumed to possess the lower spin values, while the broken line indicates the case of the higher spin values. The true figure is expected to be in-between.

One sees from **Fig. 5. 5** that fairly large contribution of the quadrupole transition must be required for $J_c^\pi=13/2^+$ compared to the case of $J_c^\pi=11/2^+$. This arises from the larger spin ditfference of the former from the spin of the metastable state, $J_m^\pi=1/2^-$. In order to reproduce the observed σ_m/σ_g value, C_{E2}/C_{E1} should be in the range between 6×10^{-3} and 4×10^{-2} for $J_c^\pi = 11/2^+$ and about 0. 1 for $J_c^\pi=13/2^+$.

One must expect that C_{E2}/C_{E1} fluctuates in a wide range from transition to transition and, therefore, it is quite unlikely that the averaged value over many transitions remains still so large as 0. 1 considering the Weisskopf estimate[2]. This consequence is consistent with that obtained in the preceding analysis. We then proclaim that the isomeric yield ratio in the thermal neutron capture of ^{94}Nb can be explained by the statistical model.

6. Thermal-Neutron-Capture Cross Sections of ^{165m}Dy and ^{165g}Dy

In **Fig. 6.1** are shown nuclear reactions induced by irradiation of ^{164}Dy with neutrons. The thermal-neutron-capture cross section of ^{165g}Dy is known, whereas that of ^{165m}Dy is not yet available. The latter can be determined radiochemically by finding the yield of ^{166}Dy as a function of irradiation length. The yield of ^{166}Dy is sensitive to the irradiation length, only while it is short because of the short half-life of ^{165m}Dy. It follows that the yield is so small that the activity measurement must be carried out with high sensitivity. The 82.5-keV γ ray has the largest branching ratio among γ rays emitted in the disintegration of ^{166}Dy. The emission rate of the 82.5-keV γ ray is, however, not considered to be well established yet: it was then measured in the present work. Detection of such a low-energy γ ray was carried out with a surface-barrier type Ge(Li) detector (LEPS) instead of the coaxial type detectors used in the preceding works.

Obtained cross-section values of both metastable and ground states were interpreted by the statistical model, together with other cross-section data.

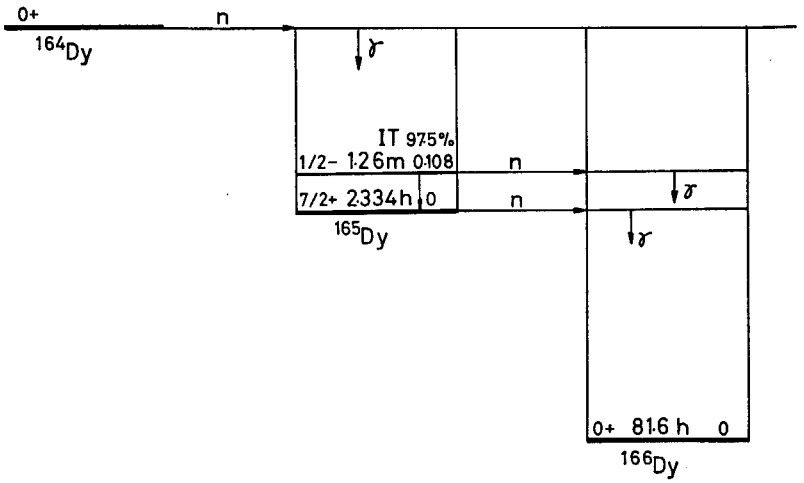

Fig. 6.1 A schematic drawing for the reactions initiated by the neutron capture of ^{164}Dy. Data on energy, spin, parity, and half-life for the metastable and the ground state of ^{165}Dy and ^{166}Dy are indicated[97, 98].

6.1. Emission rates of the 82.5-keV γ ray of ^{166}Dy and the 80.6-keV γ ray of ^{166}Ho

A ^{166}Dy-^{166}Ho source nearly in the transient equilibrium was subjected to the β-ray measurement with a gas-flow proportional counter to determine the absolute source intensity, while the 82.5-keV and 80.6-keV γ rays were measured with LEPS to obtaine the γ-ray emission rates per disintegration.

6.1.1. Source preparation

Spectroscopically pure dysprosium oxide supplied by Johson Matthey Co. was dissolved with HCl and put in a quartz ampoule, which was sealed after being dried up with vacuum pump and irradiated in a pneumatic tube ($nv_0 = 2\times10^{13}$n · cm^{-2}sec^{-1}) of the JRR-3 reactor for 1 hr. The irradiated sample was subjected to ion exchange separation with α-hydroxyisobutyric acid[96] to purify dysprosium and holmium. Mutual separation of dysprosium and holmium was not possible because of the decay of ^{166}Dy into ^{166}Ho. The dysprosium-holmium fraction was eluted as hydrochloric acid solution in the

concentrating procedure by the cation exchange method. An aliquot of the solution was mounted on Mylar film of 0.9 mg/cm² thick, dried up with silica gel in a desiccator, and covered with Scotch tape to prepare the activity source. The obtained source was 2—3 mm in dia. and 1 mg/cm² in thickness.

A ^{90}Sr-^{90}Y standard source was prepared in a similar way as the ^{166}Dy-^{166}Ho source, from a diluted solution of the ^{90}Sr-^{90}Y standard solution supplied by Laboratoire de Métrologie des Rayonnements Ionisants (LMRI), to determine the β-ray counting efficiency.

6.1.2. Activity measurement

The β-ray measurement was carried out with a gas-flow proportional counter with a gold-foil window of 1.8 mg/cm² thick operated in the PR gas range.

The γ-ray measurement was undertaken with ORTEC LEPS, whose resoluton was 0.50 keV at 82.5 keV. Calibration of the counting efficiency was done with IAEA-^{241}Am, and RCC-^{57}Co and ^{133}Ba sources. The obtained efficiency curve is shown in **Fig. 6.2**, where "Surface" implies the geometry of the source being fixed on the window-protection cap. The distance from the detector surface was 10 mm in this case. In **Fig. 6.3** is given an observed spectrum, in which assignment of the detected peaks was completed except for the 63.2-keV peak. Here, the terbium X ray arose in the β^+ decay of ^{159}Dy (half-life 144 d) produced by the ^{158}Dy(n, γ)^{159}Dy reaction.

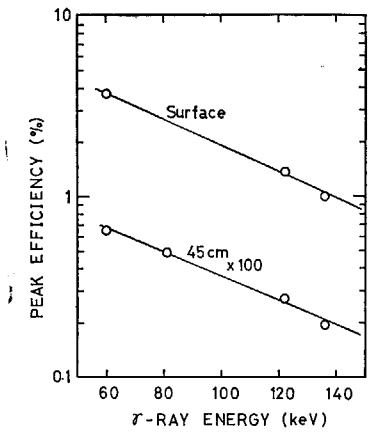

Fig. 6.2 Peak-efficiency curves for an surface-barrier-type Ge(Li) detector (Low energy photon detector: LEPS) determined with using point sources of ^{57}Co, ^{133}Ba, and ^{241}Am.

6.1.3. Results

The numbers of ^{166}Dy and ^{166}Ho nuclei are given by

$$N_1 = N_{01}e^{-\lambda_1 t} \tag{6.1}$$

and

$$N_2 = \frac{\lambda_1 N_{01}}{\lambda_2 - \lambda_1}(e^{-\lambda_1 t} - e^{-\lambda_2 t}) + N_{02}e^{-\lambda_2 t}, \tag{6.2}$$

respectively, where N_0 is the number of nuclei at the end of irradiation, λ is the decay constant, and t is the cooling time after irradiation. The suffixes 1 and 2 designate ^{166}Dy and ^{166}Ho, respectively. The second term of Eq. (6.2) is negligible for large t because $N_{02} \ll N_{01}$. The activity of each nuclide at a given value of t is obtained by means of Eqs. (6.1) and (6.2) if β counting efficiency is known.

The β counting efficiency was determined by measuring the ^{90}Sr-^{90}Y standard source. As shown

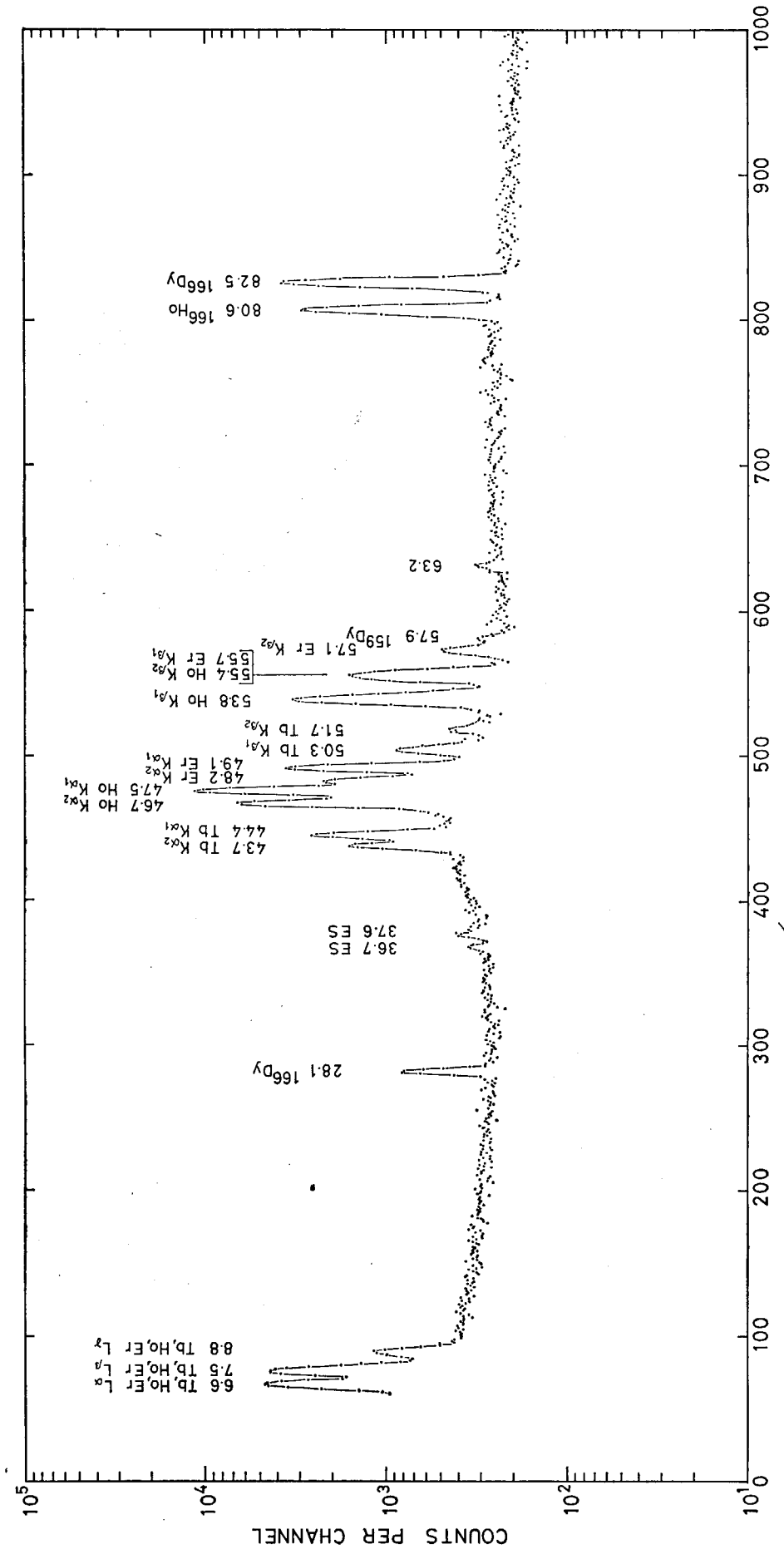

Fig. 6.3 A γ-ray spectrum of the ^{165}Dy-^{165}Ho source measured for 40 ksec after 202 hr from the end of irradiation. The symbol ES implies that the relevant peak is due to the escape of a part of the γ-ray energy as X-ray.

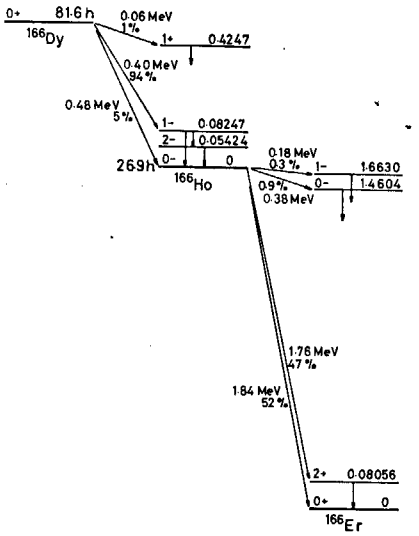

Fig. 6.4 Decay scheme of ^{166}Dy [57].

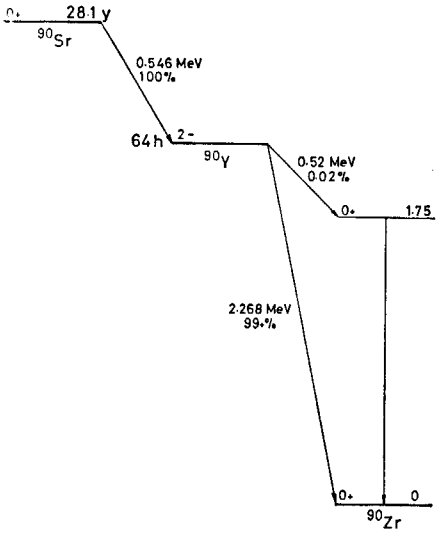

Fig. 6.5 Decay scheme of ^{90}Sr [57].

in **Figs. 6.4** and **6.5**, the decay schemes of ^{166}Dy-^{166}Ho and ^{90}Sr-^{90}Y resemble each other in a sense of emitting both high- and low-energy β rays. Therefore, the latter is considered to be appropriate as the standard in this case, though the correction due to the difference in the β-ray energy between the two sources must be taken into account. Furthermore, it was considered that the radioactive equilibrium was not completely attained in the ^{166}Dy-^{166}Ho system. The correction for self-absorption was made by calculating the β-ray absorption within the source of 1 mg/cm^2 thick. Subtraction of the contribution of the radioactive impurity ^{159}Dy was carried out by analyzing the β-ray decay curve.

In **Table 6.1** are shown the results of measuremets with three sources. The attached error is the statistical uncertainty. Other sources of the error are the errors in the counting efficiencies of both β and γ rays, which are estimated to be 1.5% each. The resulting γ-ray emission rates I_γ are listed in **Table 6.2** together with the reference values. Agreement was obtained between the present and reported values within the error. The reported γ-ray intensities turned out to be of considerable reliability after all.

Table 6.1 Experimental results on 82.5-keV(^{166}Dy) and 80.6-keV(^{166}Ho) γ-ray intensities per decay.

Source No.	Lapse of time after irradiation (hr)	Radioactivity (dps)		Observed γ ray (γ/sec)		γ Intensity per decay	
		^{166}Dy	^{166}Ho	82.5 keV	80.6 keV	82.5 keV	80.6 keV
1	173.7	49.1±0.3	69.6±0.5	7.00±0.10	4.74±0.08	0.1427±0.0015	0.0682±0.0012
2	189.8	82.4±0.4	118.3±0.5	10.98±0.17	7.40±0.14	0.1333±0.0021	0.0626±0.0012
3	201.8	130.5±0.4	188.7±0.6	17.96±0.15	12.53±0.11	0.1376±0.0012	0.0664±0.0006
				Averaged		0.1379±0.0059	0.0657±0.0035

Table 6.2 γ-Ray intensities in the decay of ^{166}Dy and ^{166}Ho.

Isotope	Energy (keV)	I_γ (per decay)	Reference
^{166}Dy	82.5	0.138±0.007	Present work
		0.13±0.03	[98]
^{166}Ho	80.6	0.066±0.004	Present work
		0.067±0.005	[99]
		0.0635±0.0075	[100]
		0.062±0.004	[101]

6.2. Cross-section measurement

The target was spectroscopically pure dysprosium oxide supplied by Johnson Matthey Co. No interfering γ ray due to impurities was found in a preliminary experiment and, therefore, no chemical purification was attempted for the target either prior to or post irradiation.

Non-irradiated dysprosium oxide was dissolved with HCl to prepare a solution containing 0.991 mg/ml of dysprosium. 0.100 ml of the solution was mounted on a thin polyethylene film (1.3 mg/cm^2 thick) and dried in a desiccator. Dysprosium chloride (2 mm in dia.) on the film was covered with Scotch tape and irradiated in the preumatic tube HP-1 of JRR-3 reactor for 3—60 min. The γ-ray measurement was carried out with LEPS immediately after irradiation. First, the γ rays of ^{165g}Dy were measured with the geometry of 45 cm apart from the detector surface. The γ rays of ^{166}Dy were measured by placing the source at 10 mm from the detector surface after ^{165g}Dy had decayed out.

Neutron flux was monitored with gold foils for short-irradiation.

6.2.1. ^{164}Dy(n, γ)$^{165m+g}$Dy reaction cross section

In **Fig. 6.6** is shown a γ-ray spectrum obtained with a sample of 10 min irradiation and succeeding 6 hr cooling. The determined energies of detected peaks agreed with those of γ rays[97] and X rays[57] given for ^{165g}Dy, except for the 52-keV peak. Here, the lead X ray was caused by the excitation of lead with γ rays of ^{165g}Dy.

The ^{165g}Dy yield was obtained with the peak area of the 94.7-keV γ ray of the largest emission rate. The resulting yield of ^{165g}Dy and the ^{164}Dy(n, γ)$^{165m+g}$Dy reaction cross section are listed in **Table 6.3**, where 2.334 hr and 0.036 [97] were used as the ^{165g}Dy half-life and the emission rate of the 94.7-keV γ ray, respectively. Furthermore, λ_3 and N_3 respectively denote the decay constant and the number of atoms of ^{165g}Dy.

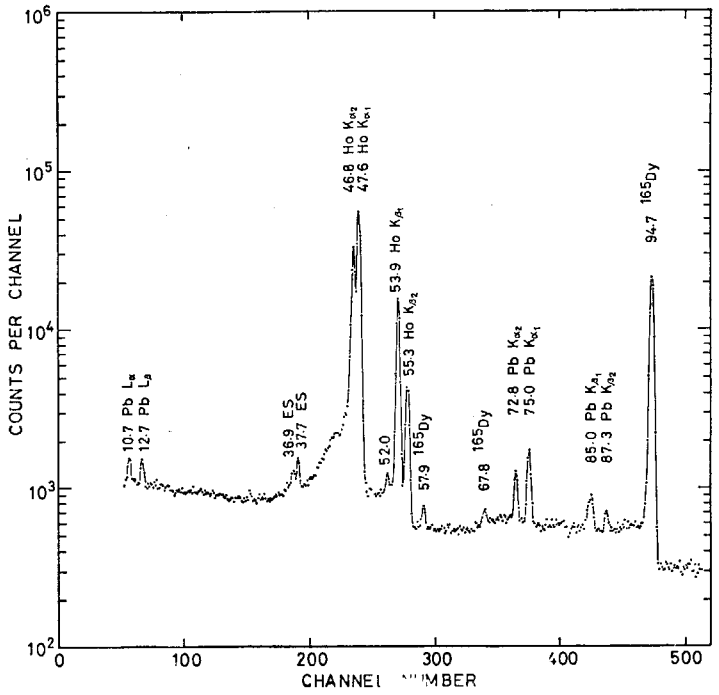

Fig. 6.6 A γ-ray spectrum of the dysprosium source measured 6 hr after the end of 10-min irradiation.

Table 6.3 Yields of ^{165g}Dy via ^{164}Dy(n, γ)$^{165m+g}$Dy reaction and the reaction cross section. The notations are explained in the text. The experiment was performed under the condition that $r\sqrt{T/T_0}=0.017$ and the thermal neutron self-shielding factor $G_{th}=0.996$.

Irradiation period(min)	nv_0 (n•cm^{-2} sec^{-1})	$\lambda_3 N_3/(1-e^{-\lambda_3 t})$ (sec^{-1})	Cross section (b)
3	$(2.17\pm0.04)\times10^{13}$	$(6.15\pm0.18)\times10^{9}$	2740
10		$(6.15\pm0.17)\times10^{9}$	2740
20		$(6.08\pm0.17)\times10^{9}$	2710
5	$(2.01\pm0.03)\times10^{13}$	$(5.83\pm0.18)\times10^{9}$	2300
7		$(5.69\pm0.18)\times10^{9}$	2740
60		$(5.62\pm0.16)\times10^{9}$	2700
		Averaged	2740±80

One finds that the cross section value obtained in each run for the ^{164}Dy(n, γ)$^{165m+g}$Dy reaction deviates very little from the others. This indicates that the experimental condition was kept fairly constant throughout the experiment. The result shows good agreement with the reported cross-section value of 2700±75 b for 2200 m sec^{-1} neutrons[1] which is nearly equal to the effective cross sectior, in this case, since $I_0' = 70$ b and consequently $s_0 = 0.03$ according to the calculation with the resonance parameters[1].

6.2.2. ^{165m,g}Dy(n, γ)^{166}Dy reaction cross sections

The ^{166}Dy yield via double neutron capture process of ^{164}Dy is given by

$$\frac{\lambda_4 N_4}{N_1(nv_0)^2} = \frac{\hat{\sigma}_{12}\hat{\sigma}_{24}}{\lambda_2(\lambda_2-\lambda_4)}[\lambda_2(1-e^{-\lambda_4 t})-\lambda_4(1-e^{-\lambda_2 t})] + \hat{\sigma}_{34}\{\frac{\hat{\sigma}_{13}}{\lambda_3(\lambda_3-\lambda_4)}[\lambda_3(1-e^{-\lambda_4 t}) - \lambda_4(1-e^{-\lambda_3 t})] + \hat{\sigma}_{12} f[\frac{\lambda_4}{(\lambda_3-\lambda_2)(\lambda_2-\lambda_4)}(e^{-\lambda_2 t}-e^{-\lambda_4 t}) + \frac{\lambda_2\lambda_4}{\lambda_3(\lambda_2-\lambda_3)(\lambda_3-\lambda_4)}(e^{-\lambda_3 t}-e^{-\lambda_4 t}) + \frac{1}{\lambda_3}(1-e^{-\lambda_4 t})]\}, \quad (6.3)$$

where suffixes, 1, 2, 3, and 4, correspond to ^{164}Dy, ^{165m}Dy, ^{165g}Dy, and ^{166}Dy, respectively. λ is the decay constant, t gives the irradiation length, N denotes the number of nuclei, nv_0 is the neutron flux, f denotes the isomeric transition rate of ^{165m}Dy, and σ_{ij} represents the cross section of the formation of the jth nuclide via the neutron capture of the ith nuclide.

The burn-out of ^{166}Dy is neglected in Eq. (6.3) since it causes only 0.3% difference in the ^{166}Dy yield even if the capture cross section of ^{166}Dy is assumed to be as large as 1×10^5 b because of short irradiation with relatively low neutron flux.

With known values of $\hat{\sigma}_{12}$ and $\hat{\sigma}_{13}$, $\hat{\sigma}_{24}$ and $\hat{\sigma}_{34}$ can be deduced from the t-dependence of $\lambda_4 N_4/[N_1(nv_0)^2]$. Equation (6.3) is rewritten in the form:

$$\frac{\lambda_4 N_4}{N_1(nv_0)^2} = \hat{\sigma}_{24}A(t)+\hat{\sigma}_{34}B(t), \quad (6.3')$$

where

$$A(t) = \frac{\hat{\sigma}_{12}}{\lambda_2(\lambda_2-\lambda_4)}[\lambda_2(1-e^{-\lambda_4 t})-\lambda_4(1-e^{-\lambda_2 t})]$$

$$B(t) = \frac{\hat{\sigma}_{13}}{\lambda_3(\lambda_3-\lambda_4)}[\lambda_3(1-e^{-\lambda_4 t})-\lambda_4(1-e^{-\lambda_3 t})] + \sigma_{12} f[\frac{\lambda_4}{(\lambda_3-\lambda_2)(\lambda_2-\lambda_4)}(e^{-\lambda_2 t}-e^{-\lambda_4 t}) + \frac{\lambda_2\lambda_4}{\lambda_3(\lambda_2-\lambda_3)(\lambda_3-\lambda_4)}(e^{-\lambda_3 t}-e^{-\lambda_4 t}) + \frac{1}{\lambda_3}(1-e^{-\lambda_4 t})].$$

Equation (6.3′) is further transformed to

$$\frac{\lambda_4 N_4}{N_1(n v_0)^2 A(t)} = \hat{\sigma}_{24} + \hat{\sigma}_{34}\frac{B(t)}{A(t)}. \tag{6.4}$$

Thus one obtains a linear equation with respect to $B(t)/A(t)$, whose slope and intersect at the ordinate give $\hat{\sigma}_{34}$ and $\hat{\sigma}_{24}$, respectively. In the calculation of $A(t)$ and $B(t)$, the following nuclear data were used: $T_{1/2}(^{165m}\text{Dy}) = 1.258$ min[97], $T_{1/2}(^{165g}\text{Dy}) = 2.334$ hr[97], $T_{1/2}(^{166}\text{Dy}) = 81.6$ hr[98], $f = 0.9776$[97], $\hat{\sigma}_{12}=1700\pm250$ b[1], and $\hat{\sigma}_{13}=1000\pm150$ b[1].

The resulting values of $A(t)$ and $B(t)$ are presented together with those of $\lambda_4 N_4$ in **Table 6.4**. The errors attached to $\lambda_4 N_4$ were evaluated considering the error amounting to 1.5% in the counting efficiency besides uncertainty in the peak area. The uncertainty of I_γ equally affects each datum, so that it was propagated only in the evaluation of the cross section.

Table 6.4 Data for analyzing the dependence of ^{166}Dy-yields on irradiation time. The notations are explained in the text.

t (min)	nv_0 (10^{13} n·cm^{-2}sec^{-1})	$\lambda_4 N_4$ (10^2 dps)	$A(t)$ (10^{-21} cm^{2}sec)	$B(t)$ (10^{-21} cm^{2}sec)
3	2.17±0.04	0.150±0.016	0.040	0.067
5	2.01±0.03	0.346±0.017	0.087	0.204
7	2.01±0.03	0.821±0.032	0.137	0.42
10	2.17±0.04	1.801±0.062	0.215	0.89
20	2.17±0.04	7.11±0.15	0.48	3.9
60	2.01±0.03	53.4±0.82	1.52	35

There is a relation

$$\hat{\sigma}_{12}f+\hat{\sigma}_{13} = 2700\pm75 \text{ b}^{1)} \tag{6.5}$$

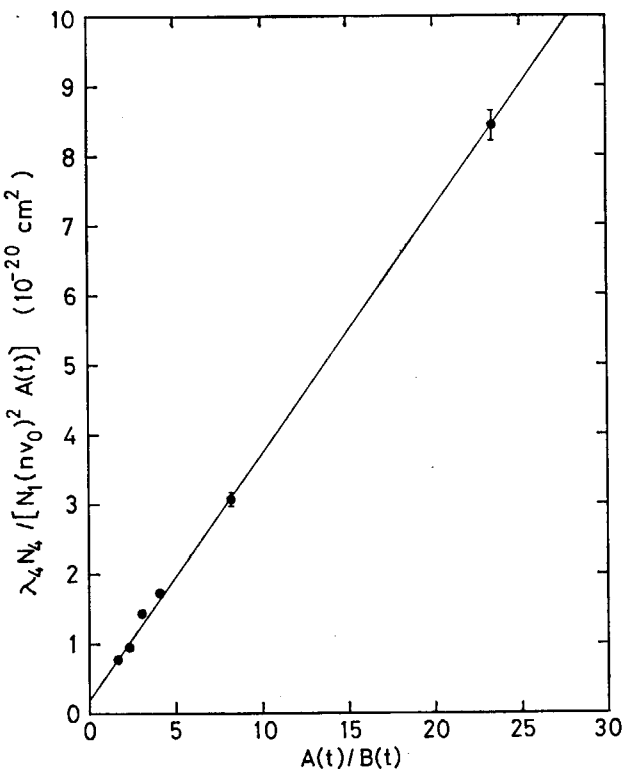

Fig. 6.7 Dependence of the yield on irradiation period. The intersect of the straight line equals to the value of $\hat{\sigma}_{24}$.

between $\hat{\sigma}_{12}$ and $\hat{\sigma}_{13}$, so that their errors are not independent of each other. In other words, the sum of $\hat{\sigma}_{12}f$ and $\hat{\sigma}_{13}$ has been measured with higher precision than each of them. It follows that a positive error in $\hat{\sigma}_{12}$ brings about a negative error in $\hat{\sigma}_{13}$. We also find difficulty in expressing the errors in $A(t)$ and $B(t)$ because either of them is a function of $\hat{\sigma}_{12}$ and $\hat{\sigma}_{13}$.

The quantity of the left-hand side of Eq. (6. 4) is plotted versus $B(t)/A(t)$, as shown in **Fig. 6. 7.** We obtained

$$\hat{\sigma}_{24} = 2000 \pm 600 \text{ b}, \tag{6. 6}$$

where the error by $\pm 0.5\%$ for N_1 and that given in **Table 6. 4** for nv_0 were taken into account as well as the uncertainty of $\lambda_4 N_4$. The result that

$$\hat{\sigma}_{34} = 3530 \pm 330 \text{ b} \tag{6. 7}$$

was deduced in turn from the 60-min irradiation data on the basis of Eq. (6. 5).

The resulting cross section data are summarized in **Table 6. 5** together with the reported values. The present work gives slightly smaller $\hat{\sigma}_{34}$ value than that of ref. 1. Comparison between them is, however, not probable in a strict sense because the experimental details of ref. 1 is not available.

Table 6. 5 Thermal neutron capture cross sections of ^{165m}Dy and ^{165g}Dy.

Reaction	Cross section (b)	Reference
^{165m}Dy(n, γ)^{166}Dy	$\hat{\sigma} = 2000 \pm 600$*	Present work
^{165g}Dy(n, γ)^{166}Dy	$\hat{\sigma} = 3530 \pm 330$*	Present work
	$\hat{\sigma} = 5000 \pm 2000$§	[36]
	$\sigma_0 = 3900 \pm 300$	[1]

* $r\sqrt{T/T_0} = 0.017$.

§ The value of $r\sqrt{T/T_0}$ is unknown. The uncertainty is given in the report of BNL-325, 2nd Edn., (1958).

6. 3. Discussion on the thermal-neutron-capture cross section of the nuclear isomer

There is a possibility of the (n, n′) reaction taking place even with neutrons of as low evergy as thermal energy[102]. Miyano and Morinaga[103] find that the ^{148m}Pm(n, n′)^{148g}Pm reaction cross section is less than 100 b, which is much smaller than the total cross section of the ^{148m}Pm(n, γ) ^{149}Pm reaction amounting to 22,000 b. Let us then assume similar situation is realized in other cases, too. That is, we shall consider the (n, γ) reaction alone in the following discussion.

If the (n, γ) reaction takes place via compound process, there is no difference expected between the metastable and ground states, except for the differences in the excitation energy and the spin. The thermal-neutron-capture cross section depends the most on how close a resonance level is to the thermal energy[104]. This is, however, not predictable for a given nuclide in general.

This problem can be statistically treated. The probability of finding a resonance level near the thermal energy would be, statistically speaking, proportional to the level density of the compound nucleus and, therefore, the capture cross section itself would be proportional to it, too.

In **Fig. 6. 8**, the thermal-neutron-capture cross sections of stable nuclides are plotted versus level densities of the compound nuclei. Both data are taken from ref. 1. Most data points lie within the band ranging from 1/10 to 10 times the mean values.

The level density of the compound nucleus was calculated by Gilbert-Cameron's method[92] used in

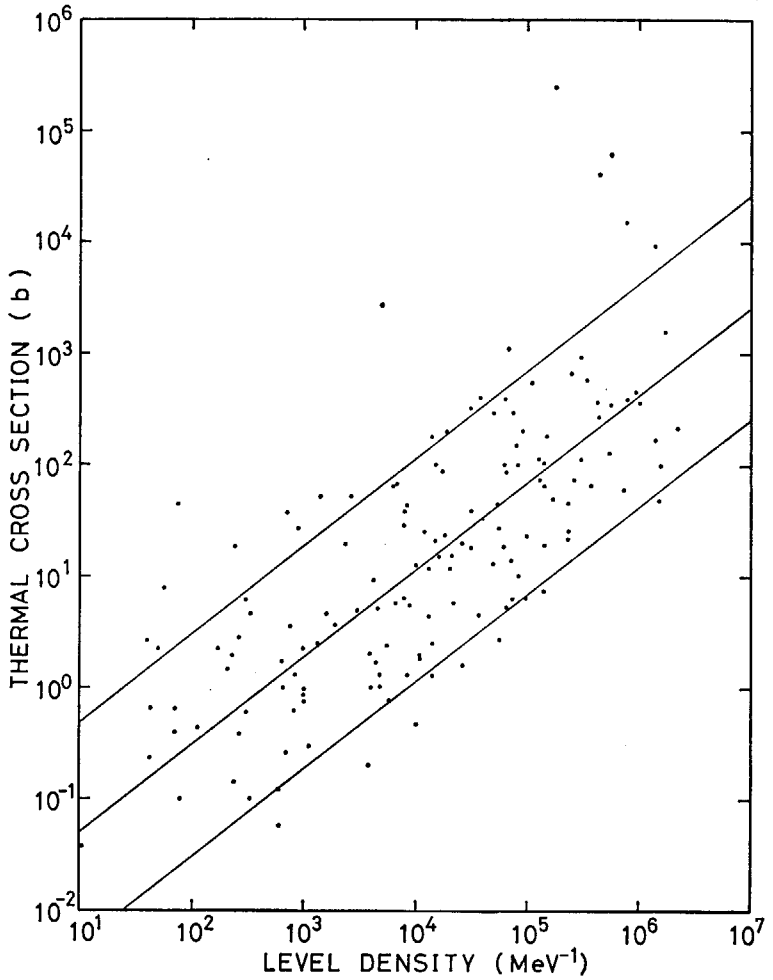

Fig. 6. 8 Thermal neutron capture cross sections plotted vs. nuclear level densities. The experimental data in reference[1] are used for both quantities.

Table 6. 6 Comparison between observed thermal-neutron-capture cross sections of isomers and calculated nuclear level densities of the compounds produced with these isomers. The notations are explained in the text.

Compound	Cross section* (b)		$\frac{\sigma^m}{\sigma^g}$	Spin§		Spin cutoff parameter	ε_m§	E_B§§	Nuclear level density (MeV^{-1})		$\frac{\rho_m}{\rho_g}$
	σ^m	σ^g		m	g		(MeV)	(MeV)	ρ_m	ρ_g	
^{59}Co	136000	1880	72	5	2	3. 3	0. 025	10. 46	8.6×10^{2}	1.13×10^{3}	0. 76
^{61}Co	58	2. 0	29	2	5	3. 3	0. 059	9. 34	1.26×10^{3}	9.2×10^{2}	1. 37
^{103}Rh	800	40	20	5	1	4. 7	0. 129	8. 98	3.4×10^{5}	1.51×10^{5}	2. 3
^{149}Pm	22000	2000	11	6	1	5. 3	0. 137	7. 27	4.0×10^{5}	1.53×10^{5}	2. 6
^{166}Dy	2000**	3530**	0. 57	1/2	7/2	5. 2	0. 108	7. 06	1.74×10^{4}	4.5×10^{4}	0. 39

* Reference[1]. ** Present work. § Reference[57]. §§ Reference[82].

section 5. 3. The s-wave neutron capture by the target nucleus of spin I forms either spin of I-1/2 or I+1/2. The level density of interest is then the sum of the level densities with the above two spin values calculated with Eqs. (5. 13) and (5. 15). **Table 6. 6** summarizes the cross section, spin, spin cutoff parameter, energy difference ε_m between metastable and ground states, neutron binding energy E_B, and level density. The capture cross section of the metastadle state is expressed as σ^m and that of the ground state is given by σ^g in order to distinguish them from the isomer formation cross sections of chapter 5. Since ε_m is small as compared with E_B, the difference in the level density is mainly brought about by the spin difference. The ratio of the level densities, ρ_m/ρ_g, lies btween 0. 4 and

2.6.

Comparing the cross-section data of the five nuclides in **Table 6.6** with the systematics shown in **Fig. 6.8**, one finds that three of the five σ^g values lie within the band, while four out of the five σ^m values are out of the band: an extraordinarily large cross setion of ^{58m}Co is considered to be due to the first resonance level lying very close to the thermal region. In the cases of ^{61}Co, ^{105}Rh, and ^{149}Pm, σ^m/σ^g values are about 10 times greater than ρ_m/ρ_g, which would be ascribed to the σ^m being out of the band by an order of magnitude. It is however, not yet clear whether this trend displays a meaningful difference of the metastable nuclei from the ground-state ones because of the scarcity of availailble data.

7. Summary

Studies of the double-neutron-capture process were carried out with much high sensitivity of the activity detection compared to the previous works, by combining the γ spectrometry with high-resolution Ge(Li) detector and chemical separation technique. Cross sections of reactions unmeasured hitherto were thus determined; namely, the $^{27}Mg(n,\gamma)^{28}Mg$, $^{94}Nb(n,\gamma)^{95m}Nb$, $^{94}Nb(n,\gamma)^{95g}Nb$, $^{165m}Dy(n,\gamma)^{166}Dy$, and $^{28}Al(n,p)^{28}Mg$ reactions.

In order to express the results in a form comparable with those measured under different neutron-irradiating conditions, the Westcott epithermal index, $r\cdot\sqrt{T/T_0}$, was explicitly determined by measuring the cadmium ratio for the formation of ^{60}Co or ^{198}Au. This made possible the comparison of the obtaind cross section of the $^{94}Nb(n,\gamma)^{95m+g}Nb$ reaction with the reported values. The result was in good agreement. An upper limit of the resonance integral in the $^{65}Ni(n,\gamma)^{66}Ni$ reaction was deduced by irradiating ^{64}Ni in irradiating holes with different epithermal indices. Previously reported cross-section data, significantly deviating from each other, were then discussed with regard to this upper limit.

We further observed the ^{28}Mg yield in the sequential $(n,p)(n,\gamma)$ reaction of aluminum by irradiation with neutrons, the $^{58}Ni(n,2n)^{57}Ni$ reaction cross section, and emmission rates of the ^{166}Dy 82.5-keV and the ^{166}Ho 80.6-keV γ rays.

The cross section of the $^{27}Mg(n,\gamma)^{28}Mg$ reaction was explained by the hard sphere capture. The study of the (n, 2n) reaction led us to an empirical equation expressing the cross sections.

The isomeric yield ratio presently observed for the capture process of ^{94}Nb was explained by the statistical model. The Huizenga-Vandenbosch prescription[6] with reasonable assumptions was found to reproduce the experimental data. More strict treatment by Pönitz's method[7] revealed that the computation was sensitively affected by the spin of the compound nucleus, the intensity of the quadrupole transition, and spins of low-lying discrete levels. It was concluded that the compound nuclear spin should be 11/2 and the low-lying levels to which alternative spin values were given were likely to have the lower spin value.

The present work clarified the thermal-neutron-capture cross section of ^{165m}Dy for the first time, which turned out to be smaller than that of ^{165g}Dy. The reverse is the situation with the four isomeric pairs whose capture cross sections are known for both members. Further studies of such capture process involving unstable nuclides would be quite interesting.

Acknowledgement

The authors are grateful to Dr. S. Baba for her valuable advice and discussion throughout this work. They are also indebted to Mr. T. Suzuki for his collaboration in the activity measurement.

References

1) Mughabghab S. F. and Garber D. I. : BNL-325, 3rd Edn. Vol. 1 (1973)
2) Blatt J. M. and Weisskopf V. F. : "Theoretical Nuclear Physics", John Wiley and Sons, New York (1952)
3) Lynn J. E. : "The theory of Neutron Resonance Reactions", Clarendon Press, Oxford (1968)
4) Morinaga H. and Isii C. : Prog. Theor. Phys., 23, 161 (1960)
5) Lane A. M. and Lynn J. E. : Nucl. Phys., 17, 586 (1960)
6) Huizenga J. R. and Vandenbosch R. V. : Phys. Rev., 120, 1305 (1960)

7) Pönitz W. P. : Z. Physik, 197, 262 (1966)
8) [^{27}Mg, ^{31}Si, ^{55}Cr] Roy L. P. and Yaffe L. : Can. J. Chem., 35, 176 (1957)
9) [^{27}Mg] Sekine T. and Baba H. : J. Inorg. Nucl. Chem., 40, 1457 (1978)
10) [^{41}Ar] Katcoff S. : Phys. Rev., 87, 886 (1952)
11) [^{51}Ti] Morinaga H., Miyano K., Fujiwara K., Chiba R., Ebisawa K. and Kawai N. : Phys. Lett., 25B, 22 (1967)
12) [^{60}Co] Brown F., Wolfson J. L. and Yaffe L. : Can. J. Phys., 31, 903 (1953)
13) [^{60}Co] Hogg C. H. and Weber L. D. : IN-1024 (1966)
14) [^{65}Ni] Pinajian J. J. : J. Inorg. Nucl. Chem., 31, 1241 (1969)
15) [^{65}Ni, ^{66}Cu, ^{198}Au] Serment V., Abu-Samra A. and Emmons A. H. : Nucl. Appl. Tech., 9, 662 (1970)
16) [^{65}Ni] Sekine T. and Baba H. : J. Inorg. Nucl. Chem., 40, 1977 (1978)
17) [^{66}Cu] Passel T. O. and Heath R. L. : Bull. Am. Phys. Soc., 3, 408 (1958)
18) [^{88}Rb] Roy J. C., Berry P. J. and Roy L. P. : Can. J. Chem., 36, 731 (1958)
19) [^{89}Sr] Roy L. P. and Roy J. C. : Can. J. Phys., 35, 1215 (1957)
20) [^{94}Nb] Douglass D. L, Mewherter A. C. and Schuman R. P. : Phys. Rev., 92, 369 (1953)
21) [^{94}Nb] Druschell R. E. and Halperin J. : ORNL-4306, 2 (1968) (unpublished)
22) [^{94}Nb] Schuman R. P. : WASH-1136, 52 (1969) (unpublished)
23) [^{94}Nb] Young T. E. and Serpa M. R. : IN-1407 (1970) (unpublished)
24) [^{94}Nb] Sekine T. and Baba H. : J. Inorg. Nucl. Chem., 40, 1973 (1978)
25) [^{105}Ru] Sharma B. L. : Nuovo Cimento, 17, 687 (1960)
26) [^{110m}Ag] Hart R. G. and Graham R. L. : Can. J. Phys., 41, 1321 (1963)
27) [^{124}Sb] Nishimura K., Ogawa S. and Tsutiya T. : J. Nucl. Sci. Tech., 16, 546 (1979)
28) [^{124}Sb] Courtemanche R., Eastwood T. A. and Werner R. D. : Can. J. Phys., 44, 2956 (1966)
29) [^{134}Cs] Bayly J. G., Brown F., Hall G. R. and Walter A. J. : J. Inorg. Nucl. Chem., 5, 259 (1958)
30) [^{139}Ba] Yaffe L., Sargent B. W., Kirsch M., Standil S. and Grundlund J. M. : Phys. Rev., 76, 617(1949)
31) [^{142}Pr] Smith R. R. and Reeder S. D. : J. Chem. Phys., 23, 2108 (1955)
32) [^{143}Ce] Roy L. P. and Yaffe L. : Can. J. Phys., 34, 238 (1956)
33) [^{154}Eu] Hayden R. J., Reynolds J. H. and Inghram M. G. : Phys. Rev., 75, 1500 (1949)
34) [^{160}Tb] Smith R. R., Reeder S. D. and Lewis R. H. : J. Chem. Phys., 25, 502 (1956)
35) [^{161}Gd] Wahlgren M. A., Stewart D. C., Lawless F. R., Hines J. J., Elynn K. F. and Lerner J. L. : Phys. Rev., 153, 1310 (1967)
36) [^{165}Dy] Ketelle B. H. : Phys., Rev., 76, 1256 (1949)
37) [^{171}Er] Miyano K. :J. Phys. Soc. Japan, 31, 1304 (1971)
38) [^{181}Hf] Wing J., Swartz B. A. and Huizenga J. R. : Phys. Rev., 123 , 1354 (1961)
39) [^{182}Ta] Murray J. J., Boehm F., Marmier P. and Dumond J. W. M. : Phys. Rev., 97, 1007 (1955)
40) [^{182}Ta] Mateosian E. der: Phys. Rev., 97, 1023 (1955)
41) [^{182}Ta] Stokes G. E., Schuman R. P. and Simpson O. D. : Nucl. Sci. Eng., 33, 16 (1968)
42) [^{187}W, ^{188}Re, ^{193}Os] Lindner M. : Phys. Rev., 84, 240 (1951)
43) [^{188}Re] Smith R. R. : J. Inorg. Nucl. Chem., 3, 157 (1956)
44) [^{198}Au] Hill R. D. and Mihelich J. W. : Phys. Rev., 79, 275 (1950)
45) [^{198}Au] Bell R. E., Graham R. L. and Yaffe L. : Can. J. Phys., 33, 457 (1955)
46) [^{198}Au] Cabell M. J. and Willkins M. : J. Inorg. Nucl. Chem., 31, 1229 (1969)
47) [^{199}Pt] Roy L. P., Roy J. C. and Merritt J. S. : Phys. Rev., 105, 1337 (1957)

48) Hogg C. H., Weber L. D. and Yates E. C. : IDO-16744 (1962)
49) Schuman R. P. and Berreth J. R. : Nucl. Sci. Eng., **12**, 519 (1962)
50) Otozai K., Sekine T., Arakawa R., Hata K., Saito T. and Baba H. : unpublished
51) JRR-2 Operation Section: JAERI-memo 4141 (1970) [in Japanese]
52) Baba H., SeKine T., Baba S. and Okashita H. : JAERI-1227 (1972)
53) Sekine T. and Baba H. : Nucl. Instr. Meth., **127**, 261 (1975)
54) Natsume H. : At. Energy Soc. Jpn., **12**, 551 (1970) [in Japanese]
55) Storm E. and Israel H. I. : LA-3753 (1967)
56) Westcott C. H., Walker W. H. and Alexander T. K. : "Proc. 2nd Int. Conf. Peaceful Uses of Atomic Energy, Geneva", United Nations, New York, **16**, 70 (1958)
57) Lederer C. M., Hollander J. M. and Perlman I. : "Table of Isotopes", 6th Edn., John Wiley and Sons, New York (1968)
58) Sekine T. and Baba H. : J. Radioanal. Chem. **45**, 155 (1978)
59) Calamand A. : STI/DOC/10/156, 273 (1974)
60) Mellisch C. E. and Crookford G. W. : Int. J. Appl. Radiat. Isot., **1**, 299 (1957)
61) Schiffer J. P. and Vandenbosch R. : Phys. Lett., **5**, 292 (1963)
62) Alburger D. E. and Harris W. R. : Phys. Rev., **185**, 1495 (1969)
63) Crouthamel C. E. : "Applied Gamma-Ray Spectrometry", Pergamon Press, New York, 106 (1960)
64) Uno Y. : "Zyuryobunseki II" (Gravimetric Analysis II), Kyoritsu Schuppan, Tokyo, 97 (1955) [in Japanese]
65) Devancy J. J: LA-1960 (1955) (unpublished)
66) Ryves T. B. : J. Nucl. Energy, **24**, 35 (1970)
67) Seren L., Friedlander H. N. and Turkel S. H. : Phys. Rev., **72**, 888 (1947)
68) Lyon W. S. and Lazer N. H. : Phys. Rev., **101**, 1524 (1956)
69) Spiling P., Gruppelaar H. and Kamp A. M. F. Op Den: Nucl. Phys., **A102**, 209 (1967)
70) Mughabghab S. F. : "Proc. Int. Symp. on Neutron Capture Gamma-Ray Spectroscopy, Petten, 1974", Reactor Centrum Nederland, Petten, 53 (1975)
71) Bird J. R. : "Proc. Int. Symp. on Neutron Capture Gamma-Ray Spectroscopy, Petten, 1974", Reactor Centrum Nederland, Petten, 160 (1975)
72) Roy J. C. and Hawton J. J. : AECL-1181 (1960)
73) Beeck J. Op. de, Speecke A. and Hoste J. : Radiochim. Acta, **4**, 32 (1965)
74) Deschuyter M., Massart D. L., Speecke A. and Hoste J. : Radiochim. Acta, **10**, 11 (1968)
75) Regge P. de, Dams R. and Hoste J. : Radiochim. Acta, **19**, 102 (1973)
76) Schumann R. P. and Mewherter A. C. : KAPL-1779 (1957)
77) Braun H. and Nazy L. : Radiochim. Acta, **10**, 15 (1968)
78) Kobayashi K., Kimura I., Nakazawa M. and Akiyama M. : J. Nucl. Sci Tech., **13**, 531 (1976)
79) Pearlstein S. : Nucl. Data **A3**, 327 (1967)
80) Flerov N. N. and Talyzin V. M. : J. Nucl. Energy, **4**, 529 (1957)
81) Barr D. W., Brown C. I. and Gilmore J. S. : Phys. Rev., **123**, 859 (1961)
82) Gove N. B. and Wapstra A. H. : Nucl. Data, **A11**, 127 (1972)
83) Theodore M. L. : Anal. Chem., **30**, 465 (1958)
84) Kocher D. C. : Nucl. Data Sheets, **10**, 241 (1973)
85) Medsker L. R. and Horen D. J. : Nucl. Data, **B8**, 29 (1972)
86) Meixner Chr. : JÜL-811-RX (1971)
87) Baba H. and Okashita H. : unpublished
88) Bethe H. A. : Rev. Mod. Phys., **9**, 84 (1937)
89) Bloch C. : Phys. Rev., **93**, 1094 (1954)

90) Dudey N. D. and Sugihara T. T. : Phys. Rev., **139**, B896 (1965)
91) Saha G. B. and Yaffe L. : Nucl. Phys., **A188**, 409 (1972)
92) Gilbert A. and Cameron A. G. W. : Can. J. Phys., **43**, 1446 (1965)
93) Groshev L. V., Demidov A. M., Lutsenko V. N. and Pelekhov V. I., : "Proc. 2nd Int. Conf. Peaceful Uses of Atomic Energy, Geneva", United Nations, New York, **15**, 138 (1958)
94) Wilkinson D. H. : "Nuclear Spectroscopy, Part B", Academic Press, New York, 852 (1960)
95) Löbner K. E. G. : Phys. Lett., **26B**, 369 (1968)
96) Natsume H., Umezawa H., Kailova V. Mi, Suzuki T. and Sato T. : "Proc. 6th Conf. Radioisotopes", Japan Atomic Industrial Forum, Tokyo, 80 (1964) [in Japanese]
97) Buyrn A. : Nucl. Data Sheets, **11**, 189 (1974)
98) Buyrn A. : Nucl. Data Sheets, **14**, 559 (1975)
99) Cline J. E., Yates E. C. and Turk E. H. : Nucl. Phys., **30**, 154 (1962)
100) Neumann H. A. : Z. Naturforsch., **21a**, 1328 (1966)
101) Burson S. B., Goudsmit P. F. A. and Konijin J. : Phys. Rev., **158**, 1161 (1967)
102) Petrov Yu. V. and Shlyakhter A. I. : Sov. J. Nucl. Phys., **23**, 631 (1977)
103) Miyano K. and Morinaga H. : J. Phys. Soc. Jpn., **23**, 576 (1969)
104) Bogart D. : Nucleonics, **10**, No. 10, 35 (1952)
105) Zweifel P. F. : Nucleonics, **18**, No. 11, 174 (1960)
106) See, for example, Platt L. G. : "Probability and Experimenta Errors in Science", John Wiley and Sons, New York (1961).

Appendices

Appendix 1. Expression of the Effective Cross Section by the Westcott Convention

Westcott *et al.*[56] give a method analyzing cross section data of reactor neutron reactions in connection with the neutron spectrum. This convention is not necessarily popular in the radiochemical field of this country, and one finds once in a while its ambiguous description. Therefore, we like to give a brief description of the Westcott convention here to clarify our presentation.

There exist neutrons in a wide energy range, from thermal energies to high energies of MeV order, in the reactor. They are classified into three groups: thermal neutrons following the Maxwellian distribution, epithermal neutrons reciprocally proportional to the energy above 0.1 eV, and fission neutrons in the MeV-energy region. Thermal neutrons, and epithermal ones to less extent though, contribute to the formation of radioactive nuclei in the neutron-capture process.

According to Westcott *et al.*[56], the effective cross section $\hat{\sigma}$ of the (n,γ) reaction is expressed as

$$\hat{\sigma} = \sigma_0(g+r\cdot\sqrt{T/T_0}\cdot s_0), \tag{A1.1}$$

where σ_0 is the cross section with 2200 m/sec neutrons. $r\cdot\sqrt{T/T_0}$ is a parameter representing the fraction of epithermal neutrons in the neutron spectrum and is called epithermal index. g and s_0 give the effect due to deviation of the cross section from the $1/v$ law in thermal and epithermal regions, respectively. Here, g is epual to 1 when the $1/v$ law holds while it depends on the neutron temperature T if not. On the other hand, $s_0 = 0$ if the $1/v$ law holds, and otherwise $s_0 = (2/\sqrt{\pi})(I_0'/\sigma_0)$. Here, I_0' is the resonance integral subtracted by its $1/v$-component.

By the use of the effective reaction cross section defined by Eq. (A1.1), the reaction rate per nucleus is given by

$$R = nv_0\hat{\sigma} = nv_0\sigma_0\,(g+r\cdot\sqrt{T/T_0}\cdot s_0), \tag{A1.2}$$

where n is the neutron density including both thermal and epithermal neutrons, and $v_0 = 2200$m/sec.

The epithermal index can be deduced from the cadmium ratio

$$R_{Cd} = \frac{\text{Activity yield without cadmium cover}}{\text{Activity yield with cadmium cover}}$$

as

$$r\cdot\sqrt{T/T_0} = \frac{g}{R_{Cd}(s_0+g/K)-s_0}, \tag{A1.3}$$

where K is a factor depending on the thickness of the used cadmium cover and is given in ref. 56.

For a thick target, one must take into account the self-shielding factors of thermel neutrons, G_{th}, and epithermal ones, G_{epi}. Equations (A1.2) and (A1.3) are then replaced, respectively, by

$$R = nv_0\sigma_0(g\cdot G_{th}+r\cdot\sqrt{T/T_0}\cdot s_0G_{epi}), \tag{A1.4}$$

and

$$r\cdot\sqrt{T/T_0} = \frac{g\cdot G_{th}}{R_{Cd}(s_0G_{epi}+g/K)-s_0G_{epi}}. \tag{A1.5}$$

Here, G_{th} and G_{epi} are given in refs. 105 and 58, respectively.

As shown above, one needs to know parameters σ_0, g, and s_0 in the reaction experiments with reactor neutrons. Such information can be extracted from experiments of changing the epithermal index in a wide range. However, a low epithermal index value generally correponds to low neutron flux, nv_0, so that precise determination of $\hat{\sigma}$ becomes difficult under such condition for reactions of

very small probability as double-neutron-capture process. It follows that σ_0 and s_0 cannot be deduced with sufficient accuracy. In the present work, the $^{65}Ni(n,\gamma)^{66}Ni$ reaction could be studied for different values of the epithermal index, but only an upper limit was obtained for s_0. In the other experiments, we merely gave the observed value of the epithermal index with the purpose of clarifying the neutron irradiation condition in such a way that intercomparison with other works is possible.

In simple radiochemical measurent of the reaction cross section, g cannot be determined and the resulting cross section reported as thermal-neutron cross section correponds to $\sigma_0 g$ instead of σ_0. It is, however, expressed as σ_0 in most cases because g is generally approximated to be 1. In the case of double-neutron-capture reaction, $\hat{\sigma}$ is named reactor (or pile)-neutron cross section or more frequently thermal-neutron cross section. We also called both $\hat{\sigma}$ and σ_0 as thermal-neutron(-capture) cross section as long as no confusion was caused, though they were distinguished in the presentation of experimental data.

Appendix 2. Computer Program for Determination of the Fission Neutron Flux by the Monitoring with the $^{58}Ni(n,p)^{58}Co$ Reaction

Let us consider an intermittent neutron irradiation as shown in **Fig. A1**, where t gives the length of the irradiation time and s is the length of intermission.

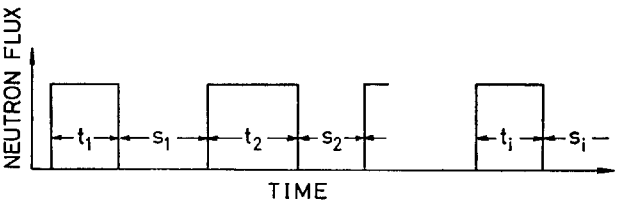

Fig. A1 An explanatory drawing for notations, t_i and s_i, used in the calculation of ^{58}Co produced in the case of intermittent irradiation.

The (n, p) reaction of ^{58}Ni produces ^{58m}Co and ^{58g}Co, and the former decays into the latter by 100% isomeric transition[57]. Let us denote the cross sections of the formation and the neutron capture of either ^{58m}Co or ^{58g}Co with σ and $\hat{\sigma}$, repectively, designated with suffix m or g, and the decay constant with λ. The following equations then give the effective decay constants of ^{58m}Co and ^{58g}Co:

$$\left.\begin{aligned} \Lambda_m &= \lambda_m + n v_0 \hat{\sigma}_m \\ \Lambda_g &= \lambda_g + n v_0 \hat{\sigma}_g \end{aligned}\right\}. \qquad \text{(A2. 1)}$$

The number of nuclei $N(t_i)$ formed immediately after the ith irradiation of the length t_i, and that surviving after s_i, $N(s_i)$, are then derived as

$$N_m(t_i) = N_m(s_{i-1})e^{-\Lambda_m t_i} + N_0 \phi_t \sigma_m \frac{1-e^{-\lambda_m t_i}}{\Lambda_m}, \qquad \text{(A2. 2)}$$

$$N_g(t_i) = N_g(s_{i-1})e^{-\Lambda_g t_i} + N_0 \phi_t \sigma_g \frac{1-e^{-\Lambda_g t_i}}{\Lambda_g} + N_0 \phi_t \sigma_m \frac{\lambda_m}{\Lambda_m}\left(\frac{e^{-\Lambda_m t_i} - e^{-\Lambda_g t_i}}{\Lambda_m - \Lambda_g} + \frac{1-e^{-\Lambda_g t_i}}{\Lambda_g}\right)$$

$$+ N_m(s_{i-1}) \frac{\lambda_m}{\Lambda_g - \Lambda_m}(e^{-\Lambda_m t_i} - e^{-\Lambda_g t_i}), \qquad \text{(A2. 3)}$$

$$N_m(s_i) = N_m(t_i)e^{-\lambda_m s_i}, \qquad \text{(A2. 4)}$$

and

$$N_g(s_i) = N_g(t_i)e^{-\lambda_g s_i} + N_m(t_i)\frac{\lambda_m}{\lambda_g-\lambda_m}(e^{-\lambda_m s_i} - e^{-\lambda_g s_i}), \quad \text{(A2.5)}$$

where N_0 is the number of ^{58}Ni nuclei and ϕ_f gives fission neutron flux.

The above equations are written in FORTRAN program, which is listed in **Fig. A2**. The output is given in the form of the produced ^{58}Co activity in dps in the irradiation of 1 mg of nickel metal with $\phi_f = 1.0\times10^{13}$ n·cm^{-2}. sec^{-1}. An example of the output is shown in **Fig. A3** and **Table A1** gives the directory of input data.

Appendix 3. Program for Calculating the Isomer Yield Ratio by Ponit's Method and the Instruction Manual

In **Fig. A4** is shown a program written with FORTRAN IV. This program consists of two subroutine programs, **TRAPOS** giving the transition probability and **LVLDGC** evaluating the nuclear level density, besides the main program. The memory size of the program is 24k words. Required input data are illustrated in **Table A2**, and an example of the output is shown in **Fig. A5**.

Table A1 The formats of the input cards for code **NICO**.

Card No.	Symbol	Columns	Format	Description
1	HFM	1—12	F12.4	Half-life of ^{58m}Co (hr); 9.1 hr if HFM=0
	HFG	13—24	F12.4	Half-life of ^{58g}Co (day); 71.3 day if HFG=0
	SIGFM	25—36	F12.4	Cross section of ^{58}Ni(n, p)^{58}Co reaction (b) ; 0.0354 b if SIGFM=0
	SIGFG	37—48	F12.4	Cross section of ^{58}Ni(n, p)^{58g}Co reaction(b); 0.078 b if SIGFG=0
	SIGMT	49—60	F12.4	Cross section of Co(n, γ)^{59}Co reaction (b) ; 1.36×10^5 b if SIGMT =0
	SIGGT	61—72	F12.4	Cross section of ^{58g}Co(n, γ)^{59}Co reaction (b); 1880 b if SIGGT=0
2	THMF	1—12	E12.5	nv_0 (n·cm^{-2}sec^{-1})
	NT	13—14	I2	Number of times of intermission of reactor operation
	COM	15—38	6A4	Comments
3	(T(I), S(I))		8F10.3	Elapse of time (hr); see **Fig. A1**; I=1, NT
4	JSTP	1	I1	=0 End of calculation =1 Continuation from reading No. 1 card =2 Continuation from reading No. 2 card =3 Continuation from reading No. 3 card

Table A2 The formats of the input cards for code **ISOM**.

Card No.	Symbol	Columns	Format	Description
1	CMNUCL	1—8	2A4	Compound nucleus
	IZ	9—12	I4	Atomic number of compound nucleus
	IN	13—16	I4	Neutron number of componnd nucleus
	COM	17—84	17A4	Comments
2	NDC	1—4	I4	Number of discrete levels containing metastable and ground states; less than 50
	ETH	5—14	F10.4	Threshold energy above which the level density is calculated with the formulae (MeV); the highest energy among the discrete levels if ETH=0
3	(EDC(I),		4(F10.6,	Energy of the I-th discrete level (MeV)
	SPDC(I),		F8.4,	Spin of the level
	IPDC(I))		I2)	=even number plus parity of the level =odd number minus parity of the level; I=1, NDC; I=1 for ground state and I=2 for metastable state

4	ECM	1—10	F10.6	Excitation energy of the compound nucleus (MeV)
	SPINCM	11—18	F8.4	Spin of the compound nucleus
	IPCM	19—20	I2	=even number plus parity of the compound nucleus =odd number minus parity of the compound nucleus
5	CM1	1—10	E10.3	Coefficient for intensity of M1 transition (Coefficient for intensity of E1 transition=1)
	CE2	11—20	E10.3	Coefficient for intensity of E2 transition
	CM2	21—30	E10.3	Coefficient for intensity of M2 transition
6	MODE	1—2	I2	=0 Calculation with a fixed spin cutoff parameter which equals that of compound nucleus =1 Calculation with spin cutoff parameters depending on the energy of levels
	IPRINT	3—4	I2	=0 Printing final results only =1 Printing populations in discrete levels during the cascade process =2 Printing populations in discrete and continuous levels during the cascade process
7	RDLM	1—10	E10.3	Calculation stops when the sum of populations in metastable and ground states exceeds 1-RDLM; 1×10^{-5} if RDLM=0
	IECN	11—14	I4	Numder of mesh in energy; 20 if IECN=0; less than 100
	JE	15—18	I4	Nunder of mesh in spin; 10 if JE=0; less than 20
8	ISTOP	1—2	I2	=0 End of execution =1 Continuation from reading No. 1 card =2 Continuation from reading No. 2 card =3 Continuation from reading No. 4 card =4 Continuation from reading No. 5 card =5 Continuation from reading No. 6 card =6 Continuation from reading No. 7 card

Fig. A2 FORTRAN IV program **NICO** for calculating the radioactivity of ^{58}Co produced via $^{58}Ni(n, p)^{58}Co$ reaction under the influence of burn-out of ^{58m}Co and ^{58g}Co in the intermittnt irradiation.

```
      C
      C   1976.2.12.
      C   CO-58 ACTIVITY INDUCED IN NICKEL.
      C   THIS CODE USED FOR INTERMITTENT IRRADIATION AND FOR CORRECTION OF
      C   THE BURN-OUT OF CO-58M AND CO-58G
      C
    1       REAL NM,NG,MEUM,MEUG,N1,NM0,NMT
    2       DIMENSION T(100),S(100),COM(6)
    3       DATA  SIGFM0,SIGFG0,SIGMT0,SIGGT0/0.0354,0.078,136000.,1880./
    4       DATA  HFM0,HFG0/9.1,71.3/
    5     100 READ(5,1,END=900) HFM,HFG,SIGFM,SIGFG,SIGMT,SIGGT
    6       IF(HFM.LT.1.E-20) HFM = HFM0
    7       IF(HFG.LT.1.E-20) HFG = HFG0
    8       IF(SIGFM.LT.1.E-20) SIGFM = SIGFM0
    9       IF(SIGFG.LT.1.E-20) SIGFG = SIGFG0
   10       IF(SIGMT.LT.1.E-20) SIGMT = SIGMT0
   11       IF(SIGGT.LT.1.E-20) SIGGT = SIGGT0
   12       WRITE(6,1005) HFM,HFG,SIGFM,SIGFG,SIGMT,SIGGT
   13       HFG = HFG*24.
   14       DCM = 0.6931/HFM
   15       DCG = 0.6931/HFG
   16       SIGFM = SIGFM*1.E-24
   17       SIGFG = SIGFG*1.E-24
   18       SIGMT = SIGMT*1.E-24
   19       SIGGT = SIGGT*1.E-24
   20     200 READ(5,2,END=900) THMF,NT,COM
   21       IF(NT.LT.1) NT=1
   22       MEUM = DCM*THMF*SIGMT*3600.
   23       MEUG = DCG*THMF*SIGGT*3600.
   24       WRITE(6,1010) (COM(I),I=1,6)
   25       WRITE(6,1015) THMF,NT
   26       WRITE(6,1020) MEUM,MEUG
   27       WRITE(6,1025)
   28       FASTF = 1.E13
   29       N1 = 6.96E18
   30       WRITE(6,1030)
   31       TTOT =0.
   32     300 READ(5,3,END=900) ((T(I),S(I)),I=1,NT)
   33       NM = 0.
   34       NG = 0.
   35       DO 500 I=1,NT
   36       NM0 = NM
   37       NM = NM*EXP(-MEUM*T(I))+N1*FASTF*SIGFM*(1-EXP(-MEUM*T(I)))/MEUM
   38       NMT = NM
   39       NG = NG*EXP(-MEUG*T(I))+N1*FASTF*SIGFG*(1-EXP(-MEUG*T(I)))/MEUG
           1    +N1*FASTF*SIGFM*DCM/MEUM*((EXP(-MEUM*T(I))-EXP(-MEUG*T(I)))/
           2    (MEUM-MEUG)+(1-EXP(-MEUG*T(I)))/MEUG)
           3    +NM0*DCM/(MEUG-MEUM)*(EXP(-MEUM*T(I))-EXP(-MEUG*T(I)))
   40       NM = NM*EXP(-DCM*S(I))
   41       NG = NG*EXP(-DCG*S(I))+NMT*DCM/(DCG-DCM)*(EXP(-DCM*S(I))-EXP(-DCG*
           1    S(I)))
   42       AM = DCM*NM
   43       AG = DCG*NG
   44       TTOT = TTOT+T(I)+S(I)
   45     500 WRITE(6,1035) I,T(I),S(I),TTOT,AM,AG
   46       WRITE(6,1040)
   47       READ(5,4,END=900) JSTP
   48       IF(JSTP.EQ.0) GO TO 900
   49       GO TO(100,200,300),JSTP
   50     900 STOP
   51       1 FORMAT(6F12.4)
   52       2 FORMAT(E12.5,I2,6A4)
   53       3 FORMAT(8F10.3)
   54       4 FORMAT(I1)
   55    1005 FORMAT(1H1,////30X,41H**** USED HALF-LIFE AND CROSSSECTION ****,//
           132X,19HHALF-LIFE(CO-58M) =,F6.2, 5H (HR), 7X,19HHALF-LIFE(CO-58G)
           2=,F6.2, 6H (DAY),
           3      /32X,19HCROSSSECTION (BARN)/35X,19HNI-58(N,P)CO-58M = ,F7.4/
           235X,19HNI-58(N,P)CO-58G = ,F7.4/35X,19HCO-58M(N,G)CO-59 = , F7.0/
           435X,19HCO-58G(N,G)CO-59 = ,F7.0)
   56    1010 FORMAT(//30X, 5H**** ,6A4, 5H ****)
   57    1015 FORMAT(//35X,23HTHERMAL NEUTRON FLUX = ,E12.5,13H(N/CM**2/SEC)/
           140X, 6H NT = ,I2)
   58    1020 FORMAT(/30X,29HEFFECTIVE DECAY CONSTANT(/HR)/
           1 36X, 8HCO-58M  ,E12.5/36X, 8HCO-58G  ,E12.5)
   59    1025 FORMAT(//20X,16H WE SUPPOSE THAT/25X,25HFAST NEUTRON FLUX = 1.E13/
           125X,33H WEIGHT OF NICKEL = 1.0 MILLIGRAM)
   60    1030 FORMAT(   ////25X,51H I IRR. TIME  CO. TIME  TOT. TIME  CO-58M
           1CO-58G/28X,50H  (HOUR)     (HOUR)     (HOUR)      (DPS)      (DPS)  /)
   61    1035 FORMAT(24X,I3,1X,3F10.2,2E11.4)
   62    1040 FORMAT(1H1)
   63         END
```

Fig. A3 An example of the output for computer program **NICO.**

```
**** USED HALF-LIFE AND CROSSSECTION ****

  HALF-LIFE(CO-58M) =  9,10 (HR)        HALF-LIFE(CO-58G) = 71,30 (DAY)
  CROSSSECTION (BARN)
     NI-58(N,P)CO-58M =  0,0354
     NI-58(N,P)CO-58G =  0,0780
     CO-58M(N,G)CO-59 = 136000,
     CO-58G(N,G)CO-59 =   1880,


**** JRR-2-48-07 RUN-1         ****


     THERMAL NEUTRON FLUX =  0,16700E+15(N/CM**2/SEC)
           NT =  2

EFFECTIVE DECAY CONSTANT(/HR)
      CO-58M   0,15793E+00
      CO-58G   0,15353E-02


WE SUPPOSE THAT
   FAST NEUTRON FLUX = 1,E13
    WEIGHT OF NICKEL = 1,0 MILLIGRAM



 I IRR, TIME  CO, TIME  TOT, TIME  CO-58M     CO-58G
     (HOUR)     (HOUR)     (HOUR)     (DPS)      (DPS)

 1     238,10      31,40     269,50 0,1087E+06 0,5313E+06
 2      21,90     121,50     412,90 0,1105E+03 0,5474E+06
```

Fig. A4 FORTRAN IV program **ISOM** for calculating the isomeric cross-section ratio in the thermal neutron capture.

```
C   CALCULATION OF NUCLEAR ISOMER RATIO IN (N,G) REACTION
C   FEB. 18,1976
C
C   CMNUCL(2) COMPOUND NUCLEUS
C   IZ        PROTON NUMBER OF COMPOUND NUCLEUS
C   IN        NEUTRON NUMBER OF COMPOUND NUCLEUS
C   COM(17)   COMMENTS
C   NDC       NUMBER OF DISCRETE LEVELS CONTAINING METASTABLE AND
C             GROUND STATE
C   ETH       THE LEVELS ARE CONTINUOUS ABOVE ETH (IN MEV UNIT)
C   EDC(I)    ENERGY OF THE I-TH DISCRETE LEVEL (IN MEV UNIT)
C   SPDC(I)   SPIN OF ITS LEVEL
C   IPDC(I)=0 PLUS PARITY OF ITS LEVEL
C          =1 MINUS PARITY OF ITS LEVEL
C             (I=1 FOR THE GROUND STATE, I=2 FOR THE METASTABLE STATE)
C   SDD(I,J)  TRANSITON PROBABILITY FROM THE I-TH DISCRETE LEVEL TO THE
C             J-TH DISCRETE LEVEL (SDD(I,I)=0., IF I IS SMALLER THAN J,
C             SDD(I,J)=0., SDD(2,1)=0.)
C   ECM       EXCITED ENERGY OF THE COMPOUND NUCLEUS (IN MEV UNIT)
C   SPINCM    SPIN OF THE COMPOUND NUCLEUS
C   IPCM   =0 PLUS PARITY OF THE COMPOUND NUCLEUS
C          =1 MINUS PARITY OF THE COMPOUND NUCLEUS
C
C   CM1       RELATIVE TRANSITION COEFFICIENT FOR M1 TRANSITION (CE1=1.)
C   CE2       RELATIVE TRANSITION COEFFICIENT FOR E2 TRANSITION (CE1=1.)
C   CM2       RELATIVE TRANSITION COEFFICIENT FOR M2 TRANSITION (CE1=1.)
C   MODE   =0  SPIN CUT-OFF PARAMETER IS CONSTANT
C          =1  SPIN CUT-OFF PARAMETER DEPENDS ON ENERGY
C   IPRINT =0  PRINT OF N,H(N),R,RDL
C   IPRINT =1  PRINT OF POPULATIONS IN DISCRETE LEVELS
C   IPRINT =2  PRINT OF POPULATIONS IN DISCRETE AND CONTINUOUS LEVELS
C   IECN   MESH NUMBER OF ENERGY
C   JE     MESH NUMBER OF SPIN
C   RDLM       CONVERGENCE LIMIT. CALCULATION STOPS WHEN RD
C              BECOMES LESS THAN RDLM,
C
C
 1       DIMENSION CMNUCL(2),COM(17),EDC(50),SPDC(50),IPDC(50),
        1          WCN(100,20,2,2),WDC(50,2),R(2),BC(100,20,2),BD(50),
        2          H(50),JES(100)
 2       COMMON /TRANS/CE1,CM1,CE2,CM2
 3   100 READ(5,1,END=900) CMNUCL,IZ,IN,COM
 4   110 READ(5,2,END=900) NDC,ETH
 5       READ(5,3) ((EDC(I),SPDC(I),IPDC(I)),I=1,NDC)
 6   120 READ(5,3,END=900) ECM,SPINCM,IPCM
 7   130 READ(5,6,END=900) CM1,CE2,CM2
 8   135 READ(5,8,END=900) MODE,IPRINT
 9   140 READ(5,7,END=900) RDLM,IECN,JE
10       IF(RDLM.LT.1.E-50) RDLM = 1.E-5
11       IF(IECN.LE.1) IECN = 20
12       IF(JE.EQ.0) JE = 10
13       IF(ETH.LT.EDC(2)) ETH = EDC(2) + DE
14       SPINZR = SPINCM - IFIX(SPINCM) + 1
15       SPMAX = 0.
16       DO 160 I=1,NDC
17   160 IF(SPMAX.LT.SPDC(I)) SPMAX = SPDC(I)
18       JMIN = SPMAX - SPINZR
19       DO 165 I=1,IECN
20       JES(I) = JMIN + 2*I
```

Fig. A4 (continued)

```
      165 IF(JES(I).GT.JE) JES(I) = JE
          DO 200 IE=1,IECN
          DO 200 J=1,JE
          DO 200 IP=1,2
      200 WCN(IE,J,IP,1) = 0.
          IF(IPCM.EQ.0) IPCM = 2
          DO 210 I = 1,NDC
          IF(IPDC(I).EQ.0) IPDC(I) = 2
      210 CONTINUE
          DO 220 IDC=1,NDC
      220 WDC(IDC,1) = 0.
          WRITE(6,905) CMNUCL,IZ,IN,COM
          WRITE(6,910) NDC,ETH
          WRITE(6,915)
          DO 230 IDC=NDC,1,-1
      230 WRITE(6,920) IDC,EDC(IDC),SPDC(IDC),IPDC(IDC)
          WRITE(6,935) ECM,SPINCM,IPCM
          CE1 = 1.
          WRITE(6,940) CE1,CM1,CE2,CM2
          WRITE(6,960) MODE
          WRITE(6,945) RDLM,IECN,JE
          WRITE(6,947)
          UCM = ECM
          CALL LVLDGC(D,IZ,IN,UCM,SPINCM,SIGM,MODE,0)
          DE = (UCM - ETH)/IECN
          N = 1
      250 IF(N.NE.1) IECN = IECN - 1
          IF(IECN.LE.0) GO TO 700
          IF(N.NE.1) IECN2 = IECN + 1
          IPIN2 = 2
          IF(IPRINT.LE.1) GO TO 260
          WRITE(6,965)
      260 DO 400 IEFN=1,IECN
          ENGFN = (IEFN - 0.5)*DE + ETH
          JE2 = JES(IEFN)
          DO 400 JFN=1,JE2
          SPINFN = JFN + SPINZR
          DO 400 IPFN=1,2
          W = 0.
          IF(N.EQ.1) IECN2 = 1
          DO 350 IEIN=1,IECN2
          ENGIN = (IEIN - 0.5)*DE+ ETH
          JE2 = JES(IEIN)
          IF(N.NE.1) GO TO 270
          ENGIN = UCM
          JE2 = 1
      270 DO 350 JIN=1,JE2
          SPININ = JIN + SPINZR
          IF(N.NE.1) GO TO 280
          SPININ = SPINCM
          IPIN2 = 1
      280 DO 350 IP = 1,IPIN2
          IPIN = IP
          IF(N.EQ.1) IPIN = IPCM
          CALL TRAPOS(SCC,ENGIN,SPININ,IPIN,ENGFN,SPINFN,IPFN)
          IF(N.GT.2.AND.SCC.LT.1.E-30) GO TO 350
          IF(N.EQ.1) GO TO 300
          IF(N.GT.2) GO TO 340
          IF(IPFN.GT.1) GO TO 340
          IF(JFN.GT.1) GO TO 340
          IF(IEFN.GT.1) GO TO 340
      300 BCN = 0.
          DO 310 IEFNN=1,IECN
          ENGFNN = (IEFNN - 0.5)*DE + ETH
          JE2 = JES(IEFNN)
          DO 310 JFNN=1,JE2
          SPINFNN = JFNN + SPINZR
          CALL LVLDGC(D,IZ,IN,ENGFNN,SPINFNN,SIGM,MODE,1)
          D = 0.5*D*DE
          DO 310 IPFNN=1,2
          CALL TRAPOS(S1,ENGIN,SPININ,IPIN,ENGFNN,SPINFNN,IPFNN)
      310 BCN = BCN + S1*D
          DO 330 IFDC =1,NDC
          CALL TRAPOS(S2,ENGIN,SPININ,IPIN,EDC(IFDC),SPDC(IFDC),IPDC(IFDC))
      330 BCN = BCN + S2
          BC(IEIN,JIN,IPIN) = BCN
      340 BCN = BC(IEIN,JIN,IPIN)
          IF(BCN.LT.1.E-30) GO TO 350
          IF(N.EQ.1) WCN(IEIN,JIN,IPIN,1) = 1.
          W = W + WCN(IEIN,JIN,IPIN,1)*SCC/BCN
      350 CONTINUE
          CALL LVLDGC(D,IZ,IN,ENGFN,SPINFN,SIGM,MODE,1)
          D = 0.5*D*DE
          WCN(IEFN,JFN,IPFN,2) = W*D
          IF(IPRINT.LE.1) GO TO 400
          WRITE(6, 970) IEFN,JFN,IPFN,WCN(IEFN,JFN,IPFN,2),ENGFN,SPINFN,
         1  SIGM,D
      400 CONTINUE
```

Fig. A4 (continued)

```
      C
      C   POPULATION IN DISCRETE LEVELS
      C
  108       IF(IPRINT.EQ.0) GO TO 410
  109       WRITE(6,975)
  110   410 DO 600 IFDC=1,NDC
  111       W = 0.
  112       IF(N.EQ.1) IECN2 = 1
  113       DO 540 IEIN=1,IECN2
  114       ENGIN = (IEIN - 0.5)*DE + ETH
  115       JE2 = JES(IEIN)
  116       IF(N.NE.1) GO TO 420
  117       ENGIN = UCM
  118       JE2 = 1
  119   420 DO 540 JIN=1,JE2
  120       SPININ = JIN + SPINZR
  121       IF(N.NE.1) GO TO 430
  122       SPININ = SPINCM
  123       IPIN2 = 1
  124   430 DO 540 IP  =1,IPIN2
  125       IPIN = IP
  126       IF(N.EQ.1) IPIN = IPCM
  127       CALL TRAPOS(SCD,ENGIN,SPININ,IPIN,EDC(IFDC),SPDC(IFDC),IPDC(IFDC))
  128       IF(SCD.LT.1.E-30) GO TO 540
  129       BCN = BC(IEIN,JIN,IPIN)
  130       IF(BCN.LT.1.E-30) GO TO 540
  131       IF(N.EQ.1) WCN(IEIN,JIN,IPIN,1) = 1.
  132       W = W + WCN(IEIN,JIN,IPIN,1)*SCD/BCN
  133   540 CONTINUE
  134       IF(N.EQ.1) GO TO 590
  135       IF(NDC.LE.2) GO TO 590
  136       DO 580 INDC=3,NDC
  137       CALL TRAPOS(SDD,EDC(INDC),SPDC(INDC),IPDC(INDC),EDC(IFDC),
           1  SPDC(IFDC),IPDC(IFDC))
  138       IF(N.GT.2.AND.SDD.LT.1.E-30) GO TO 580
  139       IF(N.GT.2) GO TO 570
  140       IF(IFDC.GT.1) GO TO 570
  141       BDC = 0.
  142       DO 560 IFDCC=1,NDC
  143       CALL TRAPOS(S2,EDC(INDC),SPDC(INDC),IPDC(INDC),EDC(IFDCC),
           1  SPDC(IFDCC),IPDC(IFDCC))
  144       BDC = BDC + S2
  145   560 CONTINUE
  146       BD(INDC) = BDC
  147   570 BDC = BD(INDC)
  148       IF(BDC.LT.1.E-30) GO TO 580
  149       W = W + WDC(INDC,1)*SDD/BDC
  150   580 CONTINUE
  151   590 IF(IFDC.LE.2) W = W + WDC(IFDC,1)
  152       IF(IPRINT.EQ.0) GO TO 600
  153       WRITE(6,980) IFDC,W,EDC(IFDC),SPDC(IFDC),IPDC(IFDC)
  154   600 WDC(IFDC,2) = W
      C
      C   FOR MULTIPLICITY OF GAMMA CASCADE
      C
  155       H(N) = WDC(1,2) + WDC(2,2) - WDC(1,1) - WDC(2,1)
      C
      C   ISOMER RATIO R(2)
      C
  156       R(2) = 1.
  157       IF(WDC(1,2).GT.1.E-30) R(2) = WDC(2,2)/WDC(1,2)
  158       WT = WDC(1,2) + WDC(2,2)
  159       RD  = ABS(1. - WT)
  160       IF(IPRINT.EQ.0.AND.N.GT.1) GO TO 640
  161       WRITE(6,948)
  162   640 WRITE(6,950) N,H(N),WDC(2,2),WDC(1,2),R(2),RD
  163       IF(WDC(1,2).LT.0.1.AND.WDC(2,2).LT.0.1) GO TO 650
  164       IF( RD.LT.RDLM) GO TO 700
  165   650 N = N + 1
  166       DO 680 IEFN=1,IECN
  167       DO 680 JFN=1,JE
  168       DO 680 IPFN=1,2
  169   680 WCN(IEFN,JFN,IPFN,1) = WCN(IEFN,JFN,IPFN,2)
  170       DO 690 IFDC=1,NDC
  171   690 WDC(IFDC,1) = WDC(IFDC,2)
  172       GO TO 250
  173   700 TN = 0.
  174       TH = 0.
  175       DO 720 M=1,N - 1
  176       TH = TH + H(M)
  177   720 TN = TN + M*H(M)
  178       IF(TH.LT.1.E-30) TH = 100.
  179       AVRN = TN/TH
  180       WRITE(6,955) AVRN
  181       READ(5,8,END=900) ISTOP
  182       GO TO (100,110,120,130,135,140),ISTOP
  183   900 STOP
  184     1 FORMAT(2A4,214,17A4)
  185     2 FORMAT(I4,F10.4)
```

Fig. A4 (continued)

```
      3 FORMAT(4(F10.6,F8.4,I2))
      6 FORMAT(8E10.3)
      7 FORMAT(E10.3,2I4)
      8 FORMAT(40I2)
  903 FORMAT(1H1,///20X,20H COMPOUND NUCLEUS = ,2A4/34X, 6H  Z = ,I3/
     1 35X, 5H N = ,I3//20X,17A4)
  910 FORMAT(//12X,29H NUMBER OF DISCRETE LEVEL =  ,I3/20X,20H THRESHOLD
     1 ENERGY = ,F10.4, 4H MEV)
  915 FORMAT(//15X, 5H NO. ,13H ENERGY (MEV), 6H SPIN , 7H PARITY/)
  920 FORMAT(15X,I3,5X,F10.4,F6.1,' (-1)**',I1)
  935 FORMAT(//20X,36H COMPOUND NUCLEUS   EXCITA. ENERGY =,F7.4, 5H MEV
     1, 7H,SPIN =,F4.1,17H ,PARITY = (-1)**,I1)
  940 FORMAT(/20X,94H COEFFICIENTS IN TRANSITION PRBABILITY S = CE1*YE1*
     1E**J+CM1*YM1*E**3+CE2*YE2*E**5+CM2*YM2*E**5   /
     230X, 7H CE1 = ,E10.3, 7H CM1 = ,E10.3, 7H CE2 = ,E10.3, 7H CM2 = ,
     3E10.3)
  945 FORMAT(/30X, 7H RDLM =,E10.3,45H,NUMBER OF ENERGY MESH IN CONTINUO
     1US REGION =    ,I4,'  ,SPIN MESH =',I2)
  947 FORMAT(      //30X,18H **** RESULTS ****)
  948 FORMAT(//20X,' N          H(N)     POPLT, META-STABLE       GROUND
     4ISOMER RATIO    RD '/)
  950 FORMAT(19X,I3,5(3X,E10.4,2X))
  955 FORMAT(//40X,13H AVERAGE N = ,F10.3)
  960 FORMAT(//21X,'CALCULATION MODE =',I2)
  965 FORMAT(1H1///30X, 5H IEFN,5H  JFN,5H IPFN,11H    WCN    ,
     18HENG(MEV),8H  SPIN  ,8H  SIGM  ,12HNO. OF LEVEL/)
  970 FORMAT(30X,3I5, E11.4,3F8.3, E11.4)
  975 FORMAT(/40X,5H NO, ,11H    WDC    ,8HENG(MEV),8H  SPIN  ,
     1  6HPARITY//)
  980 FORMAT(40X, I5, E11.4, 2F8.3, I3)
      END
```

```
      SUBROUTINE TRAPOS(S,EIN,SPININ,IPIN,EFN,SPINFN,IPFN)
      COMMON/TRANS/CE1,CM1,CE2,CM2
      S = 0.
      IF(EIN.LE.EFN) RETURN
      JDL =  ABS(SPININ - SPINFN)
      YE1 = 0.
      YM1 = 0.
      YE2 = 0.
      YM2 = 0.
      IF(JDL.GT.2) RETURN
      IPDL = IABS(IPIN - IPFN)
      IF(JDL.NE.0) GO TO 50
      IF(IPDL.EQ.1) GO TO 40
      YM1 = 1.
      GO TO 800
   40 YE1 = 1.
      GO TO 800
   50 JP = SPININ + SPINFN
      J = 0
      IF(JDL.NE.JP) J = 1
      IF(J.EQ.0) GO TO 400
      IF(JDL.EQ.1) GO TO 300
      IF(IPDL.EQ.1) GO TO 100
      YE2 = 1.
      GO TO 800
  100 YM2 = 1.
      GO TO 800
  300 IF(IPDL.EQ.1) GO TO 320
      YM1 = 1.
      GO TO 800
  320 YE1 = 1.
      GO TO 800
  400 IF(JDL.EQ.1) GO TO 600
      IF(IPDL.EQ.1) GO TO 500
      YE2 = 1.
      GO TO 800
  500 YM2 = 1.
      GO TO 800
  600 IF(IPDL.EQ.1) GO TO 700
      YM1 = 1.
      GO TO 800
  700 YE1 = 1.
  800 EDL = EIN - EFN
      ENG3 = EDL**3
      ENG5 = EDL**5
      S = CE1*YE1*ENG3 + CM1*YM1*ENG3 + CE2*YE2*ENG5 + CM2*YM2*ENG5
      RETURN
      END
```

Fig. A4 (continued)

```
      SUBROUTINE LVLDGC(DJ,IZ,IN,ENGY,SPIN,SIGM,MODE,ISTG)
C     LVEL DENSITY BY A.GILBERT AND A.G.W.CAMERON, CAN. J. PHYS. 43, 1446
C     (1965)
      DIMENSION PZ(100),PN(150),SZ(100),SN(150)
      DATA  PZ/11*0.,2.46,0.,2.09,0.,1.62,0.,1.62,0.,1.83,0.,1.73,0.,
     1      1.35,0.,1.54,0.,1.20,0.,1.06,0.,1.36,0.,1.43,0.,1.17,0.,
     2      1.24,0.,1.20,0.,1.26,0.,1.28,0.,1.35,0.,1.36,0.,1.19,0.,
     3      1.14,0.,1.12,0.,1.59,0.,1.17,0.,1.18,0.,1.22,0.,0.97,0.,
     4      0.92,0.,0.62,0.,0.68,0.,0.64,0.,0.72,0.,0.75,0.,0.71,0.,
     5      0.87,0.,0.83,0.,0.89,0.,0.79,0.,0.89,0.,0.78,0.,0.69,0.,
     6      0.61,0.,0.72,0.,0.77,0.,0.   /
      DATA PN/11*0.,2.67,0.,1.80,0.,1.67,0.,1.86,0.,2.04,0.,1.64,0.,
     1      1.44,0.,1.54,0.,1.30,0.,1.27,0.,1.29,0.,1.41,0.,1.50,0.,
     2      1.50,0.,1.43,0.,1.86,0.,1.47,0.,1.57,0.,1.46,0.,0.93,0.,
     3      0.72,0.,1.12,0.,1.29,0.,0.94,0.,1.24,0.,1.25,0.,1.14,0.,
     4      1.32,0.,1.15,0.,1.24,0.,1.43,0.,1.09,0.,1.20,0.,1.04,0.,
     5      0.70,0.,0.85,0.,0.76,0.,0.92,0.,0.99,0.,1.10,0.,0.92,0.,
     6      0.73,0.,0.70,0.,0.87,0.,0.61,0.,0.69,0.,0.55,0.,0.40,0.,
     7      0.73,0.,0.58,0.,0.86,0.,1.13,0.,0.84,0.,0.79,0.,0.82,0.,
     8      0.71,0.,0.41,0.,0.38,0.,0.67,0.,0.61,0.,0.78,0.,0.67,0.,
     9      0.67,0.,0.79,0.,0.60,0.,0.57,0.,0.69,0.,0.43,0.,0.50,0.,
     1      0.39/
      DATA  SZ/10*0.,2.91,4.17,5.72,7.80,8.97,9.70,10.10,10.70,11.38,
     1      12.07,12.55,13.24,13.93,14.71,15.53,16.37,17.36,18.52,
     2      18.44,18.19,17.68,17.09,16.65,16.66,16.59,16.35,16.18,
     3      16.41,16.60,16.54,16.42,16.84,17.22,17.42,17.52,17.82,
     4      18.19,18.58,19.11,19.83,19.14,18.35,17.40,16.54,15.68,
     5      14.75,13.71,12.67,12.18,11.61,11.09,10.78,10.53,10.41,
     6      10.21,9.85,9.36,8.97,8.56,8.13,7.68,7.33,7.11,7.16,7.05,
     7      6.81,6.56,6.95,7.52,8.03,8.41,8.86,7.71,6.36,5.47,4.78,
     8      4.37,4.17,4.12,4.29,4.61,5.04,5.48,5.96,6.40,6.87,7.20,
     9      7.74,0.,0./
      DATA  SN/10*0.,6.80,7.53,7.55,7.21,7.44,8.07,8.94,9.81,10.60,
     1      11.39,12.54,13.68,14.34,14.19,13.85,13.50,13.00,12.13,
     2      12.60,13.26,14.13,14.92,15.60,16.38,17.08,17.55,17.98,
     3      18.33,18.56,18.71,18.65,18.55,18.52,18.34,18.01,17.38,
     4      16.56,15.62,14.38,12.88,13.24,13.71,14.40,15.16,15.89,
     5      16.43,16.97,17.59,18.08,18.72,19.22,19.51,19.73,19.91,
     6      20.06,20.16,20.09,19.83,19.41,19.06,18.66,17.73,17.03,
     7      16.44,16.00,15.33,14.49,13.42,12.28,11.14,10.10,9.09,
     8      10.00,10.64,11.18,11.70,12.22,12.71,13.05,12.99,12.62,
     9      12.11,11.66,11.21,10.81,10.38,10.03,9.65,9.38,8.99,8.62,
     1      8.33,8.10,7.82,7.56,7.33,7.15,6.83,6.69,6.55,6.53,6.49,
     1      6.39,5.82,5.26,4.53,3.83,3.08,2.37,1.72,1.05,0.27,-0.09,
     2      -1.69,-2.58,-3.16,-1.72,-0.41,0.71,1.66,2.62,3.22,3.76,
     3      4.10,4.46,4.83,5.09,5.18,5.17,5.10,5.05,5.04,5.03,4.99,
     4      4.98,5.11,5.27,5.39,5.37,5.30/
      MASS = IZ + IN
      U = ENGY
      IF(ISTG.EQ.0) ENGY = ENGY - PZ(IZ) - PN(IN)
      S = -SZ(IZ) + SN(IN)
      IF(IZ.GE.54.AND.IZ.LE.78) GO TO 100
      IF(IN.GE.86.AND.IN.LE.122) GO TO 100
      IF(IZ.GE.86.AND.IZ.LE.122) GO TO 100
      IF(IN.GE.130.AND.IN.LE.182) GO TO 100
      A = MASS*(0.00917*S + 0.142)
      GO TO 200
  100 A = MASS*(0.00917*S + 0.120)
      IF(ISTG.EQ.0) WRITE(6,905)
  200 AM = MASS
      IF(MODE.EQ.0.AND.ISTG.EQ.1) GO TO 220
      SIGM2 = 0.0888*(A*U)**0.5*AM**0.6667
      SIGM = SIGM2**0.5
  220 UX = 2.5 + 150./AM
      IF(U.GT.UX) GO TO 300
      EX = UX + PZ(IZ) + PN(IN)
      TNCX = SQRT(A/UX) - 1.5/UX
      T = 1./TNCX
      RAUX = SQRT(A*UX)
      DUX = 0.05893*EXP(2.*RAUX)/(A**0.25)/(UX**1.25)/SIGM
      EZERO = EX - T*ALOG(T*DUX)
      D = 1./T*EXP((ENGY - EZERO)/T)
      GO TO 400
  300 RAU = SQRT(A*U)
      D = 0.05893*EXP(2.*RAU)/(A**0.25)/(U**1.25)/SIGM
  400 DJ = D*(2.*SPIN + 1)/(2.*SIGM2)*EXP(-(SPIN + 0.5)**2.*0.5/SIGM2)
      RETURN
  905 FORMAT(//30X,'****   DEFORMED NUCLIDE   ****')
      END
```

Fig. A5 An example of the output for computer program **ISOM.**

```
      COMPOUND NUCLEUS = NB-95
                     Z =  41
                     N =  54

      NB-94(N,G)NB-95M,G

NUMBER OF DISCRETE LEVEL =   17
      THRESHOLD ENERGY =      2.3730 MEV

  NO.  ENERGY (MEV) SPIN  PARITY

   17        2.3730   0.5 (-1)**2
   16        2.1650   1.5 (-1)**2
   15        2.1210   1.5 (-1)**2
   14        2.0700   1.5 (-1)**2
   13        1.9130   1.5 (-1)**2
   12        1.8100   1.5 (-1)**2
   11        1.6450   0.5 (-1)**1
   10        1.5900   1.5 (-1)**2
    9        1.2740   0.5 (-1)**1
    8        1.2230   1.5 (-1)**1
    7        0.9300   2.5 (-1)**1
    6        0.7990   0.5 (-1)**1
    5        0.7567   3.5 (-1)**2
    4        0.7280   1.5 (-1)**2
    3        0.7242   3.5 (-1)**2
    2        0.2347   0.5 (-1)**1
    1        0.0      4.5 (-1)**2

      COMPOUND NUCLEUS   EXCITA. ENERGY = 8.4959 MEV ,SPIN = 5.5 ,PARITY = (-1)**2

      COEFFICIENTS IN TRANSITION PROBABILITY S = CE1*YE1*E**3+CM1*YM1*E**3+CE2*YE2*E**5+CM2*YM2*E**5
            CE1 =  0.100E+01 CM1 =  0.100E-02 CE2 =  0.100E-02 CM2 =  0.100E-03

      CALCULATION MODE = 1

            RDLM = 0.100E-02,NUMBER OF ENERGY MESH IN CONTINUOUS REGION =  20  ,SPIN MESH =12

            **** RESULTS ****

      N        H(N)     POPLT, META-STABLE      GROUND     ISOMER RATIO     RD

      1   0.998E-05        0.0             0.998E-05        0.0            0.100E+01
      2   0.188E+00        0.0             0.188E+00        0.0            0.812E+00
      3   0.168E+00        0.279E-04       0.356E+00        0.785E-04      0.644E+00
      4   0.384E+00        0.189E-02       0.741E+00        0.255E-02      0.258E+00
      5   0.210E+00        0.270E-01       0.926E+00        0.291E-01      0.473E-01
      6   0.377E-01        0.276E-01       0.963E+00        0.287E-01      0.957E-02
      7   0.907E-02        0.361E-01       0.969E+00        0.311E-01      0.502E-03

                           AVERAGE N =     9.739
```